Department of Bioproducts and Biosystems

# Engineering Principles of Hydrophobin Fusion Proteins

Katri Kurppa

Aalto University

DOCTORAL DISSERTATIONS

Aalto University publication series
**DOCTORAL DISSERTATIONS** 90/2017
**VTT SCIENCE 153**

# Engineering Principles of Hydrophobin Fusion Proteins

**Katri Kurppa**

A doctoral dissertation completed for the degree of Doctor of Science (Technology) to be defended, with the permission of the Aalto University School of Chemical Engineering, at a public examination held at the lecture hall Ke2 of the school on 2nd June 2017 at 12 noon.

**Aalto University**
**School of Chemical Engineering**
**Department of Bioproducts and Biosystems**

**Supervising professor**
Professor Markus Linder, Aalto University, Finland

**Thesis advisors**
Professor Markus Linder, Aalto University, Finland

Docent Jussi Joensuu, Technical Research Institute of Finland VTT Ltd., Finland

**Preliminary examiners**
Professor Ewa Rogalska, University of Lorraine, France

Professor Henrik Birkedal, Århus University, Denmark

**Opponent**
Docent My Hedhammar, KTH Royal Institute of Technology, Sweden

Aalto University publication series
**DOCTORAL DISSERTATIONS** 90/2017

**VTT SCIENCE 153**



ISBN 978-952-60-7428-3 (printed)
ISBN 978-952-60-7427-6 (pdf)
ISSN-L 1799-4934
ISSN 1799-4934 (printed)
ISSN 1799-4942 (pdf)
http://urn.fi/URN:ISBN:978-952-60-7427-6

ISBN 978-951-38-8539-7 (printed)
ISBN 978-951-38-8538-0 (pdf)
ISSN-L 2242-119X
ISSN 2242-119X (printed)
ISSN 2242-1203 (pdf)
http://urn.fi/URN:ISBN:978-951-38-8538-0

Unigrafia Oy
Helsinki 2017

Finland

441 697
Printed matter

Aalto University

# Abstract

Aalto University, P.O. Box 11000, FI-00076 Aalto www.aalto.fi

**Author**
Katri Kurppa

**Name of the doctoral dissertation**
Engineering Principles of Hydrophobin Fusion Proteins

**Publisher** School of Chemical Engineering

**Unit** Department of Bioproducts and Biosystems

**Series** Aalto University publication series DOCTORAL DISSERTATIONS 90/2017

**Field of research** Biomolecular Materials

**Manuscript submitted** 13 January 2017 **Date of the defence** 2 June 2017

**Permission to publish granted (date)** 26 April 2017 **Language** English

☐ **Monograph** ☒ **Article dissertation** ☐ **Essay dissertation**

**Abstract**

The research presented in this thesis focuses on the design and use of hydrophobin fusion proteins for technological applications. Hydrophobins are small fungal proteins with interfacial function. This characteristic arises from a unique, bipolar structure. Hydrophobins also partition effectively in liquid two-phase systems. The aim of the work presented in this thesis was to connect the molecular function of the hydrophobin HFBI to other operational functionalities by methods of protein engineering.

Proteins have become a central focus of reseach in the fields of biotechnology and material development. The vast interest is due to the inherently detailed structure of proteins, forming complex functionalities that build up to great application potential. Nature has created detailed and precise function to these molecules, which can be harnessed to build new materials. The art of protein engineering may be used to join and modify elements in new combinations.

A central theme throughout this research was to evaluate aspects such as protein component stoichiometry, material geometry and charge effects, as well as holistic factors influencing application desing. Firstly, suitable model hydrophobin fusion proteins were designed and produced, and their functionality at liquid-liquid and solid-liquid interfaces was studied. In the following segment of this study, the functionality of the fusion proteins was assessed in model applicaions as a hybrid material with carbon nanoparticles. The results presented in this thesis demonstrate the design and use of protein functionalities for creation of biomolecular assemblies based on the self-assembly of hydrophobin HFBI.

The solution equilibrium of class II hydrophobins plays a crucial role in the usability of its fusion derivatives, alongside with the mechanistic details of the interfacial assembly. The results were evaluated in the frame of the design process of hydrophobin fusion proteins. This process consists of an engineering step, a formulation step and a final application step. Thereby, this thesis highlights the importance of considering protein architecture and stoichiometry throughout the process.

**Keywords** hydrophobin, fusion protein, surface-active, amphiphilic, QCM-D

**ISBN (printed)** 978-952-60-7428-3 **ISBN (pdf)** 978-952-60-7427-6

**ISSN-L** 1799-4934 **ISSN (printed)** 1799-4934 **ISSN (pdf)** 1799-4942

**Location of publisher** Helsinki **Location of printing** Helsinki **Year** 2017

**Pages** 144 **urn** http://urn.fi/URN:ISBN:978-952-60-7427-6

**Tekijä**
Katri Kurppa

**Väitöskirjan nimi**
Hydrofobiinin fuusioproteiinien suunnittelu ja käyttö teknologisissa sovelluksissa

**Julkaisija** Kemian tekniikan korkeakoulu

**Yksikkö** Biotuotteiden ja biotekniikan laitos

**Sarja** Aalto University publication series DOCTORAL DISSERTATIONS 90/2017

**Tutkimusala** Biomolekyylimateriaalit

**Käsikirjoituksen pvm** 13.01.2017 **Väitöspäivä** 02.06.2017

**Julkaisuluvan myöntämispäivä** 26.04.2017 **Kieli** Englanti

☐ **Monografia** ☒ **Artikkeliväitöskirja** ☐ **Esseeväitöskirja**

**Tiivistelmä**
Tässä väitöskirjassa esitetty tutkimus keskittyy hydrofobiinin fuusioproteiinien suunnitteluun ja niiden käyttöön teknologisissa sovelluksissa. Hydrofobiinit ovat pieniä homeen tuottamia proteiineja. Hydrofobiinit ovat pinta-aktiivisia molekyylejä niiden ainutlaatuisen kaksiosaisen rakenteen ansiosta, ja jakautuvat tehokkaasti veden ja detergentin muodostamissa kaksifaasisysteemeissä. Tämän työn tavoitteena oli yhdistää HFBI-nimisen hydrofobiinin pinta-aktiivisuus muihin molekyylitoimintoihin proteiinimuokkauksen keinoin.

Proteiinit ovat bioteknologisen nykytutkimuksen ja materiaalikehityksen keskiössä. Proteiinien erikoistuneet rakenteet muodostavat toiminnallisia yksiköitä, joita voidaan käyttää teknologisina rakennuspalikoina. Luonnossa kehittyneet yksityiskohtaiset toiminnot voidaan valjastaa käyttöön kehitettäessä uuden sukupolven yhdistelmämateriaaleja. Proteiinimuokkauksen avulla biomolekulaarisia yksiköitä voidaan yhdistää ja muokata lukuisilla tavoilla. Tämän tutkimuksen keskeinen teema oli fuusioproteiinien suunnitteluun vaikuttavien tekijöiden tarkastelu. Näitä ovat esimerkiksi proteiiniyksiköiden stoikiometria, materiaalien geometria ja yhteensopivuus sekä varausten aiheuttamat vaikutukset. Lisäksi tavoitteena oli luoda kokonaiskuva suunnitteluprosessista lopullisen teknologisen sovellettavuuden näkökulmasta.

Tutkimuksen lähtökohtana ovat olleet sopivat hydrofobiinin fuusioproteiinit, joiden suunnittelu, tuotto sekä käyttäytyminen neste-neste sekä kiinteä-neste rajapinnoilla kuvataan tässä väitöskirjassa. Tutkimus jatkui kehitettyjen fuusioproteiinien toiminnallisuuden tarkastelulla valituissa mallisovelluksissa. Sovellukset keskittyvät hydrofobiinin toimintaan hiilen nanopartikkelien ja vesiliuosten rajapinnalla. Tässä työssä esitetyt tulokset ovat osoitus siitä, miten proteiinien toiminnallisuuksia sekä hydrofobiinin itsejärjestätytymistä voidaan käyttää hyödyksi biomolekulaaristen kokonaisuuksien muodostamisessa.

Tulokset arvioitiin tarkastellen hydrofobiinifuusioiden suunnitteluprosessia, johon kuuluu muokkausvaihe, valmistevaihe sekä sovellusvaihe. Tämä tutkimus osoittaa erityisesti, että proteiiniarkkitehtuuri ja molekyylikomponettien stoikiometria on huomioitava tarkasti suunnitteluprosessin joka vaiheessa.

**Avainsanat** hydrofobiini, fuusioproteiini, pinta-aktiivinen, amfifiilinen,QCM-D

**ISBN (painettu)** 978-952-60-7428-3 **ISBN (pdf)** 978-952-60-7427-6

**ISSN-L** 1799-4934 **ISSN (painettu)** 1799-4934 **ISSN (pdf)** 1799-4942

**Julkaisupaikka** Helsinki **Painopaikka** Helsinki **Vuosi** 2017

**Sivumäärä** 144 **urn** http://urn.fi/URN:ISBN:978-952-60-7427-6

# Preface

As often happens in life, the realization of this thesis did not follow the expected route. It has been a long way since I began working in the fascinating world of proteins. The work in this thesis spans the years 2007-2017, and was carried out at the Technical Research Institute of Finland, VTT Ltd. Of these ten years, I spent a good part at home taking care of my children. Thinking backward, those times played a significant role in the outcome of this work.

Life. There were days when I thought this thesis might never see its final form. Surely, I am not the only one who thought this. At times, the whole concept seemed distant, with my hands full of life that did not easily coincide with academic goals. More importantly, there were the days when I felt confident in life and its timespans. That is, the recurring fact that it all usually works out in the end. Today I am happy to find myself at this checkpoint. Of course, none of this would have succeeded were I in this alone. Luckily enough I am not - inspired scientists, good friends and loving family have supported me throughout.

Gratitude. Foremost, I want to express my sincere gratitude to Professor Markus Linder, my thesis supervisor, professor and former team leader. Thank you for your encouragement, superior guidance and utmost patience during these past ten years. Your profound work on the hydrophobins has laid the ground for this thesis among many others. Just as much, I warmly thank Docent Jussi Joensuu, my thesis supervisor and colleague, for devoted supervision of my thesis work. You always miraculously found the time. Thank you for many fruitful discussions and shared experiments. Where there is a swamp and hoe, there is Jussi (and the hydrophobins).

Conditions. I thank former and current managers of VTT Biotechnology and SONE for providing the excellent research environment, and for the possibility of dividing time between projects and PhD work. I cordially thank Tekes and VTT Ltd. for funding. I also thankfully acknowledge the National Doctoral Programme in Informational and Structural Biology ISB for support and the opportunity to participate in its activities.

Teamwork. I want to thank all my co-authors for valuable discussions and sharing work on these interesting subjects. Research across disciplines is difficult as it is; thank you for the open-minded atmosphere and great collaboration. A special thank you goes to Lauri Reuter, Miika Soikkeli, Sanna Arpiainen and Vesa Hytönen for your easy-going cooperation.

A good team is the essence of experimental science. Thank you to the whole Protein Discovery and Engineering team for all your help, encouragement and friendship. Thank you to our team leader Timo Pulli for support during the finalization of this thesis.

Friendship. A heart-shaped thank you goes to my closest team members Arja, Géza and Riitta S., the small-lab nucleus. Thank you for all the discussions, patience, help and looking out for each other. Thank you Riitta for teaching me how to pipette.

My warmest thank you also to members of former teams, especially team leader Riitta Partanen for her care and attention. A special thank you to the good old Nanobiomaterial team for the inspired scientific attitude and all the fun times, especially you Päivi Laaksonen, Jani-Markus Malho and Suvi Arola. Thank you to all you VTT colleagues, with whom I have shared labs and coffee over many years.

Driving force. I want to thank all my family members and dear friends for believing in me, for sharing and caring. I especially thank my loving and wise parents Leena and Esa for always being there. I am immensely grateful for the world of creativity, people, and intellect in which I have had the privilege to grow. My beloved siblings Heikki, Hanna and Kalle form a major part of that world. Thank you for existing, thank you for your devotion. My warmest thank you also to my parents in-law Sirpa and Pauli for your unconditional help and support.

Love and inspiration. I dearly thank my husband Jani for his sturdy support and for always standing by me, lightening up difficult days during the lengthy making of this thesis. Thank you for seeing the wood behind the trees when I miss it, and for sharing our life with me.

I dedicate this thesis to my three children Klaara, Iiris and Eero, whom make my each day an adventure and are an endless source of inspiration. I love you all to pieces. You wrote this book.

Espoo, May 2017

Katri Kurppa

# Academic dissertation

| | |
|---|---|
| Supervising professor | Professor Markus B. Linder<br>Aalto University, Finland |
| Thesis advisor | Professor Markus B. Linder<br>Aalto University, Finland |
| Thesis advisor | Docent Jussi J. Joensuu<br>Technical Research Institute of Finland VTT LTD.<br>Espoo, Finland |
| Opponent | Docent My Hedhammar<br>KTH Royal Institute of Technology<br>Stockholm, Sweden |
| Preliminary examiner | Professor Ewa Rogalska<br>University of Lorraine, France |
| Preliminary Examiner | Professor Henrik Birkedal<br>Århus University, Denmark |

# List of publications

This thesis is based on the following original publications, which are referred to in the text as I–V. The publications are reproduced with kind permission from the publishers.

I Kurppa, Katri*; Reuter, Lauri*; Ritala, Anneli; Linder, Markus; Joensuu, Jussi. Antibody harvesting with a plant-produced hydrophobin-ProteinA fusion. *Manuscript submitted to Plant Biotechnology Journal 2016.*

II Kurppa, Katri; Jiang, Hua; Szilvay, Geza, R.; Nasibulin, Albert, G.; Kauppinen, Esko, I.; Linder, Markus. 2007. Controlled Hybrid Nanostructures through Protein-Mediated Functionalization of Carbon Nanotubes. Wiley-VCH Verlag GMBH. Angewandte Chemie International Edition, volume 46, issue 34, pages 6446-6449. ISSN: 1433-7851. DOI:10.1002/anie.200702298.

III Kurppa, Katri; Hytönen, Vesa; Nakari-Setälä, Tiina; Kulomaa, Markku; Linder, Markus. 2014. Molecular engineering of avidin and hydrophobin for functional self-assembling interfaces. Elsevier Science. Colloids and Surfaces B: Biointerfaces, volume 120, pages 102-109. ISSN: 0927-7765. DOI: 10.1016/j.colsurfb.2014.05.010.

IV Soikkeli Miikka; Kurppa, Katri; Kainlauri, Markku; Arpiainen, Sanna; Paananen, Arja; Gunnarsson, David; Joensuu, Jussi; Laaksonen, Päivi; Prunnila, Mika; Linder, Markus; Ahopelto, Jouni. 2016. Graphene Biosensor Programming with Genetically Engineered Fusion Protein Monolayers. American Chemical Society. ACS Applied Materials and Interfaces, volume 8, issue 12, pages 8257–8264. ISSN: 1944-8244. DOI:10.1021/acsami.6b00123.

# Author's contributions

I. (*KK and LR share equal contributions as first author).

KK took part in expression experiments in *N.benthamiana*, characterized the proteins and performed mass spectrometry measurements. KK performed all QCM-D experiments and analyzed the results. KK screened for suitable detergents for two-phase extraction and optimized the experimental conditions for ATPS. KK determined experimental and analytical methods for antibody purification in buffer solution. KK and LR performed final quantitative experiments on chosen model antibody together and LR studied the two-phase separation of fusion proteins from plant leaf extract. LR generated and characterized the BY-2 cell lines, performed the pilot scale experiments and conducted the microscopy experiments. KK wrote the first version of the manuscript and edited the final version together with LR.

II. The author conducted experimental work, interpreted the results and had the main responsibility for writing of the publication. HJ conducted TEM imaging and GS was in charge of engineering the HFBI cysteine mutant.

III. The author conducted all protein characterization experiments, performed all QCM-D experiments, interpreted the results and had the main responsibility for for writing the article. ML and VH performed construction of the recombinant production strains of HFBI-Avd.

IV. The author conducted all protein purification and characterization work, QCM-D experiments and interpreted the results. The author was in charge of planning the biomolecular work. The author wrote the article from the biochemically relevant parts.

# Contents

# List of abbreviations

| | |
|---|---|
| ATPS | Aqueous two-phase separation |
| QCM-D | Quartz-crystal microscopy with dissipation monitoring |
| SDS-PAGE | Polyacrylamide gel electrophoresis using sodium dodecyl sulphate |
| PEG | polyethylene glycol |
| FET | Field-effect transistor |
| GFET | Graphene field-effect transistor |
| CNT | Carbon nanotube |
| SWCNT | Single-walled carbon nanotube |
| MWCNT | Multi-walled carbon nanotube |
| TEM | Transmission electron microscopy |
| AFM | Atomic force microscopy |
| MW | Molecular weight |

# 1. Introduction

A group of proteins called the hydrophobins forms the core of this work. Proteins have become a central focus of research in the fields of biotechnology and material development. The vast interest is due to the inherently complex structure of proteins, forming complex functionalities that build up to great application potential. Nature has created detailed and precise function to these molecules, which can be harnessed to build novel hybrid materials.

At the same time, developments in nanotechnology have led to the need for solutions to integrate and control biophysical systems and interfaces. A cross-disciplinary effort is needed to create smart materials or sensing applications for, e.g., healthcare. Especially, biofunctionalization of surfaces is relevant in adapting physical devices to biological environments (Niemeyer 2007). Control of interfaces at material borders is a prerequisite for efficient communication – signal transduction, creating structural order in materials or molecular transport.

The art of protein engineering is used to combine and modify biomolecular elements in new combinations. Proteins can be seen as building blocks. This work describes the process of joining different functional proteins in an effort to expand their ways of use in nano- and biotechnological applications. The tailored proteins have been employed in model applications in an attempt to holistically understand the influential factors in protein design.

## 1.1 Hydrophobins

The fusion proteins described in this study are all based on a surface-active protein, a hydrophobin named HFBI. Hydrophobins are a group of small (10 kDa) proteins produced by fungi, for example the mushrooms commonly used as a food ingredient. Hydrophobins have evolved in nature to operate at different interfaces during the growth of the fungus (van der Vegt et al. 1996; Wösten & de Vocht 2000; Linder 2009). In nature, hydrophobins mediate attachment of the growing fungal hyphae to solid, hydrophobic substrates. Hydrophobins also form protective layers on parts of the fungi and are involved in the formation of appressoria cells (Khalesi et al. 2015). All hydrophobins contain eight Cys residues which bond intramolecularly to form four disulphide bridges. This special cross-linked structure of hydrophobins allows a group of aliphatic side chains to be faced outwards, forming a hydrophobic patch

on one side of the protein (Figure 1). The resulting protein structure is robust. Generally hydrophobins are classified as class I or class II depending on the pattern of amino acid side chains and resulting solubility characteristics (Wessels 1994). Structurally, the amino acid sequence of class II hydrophobins is more conserved as compared to class I hydrophobins.

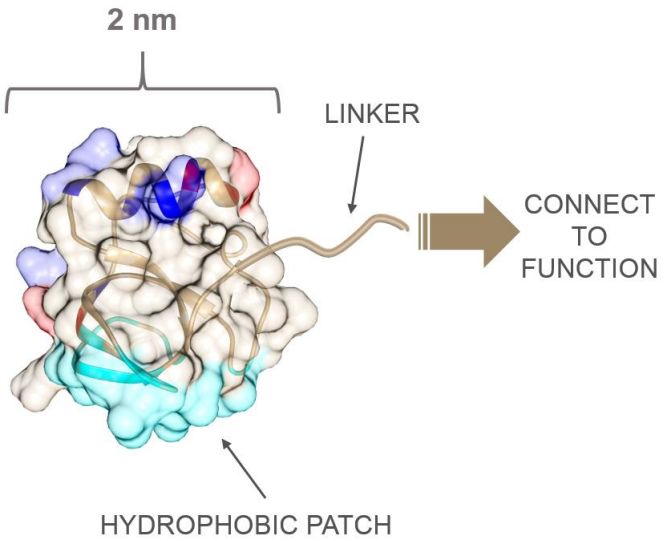


Figure 1. Class II hydrophobin HFBI was connected to fusion proteins via an N-terminal linker. The hydrophobic patch is marked in turquoise. The positively charged, surface-exposed amino acids are shown in blue and negative residues in red. The crystal structure was retrieved from the Protein data bank (ID 2FZ6; DOI: 10.2210/pdb2fz6/pdb) and the image was produced using Chimera.

The X-ray structure of HFBI shows that HFBI consists of four beta sheets and one alpha-helix with lattice parameters of a=108.9 Å, b=49.6 Å and c=85.8 Å (Hakanpää et al. 2006). Hydrophobic amino acids Leu12, Val23, Leu24, Leu26, Ile27, Leu29, Val59, Ala60, Val62, Ala63, Ala66, Leu67 and Leu68 form a surface-exposed hydrophobic patch with an area of 738 $Å^2$ (Hakanpää et al. 2006). Four disulphide bridges tie the structure from within, and allow the exposure of the hydrophobic amino acids. The hydrophilic part of class II hydrophobins consists of an α-helix. Other prominent features of the hydrophilic part include a group of charged amino acids Asp30, Lys32, Asp40, Asp43, Arg45 and Lys50. The charged residues situated opposite of the hydrophobic patch, namely Asp40, Asp43, Arg45 and Lys50, have also been referred to as the charged patch (Lienemann et al. 2013; Hakanpää et al. 2006).

The crystal structure of HFBI has also been produced in a tetrameric assembly consisting of four HFBI molecules (Figure 2a; Hakanpää et al. 2006). The structure of the tetramer is twisted and slightly curved, with more hydrophobic area exposed

on the flat side (Figure 2b). The x-ray structures have also shown detergent-associated forms of the tetramer assembly where the HFBI oligomer was bound to with detergent molecules at the outside of the curved tetramer assembly. Two tetramers were found to form a detergent-bound octamer.

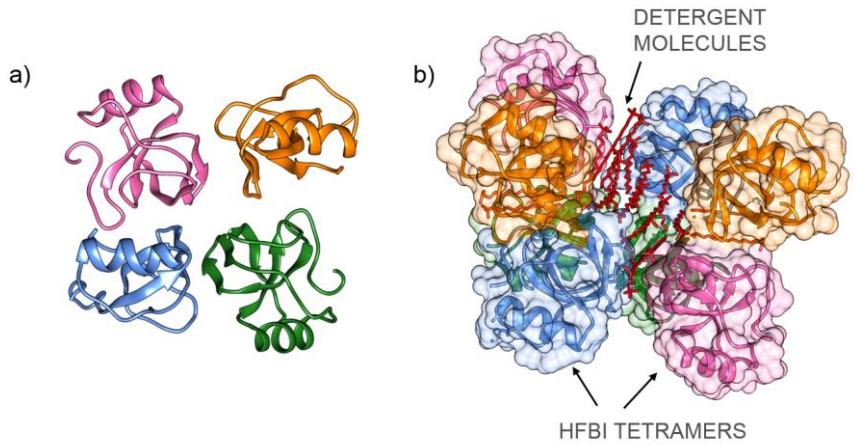


Figure 2. a) Crystal structure of HFBI showing tetrameric assembly. Chains A, B, C and D are indicated by green, blue, pink and orange colouring, respectively. b) Crystal structure of a detergent-associated HFBI octamer, formed by two interacting tetrameric assemblies. Detergent molecules are denoted by red colouring. The crystal structure was retrieved from the protein data bank (ID 2GVM; DOI: 10.2210/pdb2gvm/pdb) and the images produced using Chimera.

At the air-water interface class II hydrophobins self-assemble to form a monolayer, in which molecules have arranged in a distinct hexagonal pattern (Figure 3; (Paananen et al. 2003). This feature is due to the unique amphiphilic structure as well as favorable intermolecular amino acid interactions, based on three-dimensional structure. Functionally the most prominent feature of the hydrophobins is the hydrophobic patch. However, hydrophobin assembly is finally a matter of balance between the surrounding hydropathy environments; also self-assembly on polar surfaces has been demonstrated (Grunér et al. 2012).

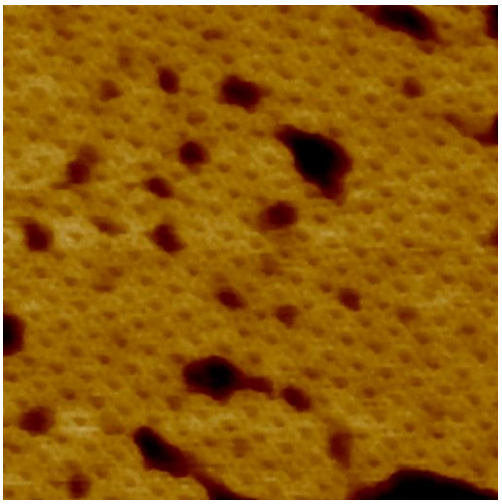

Figure 3. AFM image (100 nm x 100 nm) showing the self-assembled structure of an HFBII film at the air-water interface. Image courtesy of Arja Paananen.

The main roles of the hydrophobins include reducing the surface tension at the air-water interface, mediating adhesion to a solid substrate or formation of protective layers. These events are crucial for many organisms and several groups of surfactant type proteins exist to serve this purpose (Schor et al. 2016). These include small amphiphilic peptides, lipid-associated amphiphiles and independently acting globular proteins, such as the hydrophobins. They all have a common amphipathic structure, meaning that hydrophilic and hydrophobic side chains are clearly separated in distinctive areas. This structure is comparable to the bipolar structure of a surfactant, i.e., soap. Surfactant molecules assemble at interfaces by directing the hydrophobic tail of the molecule towards the hydrophobic phase (air or solid substrate) whilst retaining the hydrophilic head-groups in water. By doing so, the energy barrier at the interface is lowered as the water molecules can seek more favorable interactions within the aqueous phase. Functionally, the hydrophobins have many similarities with surfactant molecules. However, the structural complexity of the hydrophobins results in more complicated behavior and functionality.

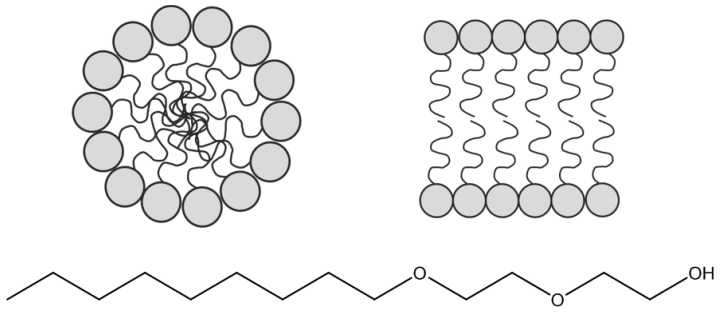


Figure 4. Surfactants are amphiphilic molecules with a hydrophobic carbon tail and a hydrophilic head group (gray sphere). Surfactants form micellar structures in an aqueous solution, with hydrophilic groups arranged on the outside of a disordered oily inner phase formed by the hydrophobic tails.

To date, several different fusion proteins of class II hydrophobins HFBI and HFBII have been constructed (Table 1). The fusion partner is typically fused to either the C- or N-terminal of the hydrophobin via a linker. The linker is typically a PEG-linkeror peptide chain. The N-terminal of the hydrophobin HFBI is situated across from the hydrophobic patch (Figure 1), while the C-terminus is found lower, near the hydrophobic patch. The N-terminus is also more available for modifications, as it elongates more out of the protein core than the C-terminus (Figures 1 and 2a).

This thesis describes the use of class II hydrophobin HFBI and its N-terminal fusion derivatives, which are discussed in detail later (Section 2).

Table 1. Fusion proteins of HFBI

| Fusion partner | Terminal | Production organism | Functionality | Reference |
|---|---|---|---|---|
| Dual-chain avidin | N | *T.reesei* | Affinity binding | Kurppa et al. 2012 |
| Glucose oxidase | C | *N.benthamiana* | Enzymatic | Joensuu et al. 2010 |
| GFP | C | *N.benthamiana* | Fluorescence | Joensuu et al. 2010 |
| Leucine zipper ZE | N | *T.reesei* | Dimerization | Laaksonen et al. 2010 |
| ProteinA | N | *N.benthamiana* | Affinity binding | Kurppa et al. 2016, manuscript |
| Cellulose binding module | N | *T.reesei* | Affinity binding | Linder et al. 2004 |
| Cellulase endoglucanase I | C | *T.reesei* | Enzymatic | Linder et al. 2004 |
| Thiol group | N | *T.reesei* | Chemical | Szilvay et al. 2007 |

## 1.2 The hydrophobic effect

The mechanism of noncovalent association of hydrophobic moieties is a consequence of the surrounding aqueous environment (Chandler 2005; Israelachvili 1991). The tendency of the nonpolar groups to escape water contact is a consequence of disrupting the hydrogen bonded structure of the surrounding water molecules. When the tetrahedral water molecules come in contact with a nonpolar sur-

face, they cannot form hydrogen bonds in their most energetically favorable configuration. The water molecules are forced to reorient themselves, creating a more ordered structure in the vicinity of the nonpolar surface. The result is decreased entropy and, consequently, increased free energy. As the water molecules do not find pairs for hydrogen bonding, they are forced out of their most energetically favorable configuration, thereby causing the hydrophobic effect. The hydrophobic effect is a key driving force in many biophysical events, such as protein folding or protein-DNA binding (Kuriyan et al. 2012).

To minimize energy, hydrophobic entities tend to face away from water, leaving more hydrogen bonding sites for the water molecules to interact with. As a consequence, a phenomenon called dewetting is observed in the void of the water molecules (Chandler 2005; Meyer et al. 2006). The structure of water is sensitive to local solute structure, such as shape and chemical structure of the nonpolar group. Understandably, the size of the hydrophobic surface, i.e., the area over which the water molecules are strained, is relevant for the strength of the hydrophobic effect. It has been shown that for larger areas of low curvature, water molecules are not capable of maintaining the hydrogen bonded network. Simulations showed that when a spherical hydrophobic particle resembling the space-filling size of a methane molecule was placed in water, surrounding water molecules were capable of maintaining the tetrahedral hydrogen-bonding structure (Chandler 2005). As a comparison, the study showed a simulation of a cluster of 135 methane molecules, filling a spherical volume with a radius of 1 nm. In this case, the structure of surrounding water molecules was no longer maintained. For large hydrophobic areas, the solvation free energy is thus entalphically dominated.

In conclusion, when a particle of low curvature and an area larger than 1 $nm^2$ was placed in water, the interfacing water molecules were not capable of maintaining the hydrogen-bonded network, resulting in depletion strong enough to cause dewetting (Chandler 2005). Comparing this value to the area of the hydrophobic patch of HFBI (7,4 $nm^2$) it is evident, that the hydrophobic effect must be a major factor dictating the behavior of the hydrophobin molecules, as well as connected fusion partners.

## 1.3 Hydrophobins at interfaces

The assembly of class II hydrophobins at the air-water interface is well described in literature. The hydrophobins HFBI and HFBII have been shown to form viscoelastic, skin-like films at the air-water interface (Szilvay et al. 2007). The surface of a drop of hydrophobin solution has been shown to flatten due to structural ordering of the proteins at the air-water interface. These features, alongside the distinctive hexagonal nanostructure of self-assembled air-water interfacial monolayer (Figure 3), are descriptive manifestations of the unique nature of the hydrophobins. The phenomena related to the air-water interfacial films of the class II hydrophobins also illustrate how vastly the hydrophobins differ from small-molecule surfactants, to which they are often compared in literature.

Another central task of the hydrophobins in nature is to mediate adhesion to solid substrates or to form protective layers. Class II hydrophobins bind to solid, hydrophobic surfaces by the hydrophobic patch to form rigid, reproducible and ordered monolayers (Linder et al. 2002; Linder 2009; Laaksonen et al. 2010). The driving-force for surface adsorption of hydrophobins is thus the hydrophobic effect. In other words, the solvation energy of the hydrophobin monomer is minimized by binding to the solid surface, thereby hiding the hydrophobic patch from water.

Interfacial self-assembly of HFBI is likely closely related to the solution behavior of the hydrophobin. For surface-active functionality to be efficient, interfacial self-assembly must be favored over the formation of solution oligomers. Indeed, crystallization studies imply that interaction with a hydrophobic surface (detergent molecule) is favored over multimer formation (Hakanpää et al. 2006). Solvent-accessible areas of the hydrophobic patches in HFBI crystal structures can be compared to examine how effectively the hydrophobic patches are buried from water contact in each assembly. The solvent accessible area of the hydrophobic patch in the monomeric, detergent-associated form was clearly smaller than in the multimeric assemblies. Thus, interaction of the hydrophobic patch with a hydrophobic surface (as detergent molecules) seems to be energetically more favorable than multimer formation.

Class II hydrophobins self-assemble at the solid-liquid interface of water and hydrophobic surfaces (Linder et al. 2002). The adsorbed layers are stable and resist forces exerted by ambient fluid flow. Due to these features, the hydrophobin platform has been applied to the biofunctionalization of various surfaces. Moreover, the hydrophobin molecule is on a size scale that is well compatible with components used in nanotechnology. This sets a basis for using engineered hydrophobins in the development of hybrid materials and bioadaptable nanodevices. Hydrophobin assemblies at the solid-liquid interface have been reported to be advantageous in interfacial applications concerning for example adhesion of matrices (Laaksonen et al. 2011; Malho et al. 2015), lubrication (Hakala et al. 2012), drug-particle protection (Valo et al. 2013), reducing nanotoxicity (Yang et al. 2013) and biosensor functionalization (X. S. Wang et al. 2010). In addition, self-assembled hydrophobin surfaces can be used as an immobilization base layer for more delicate biomolecules (Lienemann et al. 2015; Z. F. Wang et al. 2010).

### 1.3.1 Detailed understanding of hydrophobin interfacial assembly

Understanding of the molecular mechanisms related to hydrophobin function is crucial in designing functional fusion proteins, because disturbance of most relevant interaction sites may then be avoided. The most recent investigations of HFBI and HFBII self-assembly show, that the hexagonal assembly at the air-water interface originates from an arrangement of hydrophobin hexamers (Magarkar et al. 2014). This was shown by a computational study consisting of protein-protein docking and molecular dynamics simulations, in combination with cryo-EM and diffraction measurements.

The surface film of hydrophobin HFBI clearly exhibits distinctive plane symmetry. A plane symmetry group is a mathematical representation of a geometrical, two-dimensional pattern (Figure 5). Different symmetry groups are based on the number of rotation centres and possible reflection planes that can be identified in the structure. A P3 symmetry group has three rotation centres of 120 º and no reflection planes. The P6 symmetry group has one rotation centre of 60º, and in addition three 120 º rotations, but no reflection planes. Both P3 and P6 symmetry groups show a hexagonal lattice type with equal lattice constants.

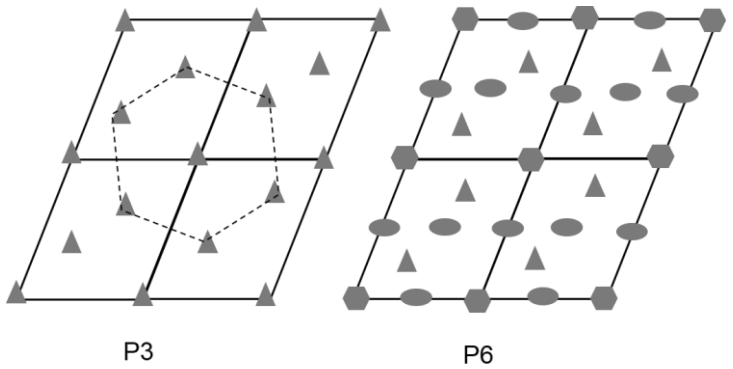


Figure 5. Geometrical symmetry groups P3 and P6 show hexagonal lattice type. The P3 symmetry group includes third order rotations of 120º (triangle). The P6 group shows sixth order rotations of 60º (hexagon) as well as second and third degree rotations (oval and triangle).Neither of these has reflection planes or lines.

Geometrical analysis suggests that the hydrophobin film structure belongs to the P6 symmetry plane group. However, cryo-EM measurements of HFBII as well as protein-protein docking experiments of HFBI and HFBII revealed a structure with lattice dimensions smaller than those of the hexamer, only with P3 symmetry (Magarkar et al. 2014). Also the Monte Carlo simulations of the formation of the self-assembled hydrophobin surface demonstrated a possible role of a P3 symmetric transition state. The rate of formation of the final hexamer-based assembly was accelerated when the metastable trimer assembly was allowed. It was also noted that self-assembly exhibited two kinetically different regions; an initial phase of increasing growth rate, followed by a steady-state region. While these observations reveal the critical molecular interactions involved in hydrophobin self-assembly, present knowledge is not sufficient to draw a direct connection between solution oligomers and interfacial structures.

The rigidity of the surface film in itself poses the requirement that all protein molecules at the surface are connected with a neighboring molecule. Such structures are all based on a *trimer* unit (Magarkar et al. 2014). A trimer unit would require the hydrophobin molecule to have three-fold symmetry, which is not the case. Protein-

protein docking experiments ruled out the option of a pentamer structure, thus narrowing molecular arrangements to hexamer structures consisting of two identical trimers, α-HFBI and β-HFBI. The structures could be matched to previously reported experimental results via the convergence of geometrical parameters and positioning of the trimer structures (Kisko et al. 2009).

Cryo-EM measurements for HFBII showed hexagonal lattices with 56 Å dimensions, and similar lattice vectors were found for both HFBI and HFBII (Magarkar et al. 2014). The hexamers were found to form a ring structure. The air interface of the hexamer was stated to be both electrostatically neutral and apolar. However, in contrast to the computational results, Fourier analysis of the cryo-EM images showed hexamers with P3 rather than P6 symmetry. Further analysis of the possible molecular arrangements revealed, that the α-HFBI and HFBII hexamer structures are able to convert from P3 to P6 symmetry through simple rotation and with only minor adjustments to the structure. The existence of this P3 structure is not supported by experimental findings, as its lattice parameters are lower than those in the observed hexamer unit. This P3 is thus considered to be a temporary structure, which possibly formed during hydrophobin assembly at the air-water interface.

Monte Carlo simulations were performed to investigate the role of the temporary trimer in hydrophobin assembly, taking the surface-active nature of the hydrophobins as a governing energetic factor (Magarkar et al. 2014). Because the viscoelastic properties of the hydrophobin film are a consequence of attractive interactions forming across a protein network, the rate of formation of the film was considered to be directly proportional to the properties. The results showed, that the formation of the hydrophobin film was significantly accelerated when the metastable P3 trimer structure was allowed. Moreover, the simulations showed that formation of the hydrophobin surface film takes place in two steps. Firstly, the surface is filled in at an increasing growth rate. Following, the film grows in steady-state, where the growth rate is independent of the initial conditions and finite size effects. Upon closer examination of the proposed trimer structures α-HFBI and β-HFBI, a dominant salt-bridge between Lys32 and Asp30 was found for the structure β-HFBI. This implies that the β structure may be more stable than the α-HFBI structure.

## 1.4 Hydrophobins in a liquid environment

Class II hydrophobins are highly soluble in water, despite the large, exposed hydrophobic patch. This can be explained by formation of multimers, where the hydrophobins interact by their hydrophobic patches to hide them from water thus lowering solvation energy. Several sets of experimental data have provided evidence of multimer formation in solution. Hydrophobins HFBI and HFBII were first observed to form tetramers in X-ray scattering measurements (Torkkeli et al. 2002). The existence of dimer and tetramer assemblies was also shown by crystallization studies of HFBI (Hakanpää et al. 2006).

The solution behavior of HFBI was studied by size-exclusion chromatography, small-angle x-ray scattering and fluorometric measurements of a specifically labelled hydrophobin.(Szilvay et al. 2006) This NCys mutant of HFBI was labelled specifically at the single available N-terminal thiol group. The presented SAXS, FRET and SEC data showed that HFBI forms solution tetramers in a concentration dependent manner, and that all HFBI is in tetramer state at concentrations >20 µM (Szilvay et al. 2006). This translates to 0.15 mg/ml using the molecular mass of HFBI M=7540 Da. The results suggest cooperative multimerization, possibly from monomers to dimers and eventually to tetramers. The concentration range for oligomer formation was later confirmed for HFBI and an HFBI fusion protein (Lienemann et al. 2013; Lienemann et al. 2015).

The details of solution behavior and the possible mechanistic connection to surface adsorption still lack explicit understanding. Nonetheless, recent work in the area has produced important results to clarify solution characteristics (Figure 7). Self-assembly at the air-water interface lowers the surface tension of the interface.

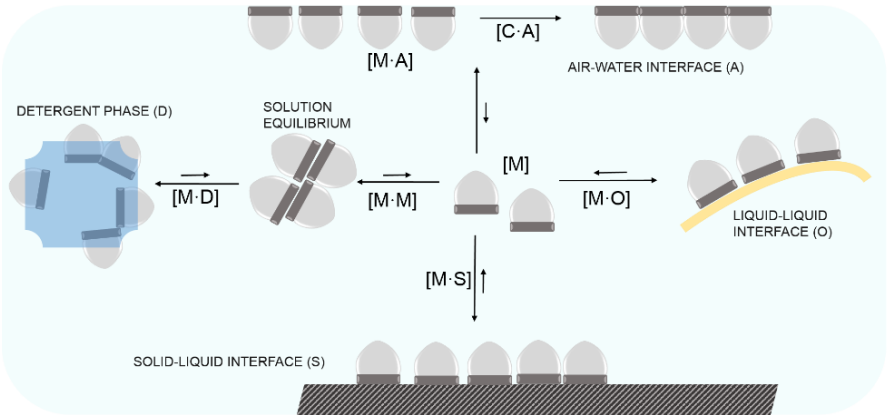


Figure 7. Illustration of hydrophobin behavior and different probable equilibrium states. The arrows indicating equilibrium transitions are indicative. The different states are marked by letters: M = monomer, C = monomer in crystalline film, A= site at air-interface, S= site at solid surface, O = site at oil interphase, D = detergent interaction.

Lienemann et al. have studied the role of the hydrophilic surface of a fusion derivative of HFBI to its function (Lienemann et al. 2013). They engineered a series of fusion proteins of green fluorescent protein and HFBI (GFP-HFBI), in which the charged residues of the hydrophilic end of HFBI were changed to a glutamine or asparagine residues. Oligomerization habits of the produced mutants were studied by flow fractionation (AF4). The conclusion of the work was, that the charged residues have a role in the functionality of GFP-HFBI. The mutant displayed different oligomerization tendency, and an increased oligomer-monomer ratio was found to correlate negatively with the mass of the surface-adsorbed layer. These observations were interpreted to mean that, increasingly, stabilization of solution oligomers

is related to enhanced protection of the hydrophobic patch, thereby decreasing the driving force for surface adsorption. QCM-D experiments showed that mutations near the hydrophobic patch decreased the mass of the layer to less than half of that of the wild-type (Lienemann et al. 2013).

The charges on amino acids Lys32 and Asp30 were found to be crucial for the function of the GFP-HFBI fusion protein (Lienemann 2013). This is in accordance with the computational study describing hydrophobin assembly at the air-water interface (Magarkar et al. 2014).

Interestingly, while the effects of charge mutations had marked effects on the oligomerization behavior of the HFBI fusion protein, only slight effects on the functionality of the non-fused HFBI were observed (Lienemann et al. 2015). Changes in elastic properties of the air-water interface film were minor when the charged amino acid residues of wild-type HFBI were replaced. Results of the size-exclusion chromatography experiments showed, that all of the charged variants as well as wild-type HFBI exist in monomeric state at concentrations <30 µM. Larger complexes were observed to form at concentrations >100 µM. The concentration range for multimer association is in agreement with results presented by Szilvay et al. (Szilvay et al. 2006).

### 1.4.1 Detailed understanding of solution behavior

The crystal structure of HFBI shows a tetrameric assembly, where the HFBI monomers exist in two different conformations (Figure 2) (Hakanpää et al. 2006). Two of the monomers in the tetramer assembly (A and C) have the β-hairpin motif in a closed conformation (c), while the other two (B and D) show an opened confirmation (o) of this loop (Figure 6a). A recent simulation study predicts, that the movement of this β-hairpin motif is related to the stability of the monomers, dimers or tetramers in solution (Riccardi & Mereghetti 2016). Movement in the hairpin region of amino acids 60-66 was suggested to be driven by the formation of the HFBI tetramer. Moreover, the formation of dimer assemblies was found to take place only from the closed conformation (c) of the hairpin region.

The theoretical findings were concluded to support two possible mechanisms for HFBI multimerization. The most probable route includes tetramerization via dimerization of two monomers in closed conformation (cc; Figure 6b). After dimerization, the hairpin on one of the monomers in the dimer changes to open conformation (co). Assembly of these dimers (co) could then produce the tetramer (coco), which would correspond to the reported crystal structure. The small energy difference between the dimer co and tetramer coco implies that conformational change of the hairpin motif occurs rather easily. Arrangement of the hairpin region modifies the hydrophobic interaction area of HFBI as well as lateral intermolecular interactions. Thus, this function was proposed to be connected to fine-tuning of hydrophobin interfacial assembly (Riccardi & Mereghetti 2016).

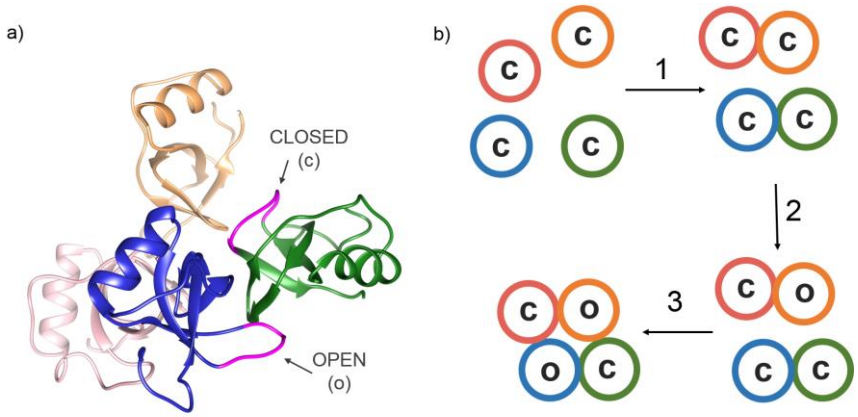


Figure 6. a) Side-view image of the HFBI tetramer showing conformational changes in loops in the β-hairpin loops (magenta). The hairpin loop on monomer chain A (green) is in closed conformation (c) and in open conformation (o) on chain B (blue). The loop is not designated on chains C (pink) and D (orange) for clarity. b) Schematic presentation of probable mechanism for tetramer assembly. The steps illustrate: 1. dimer assembly of monomers in closed conformation, 2. conformational change (c → o) in dimer and 3. final conformational adjustment induced by tetramer assembly.

### 1.4.2 Electrical behavior of hydrophobin monolayers

The electrical behavior of the hydrophobin monolayer becomes a relevant issue in many nanotechnological applications. The structure and chemical composition of the immobilized layer dictate electrical characteristics of a protein monolayer. Self-assembled monolayers of HFBI labelled with gold nanoparticles on graphene have been investigated by conducting AFM (Kivioja et al. 2009). The results showed that HFBI acted as an insulator. This observation lead to the conclusion that electrical transport in the HFBI layer occurs mainly via tunnelling. In other words, the electron wave arriving at the dielectrical protein interface does not decrease instantly but is slowly tapered off, and the probability function may be transferred through the thin molecular layer to some extent.

When dealing with charged species in electrolyte solutions and electric applications, the effect of charge interactions has significant effects. Charged species, such as proteins or ions, exert an effect on charges within a certain distance. This distance is called the Debye length $\kappa^{-1}$, and it describes the net electrostatic effect of a charge carrier. In electrolyte solutions, Debye length is defined as

$$\kappa^{-1} = \sqrt{\frac{\varepsilon^r \varepsilon^0 k_B T}{2 N_A e^2 I}}$$ Equation 1.

where $\varepsilon_r$ is the dielectric constant, $\varepsilon_0$ is the permittivity of free space, $k_B$ is the Boltzmann constant, T is temperature, $N_A$ is Avogadro's constant, e is the elementary charge and I is the ionic strength of the electrolyte.

However, protein layers have been shown to exhibit atypical behavior in respect to the concepts of electrical screening and Debye length (Stigliano et al. 2013). The nanoscale topography and chemical composition of the protein layer cause structural defects in the surrounding water, for example by local deprivation of hydrogen bonds. The resulting confinement of water around the interfacial protein layers causes changes in the polarizability of the molecular structures. In addition, organization of water molecules inside the protein layer becomes localized according to the supramolecular protein structure and its water content. Interfacial layers of hydrophobins HFBI and HFBII have been shown to have low liquid content, in the range of 10-30 % (Krivosheeva et al. 2013).

### 1.4.3 Aqueous two-phase separation

Liquid interfaces of hydrophilic and hydrophobic matter do not occur only at phase boundaries, but also in molecular structures, for example, in surfactant molecules. These interfaces are in a central role in a process referred to as aqueous two-phase separation (ATPS), which is based on phase separation of detergent molecules in aqueous solution (Figure 7). A group of non-ionic detergents exhibit reverse solubility vs. temperature behavior in water solutions (Holmberg et al. 2002). Aqueous mixtures of these surfactants phase separate as temperature is risen above the so called cloud point temperature (cp). The strength of hydrogen bonds is weakened effectively with increasing temperature due to more rapid exchange. As a consequence, the amount of water surrounding the hydrophilic EO groups is reduced.

A two-step process of extraction and recovery (ATPS) is routinely used to purify class II hydrophobins from host cell proteins. Hydrophobins partition effectively in two-phase systems formed by non-ionic ethoxyalcohol surfactants (Figure 7; Linder et al. 2001; Collén et al. 2002; Linder et al. 2004). In a second step, a long-chain alcohol (*i*-butanol) is added. It displaces the hydrophobin molecules back to the aqueous phase. This is likely based on the lack of hydrophilic bulk on the long-chain alcohol, driving the hydrophobin back to the aqueous phase to minimize solvation energy of the hydrophilic surface.

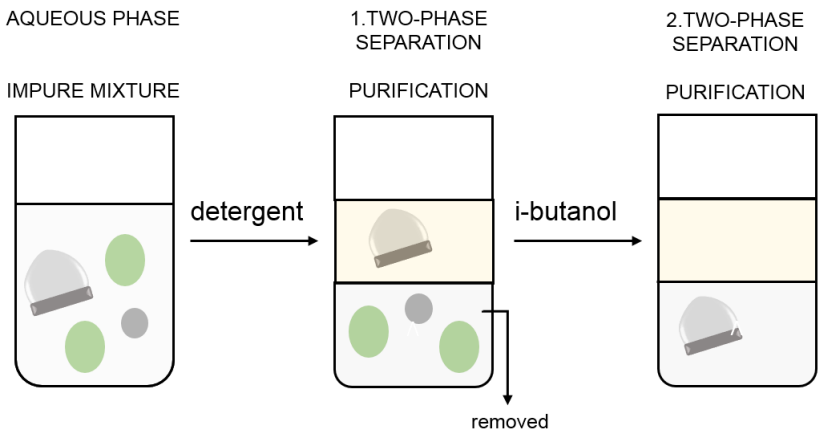


Figure 7. Schematic presentation of the principle of aqueous two-phase separation. Green particles represent impurities in starting sample.

Ethoxyalcohol surfactants have either an aliphatic or aromatic carbon tail, which can also contain branched configurations or unsaturated functional groups (Table 2). The hydrophilic end is an ethoxyalcohol chain of varying length. The cloud point temperature of a surfactant depends on both the length of the carbon tail as well as the number of polyethoxylene units on the hydrophilic end, and finally the concentration of the surfactant solution. The cloud point is also affected by solution composition.

Table 2. Common surfactants used in ATPS for hydrophobins

| Product name | Chemical composition | Chemical structure |
|---|---|---|
| Berol 532 | C11E2 | 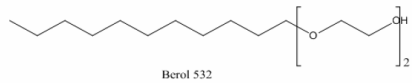 Berol 532 |
| Triton X-114 | C10E8 | 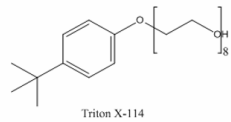 Triton X-114 |
| Agrimul NRE1205 | C12-18E5 | 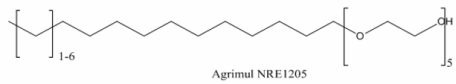 Agrimul NRE1205 |

Aqueous mixtures of these surfactants phase separate as temperature is raised above the so called cloud point temperature (CP; Holmberg et al. 2002) Hydro-

phobins interact with the amphiphilic surfactant molecules and are partitioned between the aqueous phase and the detergent phase by an unknown mechanism, presumedly based on hydrophobic interactions.(Linder et al. 2001) Interestingly, the molecular interaction of HFBI and a detergents has also been observed in crystallographic studies(Figure 2b; Hakanpää et al. 2006) The crystal structure revealed the cysteine variant NCysHFBI bound to surfactant molecules by the hydrophobic patch. The monomers of NCysHFBI were not in contact with each other.

Phase partition of molecules in the ATPS system is described by the partition factor *k*, determined by concentrations of the upper (T) and lower (B) phases (Equation 2).

$$k = C_T/C_B \qquad \text{Equation 2.}$$

One of the most important individual factors which affects the partition factor of a molecule in an ATPS system is the electrochemical component (Collén 2001). It is governed by the net charge of the proteins in question. If solution ions have different affinity for the separated phases, a potential difference across the phase boundary can occur. To minimize this effect, it is recommendable to work at a pH near protein pI or otherwise account for recognized salt effects.

Protein hydrophobicity determines the suitability of the proteins in question to separate in the phase system. Formations of higher-order oligomers, denaturation of proteins or possible conformational changes all affect the final hydrophobicity of the extracted molecules. Also the size of the proteins is naturally affected by accompanying molecules, which have to be located in the micellar structure following the surface-active hydrophobin molecule. The k-value is separate from the yield of the ATPS process. In practice, the optimal conditions may be those which increase the recovery of the protein in question, and at the same time ensure protein stability and feasible processability.

Phase separation of HFBI and HFBI fusion proteins in ATPS system was studied systematically for a range of pure detergents with increasing hydrophilicity, C10E2-C10E5 (Linder et al. 2004). The most determining factor that influenced the outcome of the ATPS process was the hydrophobicities of the molecules involved. Firstly, the hydrophobicity of the detergent, moreover the balance of the hydrophobic and hydrophilic ends (the hydrophilic-lipophilic balance, HLB), governs the structure and water content of the micellar phase. The denser, more hydrophobic surfactants (such as Berol 532) contain less water in the micelle structure, and also the hydrophilic head group is rather small in size. Consequently, the wild-type hydrophobins are very efficiently purified in ATPS systems of Berol532 (Linder et al. 2004). For hydrophobin fusion proteins it was observed, that when the volume of the micellar phase is larger, e.g., contains more water, hydrophilic fusion proteins are more easily incorporated in the detergent phases (Linder et al. 2004). Hydrophobin fusion proteins could be purified by Berol532, when the fusion partner was small and hydrophobic. The surfactant C12-18E5 (Table 2) was shown to be efficient for more hydrophilic fusion proteins (Linder et al. 2004).

Different surfactants can be used successfully in two-phase separation of hydrophobins. In addition to the hydrophilic-lipophilic balance, the surfactants have features, which cause them to function differently. Triton-X 114 (Table 2) is also efficient for purification of hydrophobin fusion proteins (Joensuu et al. 2010). Triton X-114 is an effective all-around surfactant and was used in purification of the HFBI fusion proteins that were produced in tobacco plants in Publication I.

For some non-ionic surfactants, micelle behavior is labile and easily affected by temperature or solution composition. Typically, micelle size increases with temperature, concentration and decreased length of the ethoxyalcohol (EO) tail (Holmberg et al. 2002). The shape and structure of the micelles are equally important in determining the final properties of the surfactant solution. The packing parameter cpp (Equation 3) is used to quantify these factors and determine the shape of the micelle (Goddard 1989).

$$cpp=V_H/l_c a_0, \qquad \text{Equation 3.}$$

where $V_H$ is the volume occupied by the hydrophobic groups in the micellar core, $l_c$ is the length of the hydrophobic group in the core and $a_0$ the cross-sectional area occupied by the hydrophilic group at the micelle-solution interface. The micellar shape changes from spheroidal to cylindrical and lamellar going from cpp=0 to cpp=1. In the application of the concept of cpp, it must be noted that the values of V, $l_c$ and $a_0$ are likely affected by conditions, temperature, salt, etc. For example, additives, such as medium-chain alcohols that are solubilized near the polar head groups, increase the value of $a_0$. This factor may cause differences in performance between different batches of technical surfactants.

Despite functional similarities between hydrophobins and small-molecule surfactants, drawing comparison between the two neglects the fine-tuned molecular details of the hydrophobins. It was shown by Lienemann et al. that certain charged amino acid side chains have an effect of the ATPS process of a hydrophobin fusion protein (Lienemann et al. 2013). Mutations were shown to disrupt the extraction behavior of the fusion protein GFP-HFBI, implying that charges have an effect on the behavior of hydrophobin fusion proteins in ATPS systems. However, the final outcome can be overrun by the other chemical and physical forces, which are also likely related to the characteristics of the fusion partner.

## 1.5 Industrial application of hydrophobins

Due to their distinctive properties and robust demeanor, hydrophobins show potential for various technological applications (Khalesi et al. 2015). The worldwide patent search (Espace.net) shows 408 hits for a patent search using the keyword ‘hydrophobin´. Interfacial self-assembly behavior makes the hydrophobins promising candidates for example for foam stabilization, analyte binding, or specialized coatings.

Accordingly, the focus areas of hydrophobin-related patents fall into three main categories: surface modifications, food and beverage, and cosmetics.

Availability and price have set a borderline for large-scale applications of biosurfactants in industry (Makkar et al. 2011). This applies also to hydrophobins. Large multinational companies associated with hydrophobin research include Unilever, BASF and Danisco. Currently, only the class I hydrophobin SC3 is commercially available at Sigma Aldrich at a price of 625 eur/mg. Class II hydrophobins HFBI and HFBII and their fusion proteins have been produced in gram per liter levels in T.reesei (Askolin et al. 2001) and tobacco BY-2 suspension cells (Reuter et al. 2014).

Down-stream processing can form a crucial bottle-neck and a major cost in the production of biotechnological molecules (Mukherjee et al. 2006). The down-stream process of class II hydrophobin production generally includes ATPS, which can be readily up-scaled (Linder et al. 2004; Reuter et al. 2014).

## 1.6 Fusion protein partners

The fusion proteins applied in this thesis are HFBI-ProteinA, HFBI-dcAvd and HFBI-ZE (Figure 8). These fusion partners were chosen to incorporate either structural modularity, biorecognition or affinity binding capability to the final applications. The supramolecular assembly properties and the comparative dimensions of these fusion proteins vary. These aspects are discussed in detail in Section 3. The individual properties of the fusion partners are presented in the following subchapters.

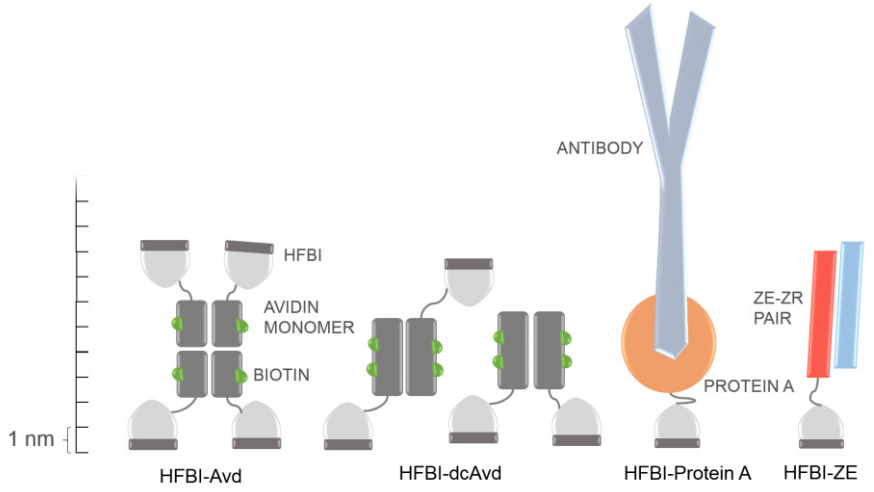


Figure 8. Fusion protein constructs used in this research exhibit varying supramolecular behavior and dimensions (increment of scale bar is 1 nm).

### 1.6.1 Avidin

Avidin was used to add a binding function to the hydrophobin core of HFBI (Publication II). Chicken avidin is a tetrameric protein found in chicken egg-white (Figure 9).(Green 1963; Green 1990) Avidin binds the small molecule biotin with high affinity ($K_d$ ~ $10^{-15}$ M). Due to this interaction the avidin-biotin pair is commonly used in biotechnological applications involving bioconjugation steps (Laitinen 2007).

Wild-type avidin consists of four identical chains which form the functional tetrameric assembly. Each of the four monomers binds one biotin molecule.(Livnah et al. 1993) A dual-chain form of avidin has been engineered to allow differentiation of the binding sites for biotechnological purposes (Nordlund et al. 2004; Hytonen et al. 2006). In dual-chain avidin (dcAvd) two of the monomer chains of wild-type avidin have been joined as one (Figure 9). Hence, the active form of dcAvd is a dimer, of which both halves bind two biotin molecules.

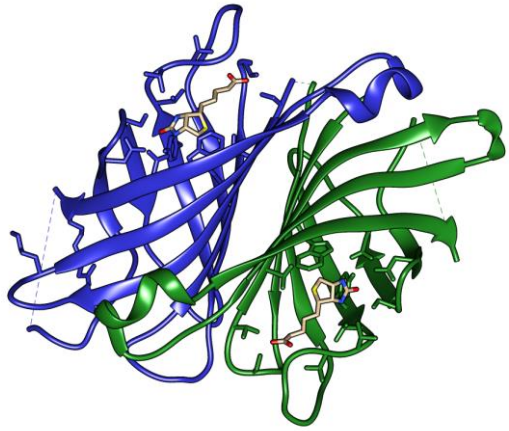

Figure 9. Crystal structure of dual-chain avidin. The crystal structure was retrieved from the Protein Data Bank (ID 2C4I; DOI: 10.2210/pdb2c4i/pdb) and the image was produced using Chimera. The β-barrels (green and blue ribbon) belong to the avidin monomer chains, which are connected as one peptide chain in dcAvd. Biotin molecules are bound to the binding sites (wire model).

### 1.6.2 ProteinA

A fusion protein compiled of HFBI (or HFBII) and ProteinA is presented in Publication I of this thesis. ProteinA is an antibody binding protein, which binds monoclonal antibodies (mAb) of the IgG class (Figure 10; Forsgren & Sjöqvist 1966; Sjödahl 1977; Deisenhofer 1981) ProteinA contains five binding domains denoted as A, B, C, D and E. Therefore, theoretically one ProteinA molecule binds up to five antibodies, but experimental data has shown the actual ratio to be approximately 1:2 (Uhlen et al. 1984; Yang et al. 2003; Moks et al. 1986).

There is one site for ProteinA binding on both heavy-chains of the antibody, meaning that each ProteinA molecule can bind two antibodies in a pH-dependent manner. The antibodies can be released from the binding sites on ProteinA by lowering the pH below 2.5. ProteinA is typically used for chromatographic purification of antibodies, where ProteinA is immobilized in column matrix (Hober et al. 2007). ProteinA based technology can also be used for immobilization of antibodies (Byrne et al. 2009).

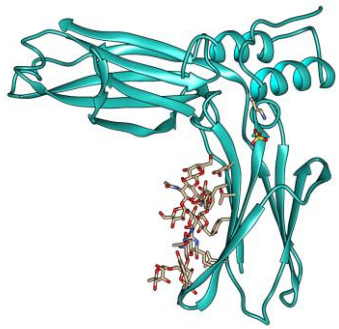

Figure 10. A crystal structure of the Fc fragment of an IgG antibody (turquoise ribbon) bound to the B fragment of ProteinA (wire model). The crystal structure was retrieved from the protein data bank (ID 1FC2; DOI: 10.2210/pdb1fc2/pdb). and the images produced using Chimera.

An increasing demand for antibodies has set a need to develop more efficient downstream processing methods (Elvin et al. 2013; Low et al. 2007). ProteinA-based chromatographic purification suffers from high cost, leakage of ProteinA and low throughput, which has accelerated the development of new purification strategies more suitable for large-scale use (Shukla & Thömmes 2010). For example, a ProteinA-oleosin fusion protein was designed for separation of antibodies based on intrinsic phase separation into an oil bodies by McLean et al. (McLean et al. 2012). Development of a liquid antibody-harvesting process based on a fusion protein of HFBI and ProteinA is described in Publication I.

### 1.6.3 Leucine zippers

The interfacial acitivity of the hydrophobin was combined with a pairing function in an aim to create a switchable, self-assembling molecule unit. A peptide dimer called the leucine zipper (Figure 11) was chosen as the switching module.(Moll et al. 2001) In nature, the leucine zipper peptides are found in cells, where they are involved in DNA binding (O'Shea et al. 1989).

The leucine zipper peptides are coiled coil structures (Lupas & Bassler 2016), which consist of two alpha-helical peptides, both 40 amino acids in length (Figure 12). The leucine zipper peptide structure is characterized by a repeating heptad unit

abcdefg (Monera et al. 1994). Two turns of the α-helix comprise the heptad arrangement of seven amino acid residues (Figure 11a). In the heptad unit, the a and d positions denote hydrophobic amino acid residues, such as leucine. Positions e and g belong to charged amino acid residues. Repetition of the heptad units forms an amphiphilic structure, with a band of hydrophobic leucine residues aligned along the length of the α-helix. Hydrophobic interactions of countered leucine residues on the helixes form a heterodimer, assisted by four attractive salt bridges g → e'. The homodimer has correspondingly two attractive and two repulsive salt bridges. The peptide dimer eventually forms a superhelical quaternary structure (Figure 11b).

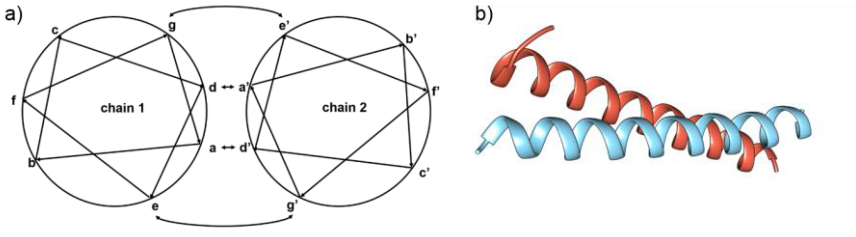


Figure 11. a) Presentation of helical wheel model of the leucine zipper dimer and binding interactions in the heptad repeating unit denoted by letters a-g. b) Crystal structure of a leucine zipper domain in a dimeric state. The crystal structure was retrieved from the protein data bank (ID 4DMD, DOI: 10.2210/pdb4dmd/pdb) and the images produced using Chimera

A pair of designed parallel heterodimerizing leucine zippers with a stability of $10^{-15}$ M were applied by Zhang et al. to create self-assembling protein scaffolds (Zhang et al. 2005). This zipper peptide sequence ZE was slightly modified and engineered to form a hydrophobin fusion protein (Laaksonen et al. 2010).

# Aims of the study

This research focuses on the use of tailored hydrophobin fusion proteins in model applications. Hydrophobins are small fungal proteins with interfacial function. This characteristic arises from a unique, bipolar structure. Hydrophobins also partition effectively in liquid two-phase systems. The aim of the work presented in this thesis was to connect the molecular function of the hydrophobins to other operational functionalities by methods of genetic engineering.

Firstly, suitable model hydrophobin fusion proteins were designed and produced and their functionality at liquid-liquid and solid-liquid interfaces was studied. In the following segment of this study, the functionality of the fusion proteins was assessed in model applications as a hybrid material. A central theme throughout this thesis is to evaluate aspects such as *protein component stoichiometry, material geometry and charge effects*, as well as *holistic factors influencing application design* using hydrophobin proteins.

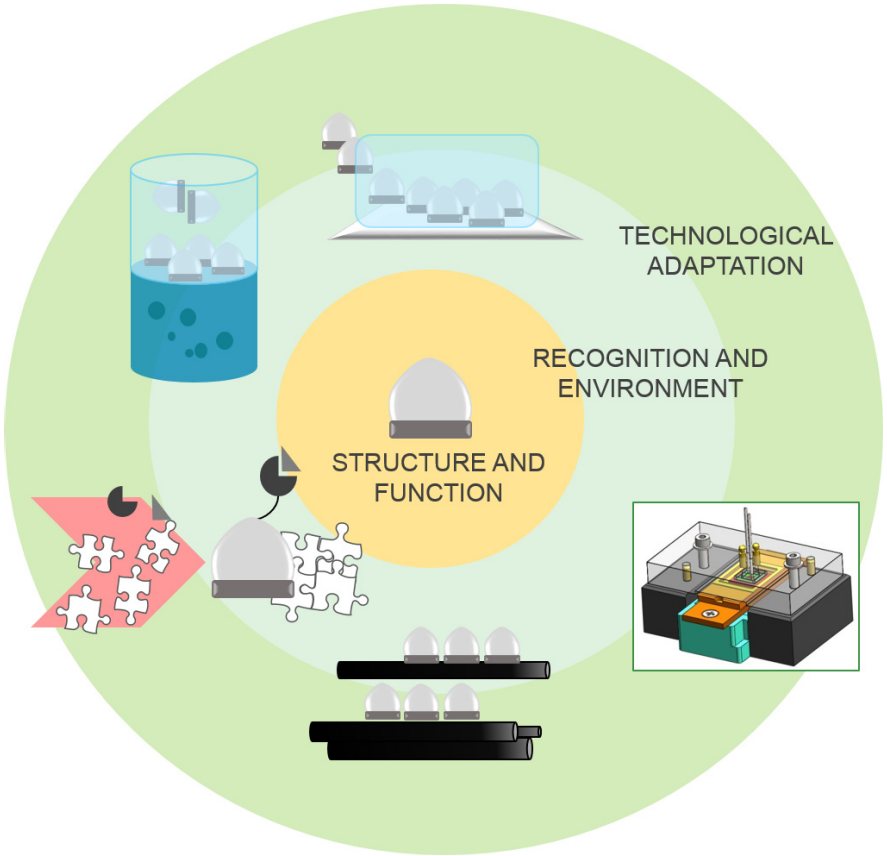


Figure 12. Schematic presentation of the aims of this research.

# 2. Materials and methods

This section will provide reference to the fusion proteins used in this research (Table 3). Central techniques used for characterization and application development are also introduced.

## 2.1 Proteins

Fusion proteins used in the research included in this thesis are listed in Table 3.

Table 3. Fusion proteins applied in this thesis with reference to appended publications

| Fusion protein or conjugate | Production organism | Functionality | Publication |
|---|---|---|---|
| HFBI-ProteinA | *N.benthamiana* | Affinity binding | I |
| HFBII-ProteinA | *N.benthamiana* | Affinity binding | I |
| Au-NCysHFBI | *T.reesei* | Nanoparticle | II |
| HFBI-Avd | *T.reesei* | Affinity binding | III |
| HFBI-dcAvd | *T.reesei* | Affinity binding | III |
| HFBI-ZE | *T.reesei* | Dimerization | IV |

## 2.2 Aqueous two-phase separation

Aqueous two-phase separation (ATPS) was used to purify the produced hydrophobin fusion proteins (Figure 8). Two technical grade detergents are commonly used in the purification routine of class II hydrophobins and their fusions, known by tradenames Berol532 and Agrimul NRE1205 (Table 2).

To purify hydrophobin fusion proteins, ATPS was performed starting from crude leaf extract or supernatant of *T.reesei*. For *T.reesei* supernatants the ATPS was conducted at pH 5 using Berol 532 (HFBI-dcAvd). The back-extracted fractions were finally purified by high-pressure liquid chromatography and recovered yields were calculated by integration of the chromatograms. HFBI-ProteinA was purified from crude *N. benthamiana* leaf extract at pH 7, and final purification was done by affinity chromatography. The recovered yields were analysed by SDS-PAGE.

HFBI-ProteinA was first allowed to bind to the target antibodies in buffer solution. The experiments were conducted at room-temperature and neutral pH to avoid antibody fouling. Possibilities to influence the two-phase system were thus restricted to the choice of surfactant, buffer composition and possible additives. The solution was then added to a batch of pre-weighed detergent and mixed carefully. In the

case of Triton X-114 the detergent is the lower phase and, hence, the upper phase (residue) was collected. To selectively release the antibodies from HFBI-ProteinA, the detergent phase was washed with acidic buffer. After phase separation had re-occurred, the acidic top phase was collected and neutralized to avoid antibody de-naturation.

The functionality of the HFBI-ProteinA fusion protein was tested also in the presence of host cell background For this, samples of plant-leaf extract were spiked with the target antibody Rituximab and the HFBI-ProteinA fusion protein. Finally, the whole solution was subjected to the two-phase system described above.

## 2.3 QCM-D

A quartz-crystal microbalance with dissipation monitoring was used in this research to study the assembly of the hydrophobin fusion proteins at liquid-solid interfaces. The QCM-D technique uses an oscillating piezoelectric quartz crystal which is set to vibrate at its resonance frequency (Figure 13; Rodahl et al. 1997) The crystal surface can be spin-coated with various materials.

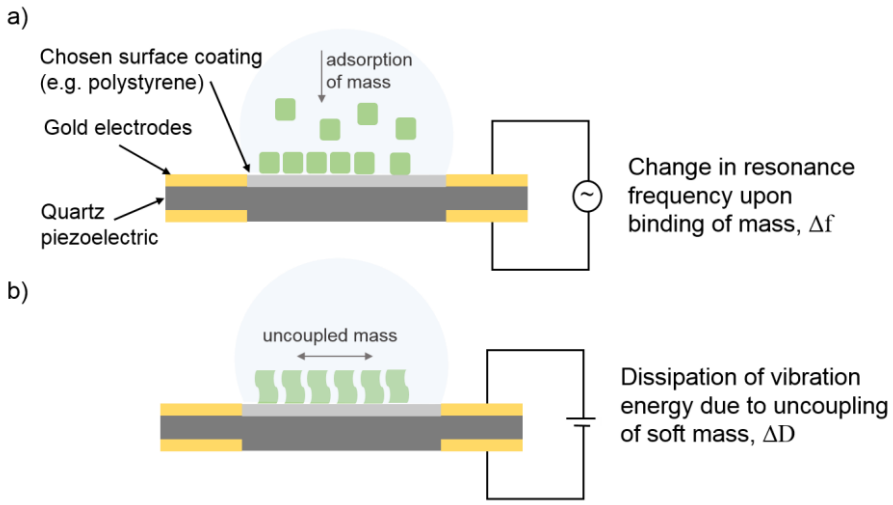


Figure 13. Operating principle of QCM-D technology. a) When mass is adsorbed to the surface of the sensor crystal, the resonance frequency of the crystal is changed. The change in frequency $\Delta f$ is proportional to the adsorbed mass $\Delta m$ for rigid molecular layers. b) The adsorbed molecules dampen the oscillation of a freely oscillating crystal, yielding the dissipation factor D. Dissipation describes the viscoelastic properties of the adsorbed layer.

During measurement, the crystal is firmly placed in a closed fluid chamber and surrounded by the chosen measurement fluid. The measurement chamber is connected to a temperature-stabilized flow channel and the fluid flow is operated by a peristaltic pump. As molecules reach the surface of the measurement crystal and adsorb to the vibrating surface, the oscillation frequency of the crystal is decreased by the increased mass. The change in resonance frequency $\Delta f$ and overtones 3,5,7, 9 and 11 are monitored. The measured $\Delta f$ can be translated to mass $\Delta m$ using the Sauerbrey equation (Equation 4).

$$\Delta m = -\frac{C \cdot \Delta f}{n_3} \qquad \text{Equation 4}$$

where C = 17.7 $ngHz^{-1}cm^{-2}$ for a 5 MHz quartz crystal and $n_3$ = 3, the overtone number.
Dissipation describes the viscoelastic properties of the mass bound to the crystal surface. Once the electric circuit driving the crystal is cut, the sensor crystal is left to oscillate freely. As a result, the oscillation starts to gradually dampen down as oscillation energy is lost. This change is measured as the dissipation factor, D (Equation 5).

$$D = \frac{E_{lost}}{2\pi E_{stored}} \qquad \text{Equation 5}$$

A large, uncoupled mass bound to the surface will cause the crystal to pause faster. On the contrary, a firm molecular layer is more coupled with the oscillation of the crystal and will dissipate the oscillation energy more slowly. The Sauerbrey relation (Equation 4) is valid only for firm molecular layers, i.e., when mass is adequately coupled to the oscillation of the crystal. For soft, viscoelastic layers the contribution to $\Delta f$ is unsensed by the sensor crystal and viscoelastic models must be applied to examine the properties of the bound mass.

## 2.4 Carbon nanomaterials

This section presents an overview on the carbon nanomaterials used in this research (Figure 14; Publications II and IV)

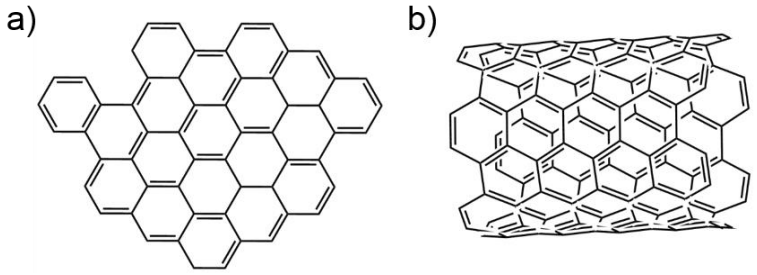


Figure 14. a) Graphene is an allotrope of carbon, which consists of one molecule layer of conjugated benzene rings. b) Carbon nanotubes are rolled-up sheets of graphene.

### 2.4.1 Graphene

Graphene (Figure 14a) is a two-dimensional, one-atom thick layer of $sp^2$-bonded carbon atoms (Novoselov 2004; Novoselov et al. 2012). Carbon atoms in graphene form a hexagonal lattice structure (Figure 14a). The graphene monolayer is a building block for other carbon allotropes. A stack of graphene layers forms graphite, the more commonly known form of carbon. Graphene is outstanding in terms of its mechanical and conductive properties; graphene is over 100 times stronger than steel (Lee et al. 2008; Mayorov et al. 2011; Geim & Novoselov 2007).

Electronically, graphene is a zero-gap semiconductor material, meaning there is no gap between the energy states of the conductance and valence band electrons (Castro Neto et al. 2009; Geim & Novoselov 2007; Novoselov 2007). The conductance and valence bands of graphene meet at the Dirac point (Figure 15). Graphene exhibits a low density of energy states near the Dirac point, which makes its electronic properties very sensitive to the surroundings at this point (Novoselov et al. 2005). Electrons interact with the honeycomb lattice to produce massless Dirac fermions, electrons and holes as they move from the valence band (highest occupied molecular orbital, HOMO) to the conductance band (lowest occupied molecular orbital, LUMO).

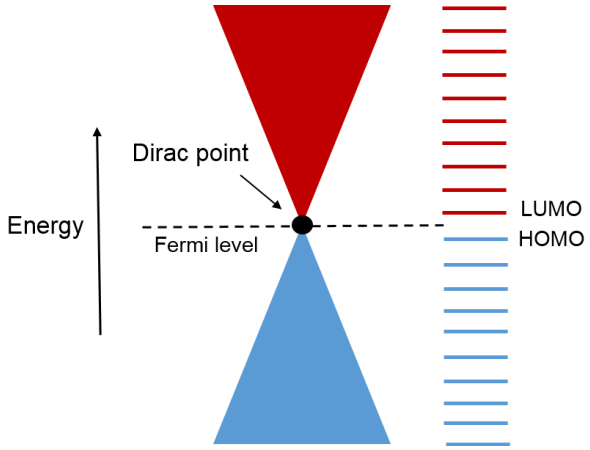


Figure 15. Schematic presentation of energy distribution of electrons in graphene. The crossing point of the valence band and conductance band is the Dirac point.

### 2.4.2 Carbon nanotubes

Carbon nanotubes (CNT) can be described as rolled-up sheets of graphene (Figure 14b) (Iijima 1991; Baughman et al. 2002). They are long, cylindrical particles which are hollow inside. Carbon nanotubes are categorized as single-walled (SWNT) or multi-walled (MWNT), depending on their wall structure. They exist as bundles, which are stacked together longitudinally due to π-stacking of the C-C $sp^2$ bonds. Carbon nanotubes are highly hydrophobic, but can be solubilized in water similarly to graphene, i.e. by chemical modification and ultrasonication, or by using organic solvents (Tasis et al. 2006; Hirsch 2002). Also biomolecules can be used for solubilisation of carbon nanotubes (Asuri et al. 2006; Zheng et al. 2003).

Carbon nanotubes are extremely strong and stiff, with a tensile strength 10-50 times that of stainless steel. Electronically carbon nanotubes are different from graphene, CNT's are always either metallic or semiconducting. Carbon nanotubes also exhibit very good thermal conductivity as well as unique optical properties (Baughman et al. 2002).

### 2.4.3 Exfoliation and adsorbent interactions

Separation of individual graphene sheets or carbon nanotubes in solution is called exfoliation. Exfoliation in liquid phase is traditionally achieved by using aromatic organic solvents such as toluene. Water solubility can be attained by chemical modifications (Loh et al. 2010). Covalent modification of the carbon surface by for example oxidation increases water solubility of the carbon material, but disrupts the valuable $sp^2$ structure of the particle surface and thereby deteriorates material performance.

To ensure material performance, noncovalent functionalization methods can be used. These include modification with hydrophobins (Laaksonen et al. 2010). Noncovalent exfoliation of carbon nanotubes or graphene proceeds via interaction with surfactants or suitable biomolecules, such as proteins (Marchesan & Prato 2015). In addition to the solubilizing effect, the adsorbed surface-active molecules can further interact with graphene: transfer electrons, induce holes, scatter carrier transport, or create localized spots with high gate voltage. The nature of the induced effect is surfactant dependent, and is a consequence of the amphiphilic structure and surfactant dipole strength.

Engineering of nanoscaled surfaces requires control over surface chemistry and molecular orientation is affected by van der Waals forces (Novoselov et al. 2016). In nanoscale, the final realization of forces and interactions involved depends greatly on particle size and geometry (Autumn et al. 2002). In addition to physical surface forces, the interfacial arrangement of ions in water solution influences the electric characteristic of a surface. In the case of biomolecular surfaces, cavities or variation of chemical structure may confine water molecules and ions into unpredictable orientations, causing dewetting, but also polarization effects (Stigliano et al. 2013).

### 2.4.4 Graphene field-effect transistor

A field-effect transistor (FET) is a semiconductor device which is composed of three electrodes, the source, the drain and the gate (Young & Freeman 1996). The source and drain are connected by a gate electrode. The current between the source and drain is controlled by their respective potential difference, and by the charge on the gate. No current runs through the gate. In the case of a graphene field-effect transistor (GFET), a graphene sheet connects the source and drain, forming the channel (Stine et al. 2013).

Hydrophobin fusion proteins were used to functionalize the graphene surface in a field-effect transistor based biosensor (BioFET) (Figure 16;.Riikonen et al. 2013) The graphene channel was connected to four electrodes: source, drain, gate ($V_{gate}$) and reference ($V_L$). The graphene channel was immersed in a fluid chamber filled with measurement buffer. The conductivity of the graphene channel was monitored at the Dirac point.

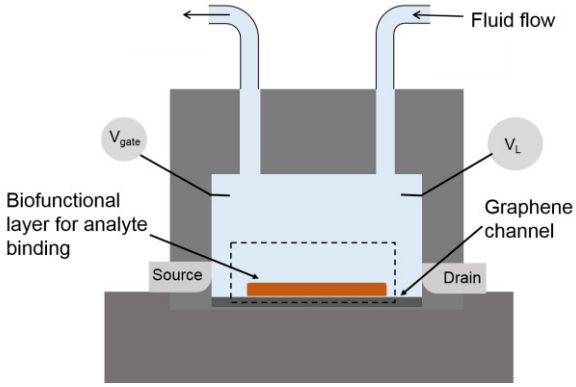


Figure 16. Schematic presentation of a G-FET device in biosensor setup.

# 3. Results

## 3.1 Hydrophobin fusions in 3D systems

The interfacial activity of the hydrophobin was connected to the antibody binding capability of ProteinA (I). The ATPS technique was applied to create a liquid-based method for molecular handling using the hydrophobin as a tag in the two-phase system (Figure 17).

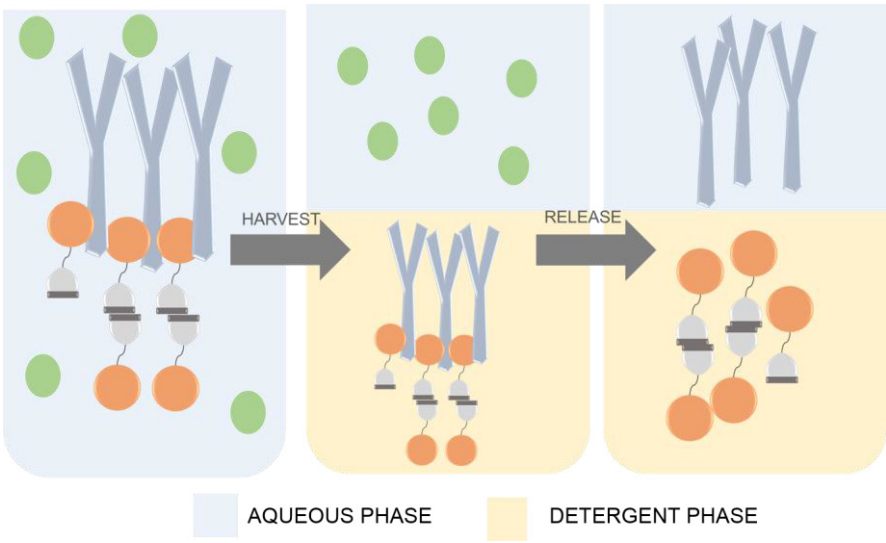


Figure 17. Schematic representation of HFBI-ProteinA antibody harvesting process. The green shapes denote impurities.

A fusion protein of HFBI or HFBII and ProteinA was designed and produced in the tobacco plant *N.benthamiana* with good yield. The fusion protein was successfully purified by ATPS using Triton X-114. The recovered yield of HFBI-ProteinA was 62±5%. The partition coefficients *k* for HFBI-ProteinA were 4.8±0.9 and for HFBII-ProteinA 2.4±0.6. Native ProteinA did not partition to the surfactant phase in the same ATPS conditions, as shown by a *k*-value of 0.4±0.1.

Functional characterization of HFBI-ProteinA and HFBII-ProteinA was completed by QCM-D measurements. Both fusion proteins were observed to tightly bind to the hydrophobic polystyrene substrate. Both of the fusion proteins bound the Rituximab antibody in an amount comparable to physisorbed native ProteinA. HFBI-ProteinA bound 1.5 moles of Rituximab per mole of HFBI-ProteinA. The corresponding value for both HFBII-ProteinA and native ProteinA was 1.2. Control measurements showed that no antibody bound to layers of wild-type HFBI or bovine serum albumin.

The formed molecular surfaces were reproducible and regenerable (Figure 18). The bound antibodies could be released by rinsing the surface with acidic glycine buffer. The underlying HFB-ProteinA layer was left intact. After neutralization of the solution pH, a new round of antibodies could be bound to the HBF-ProteinA layer without a significant loss in binding capacity.

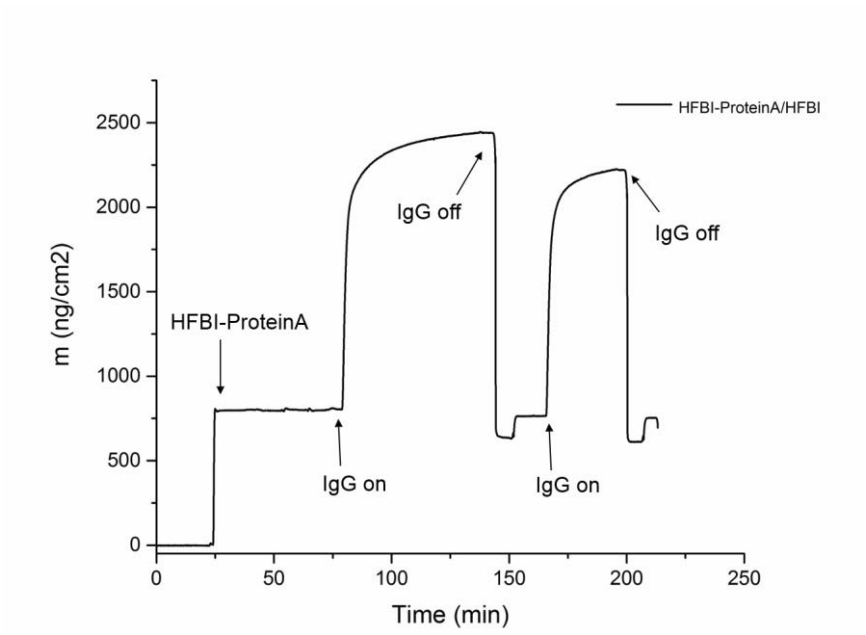


Figure 18. a) Preliminary QCM-D measurements demonstrate the regenerability of the surface layer of HFBI-ProteinA. The measurement shows the initial adsorption of HFBI-ProteinA, followed by two rounds of IgG binding (IgG on) and release (IgG off). The basal HFBI-ProteinA layer is not affected by the sequential process of analyte binding and release.

A lower areal density of functional groups can increase the effective analyte response through reducing steric hindrance. This can be advantageous, for example, in the case of large analyte molecules, such as antibodies. Diluting hydrophobin fusion proteins with wild-type hydrophobin has been previously observed to enhance surface packing by reducing steric hindrance at the surface (personal discussion). In this research, preliminary QCM-D measurements indicated, that there was no significant difference in the amount of bound IgG whether the hydrophobin was surface was formed by HFBII-ProteinA alone or by a 5:1 molar mixture of HFBII-ProteinA/HFBI (Figure 19).

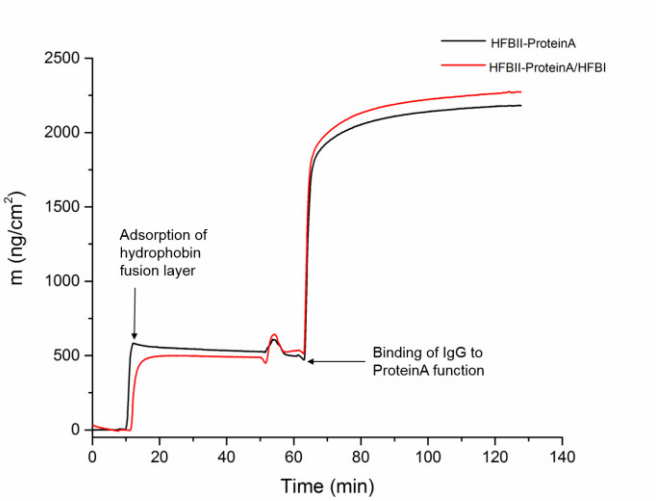


Figure 19. Preliminary QCM-D measurements indicate, that the amount of IgG bound is not significantly improved by co-assembly of HFBII-ProteinA with HFBI.

QCM-D measurements allowed examination of the molecular layers by viscoelastic modelling (Figure 20). The QCM-D signals were followed at several overtones $f_n$ of the resonance frequency f (n = 3,5,7,9 and 11) and the viscoelastic Kelvin-Voigt model was used to examine the thicknesses of the bound protein layers. The model was applied to both layers separately. The density of the layer was assumed as 1000 kg/m$^3$ and viscosity 0.001 kg/ms. Ordering of the basal hydrophobin monolayer places chemical functionalities of connected groups (ProteinA and IgG) in defined locations causing elevated shear force.

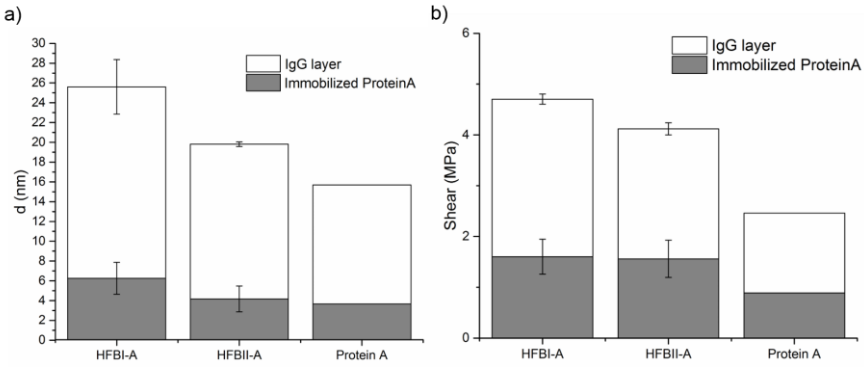


Figure 20. a) Thicknesses of layers by estimated by viscoelastic modelling (Kelvin-Voigt). b) Modelled values of shear force in HFBI-ProteinA/IgG layers. Wild-type ProteinA is shown as a reference.

On the basis of the characterization results, the hydrophobin was harnessed in use in a surfactant-buffer two-phase extraction system. The molecular complex of HFBI-ProteinA and an IgG antibody Rituximab were mixed with the two-phase detergent/buffer system of Triton X-114 and phosphate buffer. Initial experiments immediately showed that HFBI indeed was able to guide the fusion protein/antibody complex to the detergent phase. SDS-PAGE gel imaging verified a decreased concentration of antibodies in the residual buffer phase (Figure 21). Correspondingly, enrichment of antibodies was observed in the buffer after release from the detergent. However, the partitioning of the antibody in initial experiments was much poorer than was expected on the basis of HFBI-ProteinA behavior in ATPS. Phase separation was also unstable.

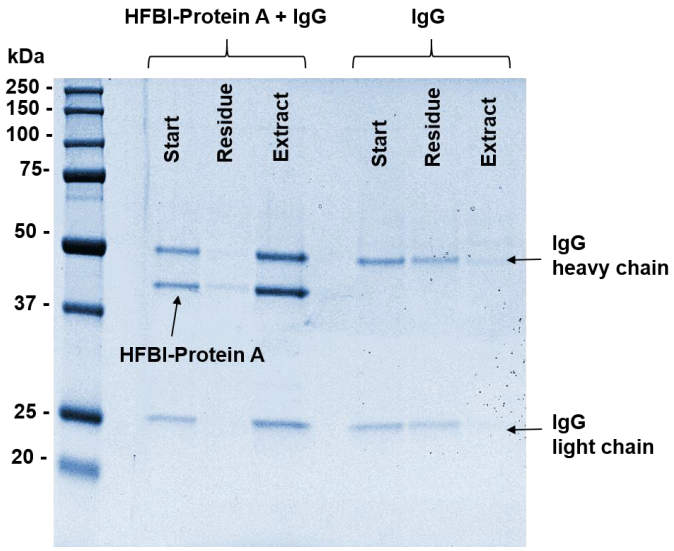


Figure 21. SDS-PAGE gel image demonstrating proof of concept for the HFBI-ProteinA-based antibody harvesting process.

In an effort to enhance partitioning of the HFBI-Protein /IgG complex to the detergent phase, addition of a crowding agent (PEG, MW 6000, 10 w-%) was tested (unpublished data). The added polymeric component was expected to increase pressure for movement of the HFBI-ProteinA/antibody –complex to the detergent phase (Collén et al. 2002). However, although the addition of PEG supported the phase separation event in the system, the crowding agent interfered with subsequent SDS-PAGE analyses. This could be avoided by precipitation of the samples prior to loading. However, the additional step was concluded to add uncertainty in terms of antibody stability and possibly lowered yield. The use of polymeric additives was thus omitted from the process and development of the harvesting routine was continued with the buffer/Triton X-114 system.

Hydrophobin-based harvesting of antibodies was demonstrated finally using samples spiked with plant leaf extract (I). This sample background was chosen to model the function of the HFBI-ProteinA in more realistic complex fluids. Using HFBI-ProteinA, a recovered yield of 28±1% of Rituximab was measured (I). This was clearly higher than the recovery of bare Rituximab (12±2 %).

## 3.2 Fusion proteins for adsorption to solid surfaces

The interfacial function of HFBI was connected to a different type of binding function in the fusion protein HFBI-dcAvd (Publication III). The connection of avidin and hydrophobin was initially constructed in two different stoichiometries (Figure 8), leading either to either a 1:1 ratio of hydrophobin/biotin-binding site in HFBI-Avd and 1:2 hydrophobins/biotin-binding site in HFBI-dcAvd.

Both fusion proteins were produced successfully in *T.reesei*. However, the different assemblies displayed very different solubility. The HFBI-Avd fusion was tightly bound to the mycelium after cultivation, while HFBI-dcAvd was found to be soluble in the culture medium. The same tendency was noted during protein purification. HFBI-Avd was released from the mycelium by SDS and could not be retained in solution without SDS or ethanol. In contrast, HFBI-dcAvd was secreted during production and could be easily handled in the solution. HFBI-dcAvd was purified in normal manner by ATPS using Berol 532. The concentration of the extract after two-phase separation was 0.65 mg/l. Cation exchange chromatography was used for final purification.

To allow good comparison, the biotin-binding capability of the HFBI-dcAvd fusion was studied by the same techniques that were used priorly to characterize dcAvd (Nordlund et al. 2005). Measurement of the fluorescence of tryptophan residues in the biotin binding sites during titration with free biotin was used to determine the effective number of biotin-binding sites. The obtained value for HFBI-dcAvd was 2.4, which was slightly lower than has been reported previously for dcAvd (3.9).(Nordlund et al. 2005) The fluorometric measurement was compared to results of a 3H-assay, which yielded a value of 2.9 as the number of biotin-binding sites for HFBI-dcAvd.

The biotin affinity of HFBI-dcAvd was investigated by studying the dissociation of radiolabelled 8,9[$^3$H]-biotin.These measurements produced a dissociation constant $k_{diss}$ of 7.6±0.8 $\cdot 10^{-6}$ $s^{-1}$ for HFBI-dcAvd. A value of $k_{diss}$ =3.0 $\cdot 10^{-6}$ $s^{-1}$ has been previously reported for dcAvd (Nordlund et al. 2005).

The HFBI-dcAvd fusion protein was observed to self-assemble reproducibly on a polystyrene substrate in QCM-D measurements. The Saurbrey mass of the surface layer was 825 ng/cm$^2$. Considering the molecular masses based on the protein sequence, the result indicated the formation of a molecular monolayer. The dissipation values were typically low, $<1 \cdot 10^{-6}$, confirming again the rigidity of hydrophobin mediated surface-adhesion.

The equilibrium binding isotherms of HFBI and HFBI-dcAvd were measured by QCM-D using protein solutions of different concentrations. The Sauerbrey mass

(Equation 4) of the saturated HFBI surface layer was measured to be 290±17 ng/cm$^2$ and 825 ng/cm$^2$ for HFBI-dcAvd. The dissociation constants for both HFBI and HFBI-dcAvd were in the order of $10^{-7}$ to $10^{-8}$ M. The dissociation constant for HFBI-dcAvd was slightly lower, the 95 % confidence interval for HFBI being 0.02-0.2 µM and for HFBI-dcAvd 0.1-0.5 µM. QCM-D measurements show that the dissipation (Equation 5) of the adsorbed HFBI layer is very low, $< 1 \cdot 10^{-6}$. This indicates that the formed layer is rigid and well-coupled with the oscillation of the crystal.

Biotinylated substrates were bound to the self-assembled HFBI-dcAvd layer to confirm the operational functionality of the dual-chain avidin module. The binding of biotinylated fusion protein of green fluorescent ProteinAnd hevein (bGH) was measured by QCM-D. The HFBI-dcAvd was found to readily bind the biotinylated protein in a 1:1 ratio. The molecular ratio was estimated on the basis of Sauerbrey masses (Equation 4) and molecular masses of bGH and HFBI-dcAvd. When bGH was immobilized via HFBI-dcAvd the layer structure was rigid, yielding a low dissipation factor D (Equation 5) in the order of $10^{-6}$. Control experiments showed, that bGH did not bind to a surface of wild-type HFBI in comparable amounts. The Sauerbrey mass of bGH on the HFBIdcAvd substrate was 530 ng/cm$^2$, whereas on wt HFBI only a layer of 70 ng/cm$^2$ was adsorbed.

The HFBI-dcAvd monolayer was produced using solutions of 0.01 mg/ml concentration. In the same conditions, avidin did not bind to the surface in a mentionable amount. In subsequent control measurements, layers of mass equivalent to a monolayer of avidin could be produced when avidin concentration was increased to 1 mg/ml. This avidin layer was observed to bind high amounts of the biotinylated substrate, clearly higher than possible for an ordered monolayer. Indeed, dissipation in the layer was elevated after binding of the substrate, indicating a loose and unordered molecular layer. In addition, reproducibility of the physisorbed avidin surfaces was poor compared to the HFBI-dcAvd layers.

## 3.3 Hydrophobin functionalized surfaces in 3D systems

Hydrophobin assembly at solid-liquid interfaces was demonstrated also in 3D assemblies of HFBI and carbon nanotubes (II). Carbon nanotubes could be water-solubilized and exfoliated in solutions of class II hydrophobins at room temperature using ultrasonication. The interaction of HFBI and carbon nanotubes was first verified by studying the solubilisation of dry carbon nanotubes in aqueous solutions of HFBI, assisted by sonication. HFBI was observed to effectively solubilize carbon nanotubes. Single-walled carbon nanotubes (SWNT's) could be solubilized to 200 µg/ml by HFBI solutions of 0.25 mg/ml (0.03 mM). The amount of carbon nanotubes solubilized by BSA in the same conditions was found to be negligible. The solutions were produced by ultrasonication and were found to be stable to handling and months of storage at room temperature.

UV/Vis spectroscopy was used for initial characterization of the HFBI-SWNT solutions. Transmittance values of the solutions at 550 nm were 28 % for HFBI-SWNT and 96% for BSA-SWNT. The absorbance spectrograms displayed poorly resolved

Van Hove peaks that are characteristic to solubilized SWNTs. Circular dichroism was measured to examine possible changes caused to the protein structure. No changes to the HFBI structure were detected.

Transmission electron microscopy was used to examine the assembly of carbon nanotubes with hydrophobin molecules. Initial experiments confirmed that individual carbon nanotubes were solubilized in the HFBI solution. The carbon nanotubes were trapped in a film of hydrophobin, which stretched across the holey carbon grid. However, it was impossible to separate the CNT-bound hydrophobins from the extending film.

To get a closer view on the molecular assembly of the HFBI-CNT hybrids, the hydrophobin was labelled with gold nanoparticles. This was achieved by using an engineered hydrophobin mutant, the NCysHFBI (Szilvay et al. 2006). In NCysHFBI, the N-terminus is continued with a peptide linker of 13 amino acids, ending at a cysteine residue. NCysHFBI is produced and purified as a dimer $(NCysHFBI)_2$, bound by a disulphide bond of the thiol groups. The thiol groups were generated by reduction with dithiotreitol and subsequently used to couple the protein to maleimide functionalized gold nanoparticles. This bioconjugation step ensured a determined 1:1 stoichiometry of the HFBI and Au nanoparticles, allowing structural distinction in transmission electron micrographs.

The positioning of the HFBI molecules was verified by visualization of the gold nanoparticles in the micrographs. TEM images of SWCNT's solubilized by Au-NCysHFBI confirmed the assembly of carbon nanotubes with specifically bound hydrophobin molecules. The gold nanoparticles were arranged regularly by the SWNCT wall at a 2.6±0.4 nm interdistance. As a control, HFBI was mixed with the Au nanoparticles and the mixture was used for CNT solubilisation. Evaluation of these samples by TEM showed a random distribution of gold nanoparticles evenly spread across the whole film.

The reduced form $(NCysHFBI)_2$ was also tested for used in solubilisation experiments, but did not show any enhanced performance. However, the films of $(NCysHFBI)_2$ were observed to be more resistant to damage caused by the microscope beam.

## 3.4 Hydrophobin fusion proteins for electronic applications

To study the feasibility of nanocarbon modification with hydrophobin fusion proteins, biofunctionalization of graphene surfaces was pursued. The suitability of hydrophobin for use in bioelectronics applications was demonstrated in Appendix IV.

Two different HFBI fusion proteins were used to biofunctionalize the graphene channel of a G-FET biosensor. The conductive graphene surface was connected to the surrounding aqueous environment via a self-assembled layer of the HFBI-fusion protein. Changes in the vicinity of the graphene surface affect electrical conductivity and could be directly measured. Formation of the monolayers at the interface of CVD graphene and buffer was examined by AFM in both wet and dry states. Both proteins HFBI-ZE and HFBI-ProteinA were observed to form dense monolayers of

4-5 nm thickness immediately upon introduction of the protein solutions to the graphene surface. Drying was observed to cause cracks in the protein layers, but the monolayer was resumed within 5 minutes after rewetting with the original buffer.

Functionality of the surface layers of HFBI-ZE and HFBI-ProteinA were examined by QCM-D measurements. HFBI-ZE formed a monolayer on polystyrene, yielding a Sauerbrey mass (Equation 4) of 270 ng/cm$^2$, corresponding to a monolayer as estimated using the molecular mass and hydrophobin dimensions (12 kDa). The dissipation value (Equation 5) for surface-adsorbed HFBI-ZE at pH 7 was 2-2.5$\cdot 10^{-6}$. This is somewhat higher than for monolayers of wild-type HFBI ($D<1\cdot 10^{-6}$). When the peptide ZR was added to the HFBI-ZE surface, the dissipation value decreased, but no change in frequency was observed. At pH 5 the dissipation value of HFBI-ZE was measured to be $<<1\cdot 10^{-6}$. Surface plasmon resonance measurements verified the binding of the HFBI-ZE to ZR in approximately 1:1 ratio.

QCM-D measurements showed that HFBI-ProteinA bound to the polystyrene surface forming a layer with a Sauerbrey mass of 752 ng/cm$^2$, corresponding to a molecular area of 9 nm$^2$ using a 44 kDa molecular mass. Molecular dimensions of 2.5 nm x 4 m were used for the estimation of molecular area of HFBI-ProteinA. The mass was thereby estimated to correlate with an average 3.2±0.2 nm spacing between the proteins. These values were estimated on the basis of the ProteinA subunit B (Protein Data bank ID 1BDC). Addition of the IgG1$\lambda$ antibody increased the Sauerbrey mass by 1331 ng/cm$^2$, corresponding to an IgG/HFBI-ProteinA ratio of roughly 1.9:1.

To study the absorption of HFBI-ProteinA to the CVD graphene surface used in the final application, a piece of CVD graphene was attached to a $SiO_2$ sensor crystal. When the binding of HFBI-ProteinA was measured, the protein was observed to bind to the $SiO_2$ surface partly covered with CVD graphene control, as well as the $SiO_2$ surface used as a control. The Sauerbrey mass of HFBI-ProteinA was similar in both cases, although clearly lower than on polystyrene. However, the amount of IgG bound to the graphene covered surface was five times greater than to the reference $SiO_2$ surface.

Functionality of the developed sensor was demonstrated by measuring analyte conditions in model solutions by using two different HFBI functionalized surfaces, HFBI-ZE and HFBI-ProteinA. The binding of the negatively charged HFBI-ZE to the graphene surface caused the Dirac peak to shift to more positive voltage. When the positively charged peptide ZR was bound to the HFBI-ZE layer from a 10 µM solution, the Dirac peak was observed to return to the clean sensor state, indicative of neutralization of the zipper charges upon dimerization. The detection range for the HFBI-ZE-ZR system was found to be between 10 fM - 10 µM and detector response occured in less than 1 s.

The corresponding measurements were conducted using the HFBI-ProteinA functionalized graphene surface. Binding of both HFBI-ProteinA and IgG induced a negative shift of the Dirac peak. The detection range was found to range from 80 fM to 80 nM, also displaying a fast initial response followed by slower saturation.

Selectivity of the hydrophobin functionalized surface was studied by crossing the used analytes. When IgG1 was added to the sensor surface functionalized with

HFBI-ZE, a less than 1% response in channel resistance was measured. Control measurements of ZR binding to a clean graphene surface and a monolayer of wild-type HFBI were also performed. In both cases the measured sihift of the Dirac peak was an order of magnitude lower than for the specific interaction of ZR on the HFBI-ZE surface.

# 4. Discussion

Construction of recombinant fusion proteins allows straightforward access to functional biomolecules. However, connecting different proteins together does not necessarily result in a sum of the different functionalities. The as-created fusion protein is a completely new molecule and may exhibit unpredicted behavior. The combined protein functionalities may not operate as they would if they were secluded. Effects of protein fusioning finally depend on the created protein construct as well as the chemical and physical microenvironment in which the fusion protein is to be applied. The results presented in Section 3 allow identifying certain general circumstances, where the presence of the fusion protein may challenge hydrophobin functionality. (Figure 22).

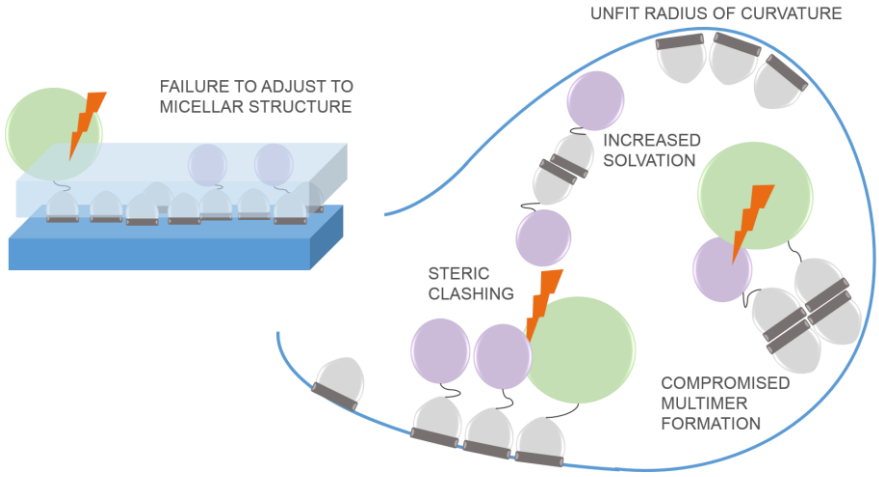


Figure 22. Schematic presentation of actors compromising functionality of hydrophobin fusion proteins.

The task of constructing and applying functional fusion proteins can be presented as a stepwise process (Figure 23). Final technological application of biomolecules includes many cross-disciplinary landmarks, in which the fusion proteins must be examined in diverse settings. The value of a recombinant protein is finally dictated by its suitability for use in a target application. This sets a demand for smart protein engineering, but also requires skill in protein formulation and biophysical application. Recognizing main issues related to each step of the development process will thus facilitates actual industrial implementation.

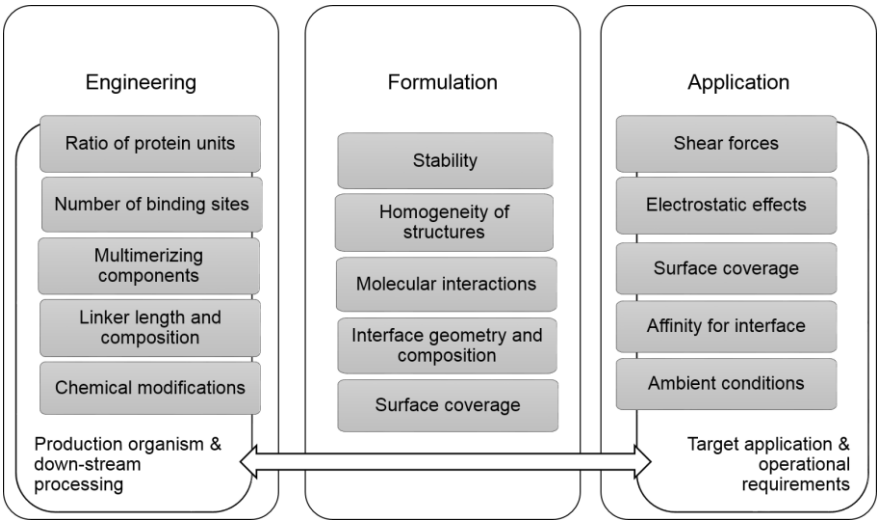


Figure 23. Design process of hydrophobin fusion protein technology.

Access to the final functional proteins follows a route involving three steps (Figure 23). The results presented in Section 3 will be examined in this context to gain a more general view of factors associated with hydrophobin fusion technology.

The engineering step proceeds from selection of functional fusion partners to engineering a line of fusion constructs with varying properties and composition. This step continues with production of the designed constructs and finally, protein purification. The engineering step is governed by the choice of production organism, which dictates the overall flexibility of the whole design process in terms scale-up and timeline. The production organism may also impose restrictions on structural elements of the proteins.

The formulation step entails experimental efforts aimed at verifying the functionality of both all protein parts individually, and establishing optimal conditions for final use of the fusion protein. In other words, formulation entails characterization of the whole molecular system. Steps aiming at stabilization or activation for final application should also be considered at this stage.

Finally, the fusion protein is harnessed to use in the application step. This step includes examination of the final setup from multiple aspects, defined by the end-technology. The application step can bring out unexpected behavior related to additive interactions in the final system. To tune the system, the engineering process must return to characterization step to optimize conditions or, ultimately, to the engineering step.

*Engineering step*

The main factors contributing to hydrophobin fusion protein behavior are related to protein stoichiometry and multimerization habits. Molecule stoichiometry was found

to be a critical factor for the functionalities of HFBI-Avd and HFBI-dcAvd, where both of the fusion partners respectively form multimers in solution. HFBI-Avd was not operational, because of challenges in solubility after release from the mycelium. HFBI-dcAvd on the other hand could be handled in a feasible manner. The high multimerization affinity of avidin monomers in HFBI-Avd hindered independent multimerization and solubility of the fusion protein. Within the limits of this imposed geometrical restriction, the solvation energy of the hydrophobic patches could be sufficiently lowered only by adsorption to mycelial structures.

Also HFBI-ProteinA performed well at the liquid-solid surface. The amount of bound IgG was found to be insensitive to whether the surface consisted of only HFBI-ProtA or had been co-assembled with HFBI. This observation indicates that the wild-type hydrophobin and fusion protein do not compete equally for surface adsorption sites, perhaps due to different stabilities in multimer equilibria. It is also possible, that the amount of bound analyte on co-assembled surfaces would differ more for analytes smaller than the IgG molecule.

Transition of the HFBI-ProteinA fusion to a 3D system revealed a more complicated situation. The recovered ATPS yields were low and phase separation was unstable. The degree of association in the HFBI-ProteinA/IgG interaction leads to a large molecular complex and may hinder hydrophobin multimerization, thereby weakening the driving force for hydrophobin interaction with detergent. One ProteinA molecule can bind up to five antibodies, each of which have two possible binding sites for ProteinA. Considering this, it is clear that a random compilation of large, interconnected proteins would result. Thus, reducing the size of the complexes by adjusting the ratio of associated HFBI:IgG in the protein engineering step may be beneficial and should be studied in the future.

Considering the area of the hydrophobic patch and the hydrophilic area of the adjacent hydrophilic end containing ProteinA and bound antibody, it would be plausible to assume, that the large hydrophilic molecules might hinder the surface-activity of the hydrophobin. The hydrated molecular surface area exceeds the area of the hydrophobic patch by orders of magnitude and could possibly surmount the driving-force of hydrophobin assembly. However, even when the hydrophobin was connected to a large hydrophilic complex, association with the detergent phase was not completely sacrificed. This may be understood through a loose correlation to micellar geometries, in which the hydrophilic bulk of the head group does not affect micelle geometry, but only the cross-sectional area of the hydrophilic moiety is relevant (Equation 3). It is impossible to determine, whether hydrophobin association with the detergent phase occurs via the monomeric form of the protein, or rather the multimeric assemblies become incorporated in detergent micelles of corresponding geometry.

Another possible explanation for the low recovery yields in the antibody harvesting system are problems in the binding of the antibodies to the ProteinA module. Necessary geometrical arrangements may be restricted if hydrophobin multimerization prevails solution behavior. This problem could be especially prominent in the case of the HFBI-ProteinA fusion protein, because of the large size of the binding antibodies. Steric clashing of vicinal molecules may disturb binding of the antibodies

to the ProteinA binding sites even in a 3D system. Indeed, entrapment of water molecules due to localized restrictions in molecular assemblies has been presented to lead to decreased entropy and thus energetically unfavoured states (Chandler 2005; Stigliano et al. 2013).

Regarding adsorption at the solid-liquid interface, the main advantages of hydrophobin fusion technology are 1) structural order and 2) high-affinity for surface binding. These features result in defined orientation of the fusion partners and reproducible surface coverage. Self-assembly of hydrophobin at the liquid-solid interface was not observed to be disturbed by the fusion partners. The resulting molecular complexes were not observed to loosen from the substrate despite increased solvated surface area. This was the case for all fusion proteins, and it is indication of the strength of the interaction of HFBI and the solid hydrophobic surface.

For certain applications a high number of bound analyte is desirable. However, possible steric effects of the bound molecules may decrease the degree of surface coverage. This should be taken into account in construct design. Although the two-step mechanism of self-assembly has been proposed for only the air-water interface, the natural function of the hydrophobin implies, that a two-step process is required for efficient surface coverage. The initial occupancy of hydrophobin at an interface is random and the molecules are rapidly expelled from aqueous solution to the surface due to the dewetted hydrophobic patch. As more monomers keep approaching the surface, the previous molecules have to be able to diffuse laterally to adjust the incoming monomers. The mode of contact between the surface and the hydrophobic patch, would be in a major role in this event. Friction between the surface and the hydrophobic patch, as well as steric clashes of bound fusion partners may create an energetic barrier for the lateral movement of the surface-bound monomers. The effect of the fusion partner may be more pronounced at the solid-liquid interface, as the solid surface does not allow protrusion of molecular parts during a possible reorientation.

In addition to stoichiometry, molecular geometry determines solution behavior and functionality of hydrophobin fusion proteins. Wild-type hydrophobins form a variety of multimeric solution states, and experimental findings suggest that the same is true for hydrophobin fusion proteins. The shape of the oligomers and positioning of fusion proteins is determined by molecular contacts between hydrophobin monomers. Multimerization habits and challenging geometries may be controlled by genetic engineering of fusion partners. This was found to be beneficial in the case of avidin fusion proteins. For surface adsorption, it is important that the molecular orientation of the fusion partners does not hinder contact with the surface. This may be solved by avoiding multimerizing fusion protein partners as well as by considering linker length and rigidity.

Considering the tetramerization mechanism proposed by Riccardi et al (Riccardi & Mereghetti 2016), it is clear that any fusion protein or function connected to HFBI should not disturb movement of the β-hairpin loop. The amino acids 60-66 of this region are in direct connection to the N-terminal, separated by a peptide chain of 10 amino acids. In the wild-type HFBI crystal structure the N-terminal is fixed to the protein core by hydrogen bonding. However, conformational changes in the loop

from which the N-terminal extends may be hindered if a strong opposing force is present at the N-terminus. Such may be the case for example for large multimeric fusion partners displaying strong binding interactions, such as avidin or ProteinA.

The results described in this research underline the fact, that molecular mechanisms of hydrophobin assembly should not be understood simply in view of the amphiphilic structure. On the contrary, it is the amphiphilic structure which gives rise to diverse interactions with the surrounding environment. It seems clear that the energetical penalty of exposing the dewetted hydrophobic patch cannot be avoided; an increased degree of solvation at the hydrophilic end of the molecule does not diminish the driving force for the hydrophobic interaction.

However, although the surface-activity of the hydrophobin is seemingly unaffected by fusion partners, the existence of connected large molecules has other effects on the self-assembled structures. Hydrophobic molecules interact with water also in other ways than merely expelling water from the hydrophobic surface. Theory supports the presented observations on behavior of hydrophobin fusions. In the case of amphiphilic molecules, solvation of the hydrophobic area is not an excluded phenomenon (Chandler 2005). Hydrophilic parts of the molecule are involved in strong interactions with water molecules. On the other hand, orientation of the hydrophilic parts is dictated by positioning of the hydrophobic parts which are buried from water contact. These interactions cause restrictions to the free movement of surrounding water molecules. As a result, water molecules become locally entrapped.

The free energy of transferring an amphiphile to water is the same as the energy for transferring the hydrophobic part to water, because the hydrophilic part will always stay solvated (Chandler 2005). Formation of a micelle is thus opposed by two free-energy contributions: the formation of a stable interface and, secondly, the reduction of available configurations of water molecules, which entails entropic loss. These factors govern micelle size. As the number of molecules in a micelle grows, there is no space to maintain a dense interior while simultaneously placing head groups on the exterior.

According to theory, the factors associated with micelle formation are the width of the hydrophobic tail (α) and the length over which hydrophilic parts and hydrophobic parts are separated (δ; Chandler 2005) These factors determine micelle radius L in terms of number of associated molecules, n:

$$L=(\alpha^2\delta)^{1/3}n^{1/3} \qquad \text{Equation 6.}$$

The number of associated molecules in a micelle is thus given by

$$n = \beta\gamma\delta^2, \qquad \text{Equation 7.}$$

where $\beta=1/k_BT$ , $\gamma$ is the oil-water surface tension, $k_B$ is the Boltzmann constant and T is temperature. Applying this theory to a hydrophobin tetramer (n=4) gives a micelle radius L of 2.8 nm. The diagonal length of the HFBI tetramer is roughly 6.5 nm, as estimated by measuring from the crystal structure. This is in compliance with the theoretical presentation (Equations 6 and 7).
The main points to be considered in the engineering step are thus narrowed to geometry and steric hindrance. The presence of large fusion partners may disrupt the stability of solution oligomers due to entropic loss. This factor may be even more prominent in the case of multimeric tertiary structures. Disruption of solution assemblies may result in poor solubility of the molecules which is problematic during production and purification. In addition, control over molecular positioning in applications is lost due to energetically unstable solution assemblies and suboptimal packing efficiency at solid-liquid surface.

*Formulation step*

The formulation step of the design process includes examination of solution composition, molecule concentrations and optimization of the molecular composition at the interface. This step, although often self-evident and therefore disregarded, is actually a crucial step for successful implementation of final applications.

The binding affinity of hydrophobins to the polystyrene surface is low if compared for example to the exceptionally high biotin binding affinity of avidin ($10^{-15}$ M) and slightly lower for the fusion protein HFBI-dcAvd than for wild-type HFBI. The observed difference may be interpreted to be caused by the large, hydrated bulk of dcAvd, which poses a counteracting force for hydrophobin surface adsorption. A fusion partner may thus destabilize the surface assembly in similar manner as for oligomerization. The Langmuir isotherm fails to take into account molecular interactions between vicinal, adsorbed molecules. This may diminish the differences in surface affinity of the wild-type hydrophobin and its fusion protein. However, a crystalline surface structure has not been shown for hydrophobins at the solid-liquid surface, which suggests that there are probably mechanistic differences in adsorption at solid-liquid interface and the air-water interface.

The pH dependent dissipation values measured for HFBI-ZE at the solid-liquid interface point out the fact, that the fusion partner may significantly affect the behavior of the interfacial molecular layer with respect to solution composition. Structural rearrangements and changes in the viscoelasticity of the protein layer also likely affect the electrical behaviour of the protein surface. Thus, careful analysis of interfacial structures in the final application conditions is essential to be able to distinguish target signals, i.e., analyte binding.

Preliminary observations on difficulties in co-assembly of HFBI-ProtA and HFBI at the solid-liquid interface imply, that wild-type hydrophobin and hydrophobin fusion proteins possess different dissociation constants of multimer assembly. This in turn would affect the proportion of monomers available for surface adsorption. In the case of co-assembly, parallel events of solution multimerization and surface adsorption of the fused and unfused hydrophobins compete (Figure 24). The multimeric

forms of the fusion proteins may be less stable in comparison to those of the native hydrophobin, thus presenting more monomeric form available for surface adsorption. The formation of co-assembled surfaces would thus be related to the concentration range of solution multimerization.

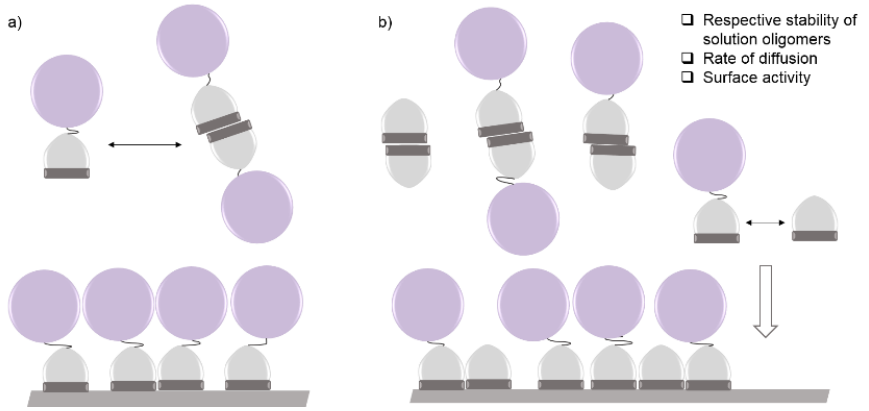


Figure 24. Biofunctionalization of surfaces with hydrophobin fusion. a) Surface coverage may be governed by steric effects of fusion partner. b) Different solution dynamics of fused and non-fused hydrophobins may cause unequal competition for available surface adsorption sites.

When aiming at biofunctionalization of solid surfaces, the geometry of the surface should be complimentary with the hydrophobic patch. The rather rigid nature of the hydrophobin molecule likely requires a suitable geometric counterpart. The relationship between the diameter of carbon nanotubes and protein interactions has been recognized and it has been suggested that CNT diameter needs to be >10 nm for long-lasting contact with interacting macromolecules (Marchesan & Prato 2015). Results regarding carbon nanotube functionalization indicated that carbon nanotubes were fully covered with Au-NCysHFBI at regular interspacing. The observed measure corresponded well to the diameter of the HFBI molecule. The radius of curvature of the smallest individual carbon nanotubes is possibly too large to fully bind to the hydrophobic patch of HFBI.

The carbon nanotube surface has been observed to induce conformational changes in the peptide backbone of certain interacting proteins, to adjust to the radius of curvature of the CNT (Marchesan & Prato 2015). In the case of the hydrophobins such deformation is not likely due to the rigid sulphide bridged structure. However, the hydrophobins were able to assemble at the water-carbon interface and the resulting solutions were very stable. The hydrophobic force exerted by the carbon surface could possibly cause effective distortion, i.e. closer packing, in the hydrophobic side chains, even though large structural rearrangements did not occur based on CD measurements (II).

According to general understanding, the interaction between the carbon nanotube surface and the hydrophobin occurs mainly via hydrophobic interactions of aliphatic residues in the hydrophobic patch and the aromatic carbon surface. However, aromatic rings can also act as acceptors to hydrogen bonds or cationic charge. Cationic charge is present near the hydrophobic patch of HFBI in residues Lys32 and Asp30. Participation of these amino acid residues would require a suitable geometric orientation due to the orientation of the nitrogen orbitals (90° angle; Figure 25). This additional mechanistic detail may be involved in positioning of hydrophobins at aromatic carbon surfaces. If the low curvature of the carbon nanotube hinders intermolecular interactions between hydrophobin monomers, the proteins may be anchored via cation donation of the positively charged groups, explaining thus the regular arrangement of hydrophobins even in the void of optimal binding surface.

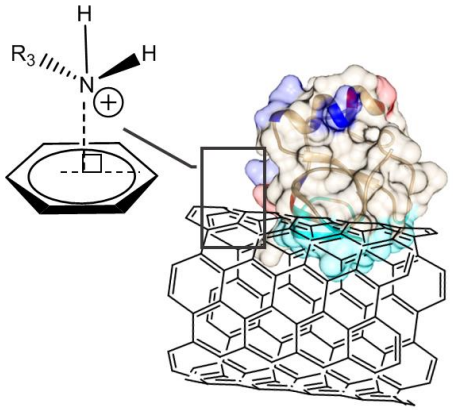


Figure 25. The interaction between hydrophobins and carbon nanotubes is challenged at small nanotube diameters due to high curvature. The positively charged amino acids near the hydrophobic patch may act as cation donors and participate in positioning of the hydrophobins on the carbon.

Hydrophobins show diverse, oligomeric solution structures based on interaction of the hydrophobic patches. Solution structures may be stabilized by additional interactions, such as hydrogen bonds or ionic bonds. It seems however, that the hydrophobic force between the hydrophobic patches of two hydrophobin monomers is rather weak. This would be plausible considering the natural function of the hydrophobins. Experimental methods used to study dynamic solution behavior rely on fluid flow, which exerts cutting forces in the liquid, possibly strong enough to break all but the smallest base units. For hydrophobin this might be the dimer, or tetramer, and observation of larger assemblies fails It is easily understood how the tetramer could form a continuing lamellar structure. The crystal structure of the hydrophobin oligomers shows, that the hydrophobic patches are not exactly aligned, but twisted (Figure 2a), possibly allowing subsequent units to link to the assembly.

The fact that neither the interfacial activity nor the ATPS process is largely disturbed by the connection of fusion partners, would support the fact, that the cross-sectional area of the fusion partner is more important than the whole size of the protein. The driving force for the hydrophobin to self-assemble at interfaces is not lost upon fusion to other proteins. In other words, the effective amphiphilicity of the hydrophobin is not disturbed. Due to the sulphur-bridged inner structure, the hydrophobins are rigid and robust, they do not lose structure. However, this does not mean that the chemical surface of the hydrophobin molecule is inert to ambient conditions. Factors that affect the hydrophobic effect also affect hydrophobin structure and function. This means, that certain changes, such as temperature or salt concentration can cause tighter packing of the hydrophobic parts, whereas hydrophilic parts become more hydrated. Thus, the hydrophobin structure can be effectively distorted.

Geometrical changes in the hydration shell of the amphiphilic hydrophobin protein could play a role in the two-phase separation process in respect to choice of detergent. Accordingly, increased hydrophilicity in the detergent EO chain has been noted to be beneficial for the two-phase separation of the more hydrophilic hydrophobin fusion proteins. These surfactants include more water and physical space around the head groups in the micellar phase. In addition, longer EO chains have more conformational freedom to comply with the extending, curved protein surface.

*In vitro* assays take place in dilute aqueous solutions containing vast volumes of free water. It may be that in such a situation, confinement of water molecules has more pronounced effects. Biomolecules *in vivo* operate in a chemical microenvironment which is largely shaped by electrostatic and hydrophobic interactions with surrounding chemical groups. Although the structure of water is locally disrupted at molecular interfaces, lost hydrogen bonds may be compensated by other interactions with vicinal molecules. Protein aggregation is a consequence of uncontrolled hydrophobic interactions taking over, but also this problem is solved *in vivo* via specific stabilizing molecular interactions.

Macromolecular crowding agents are sometimes used in vitro to mimic in vivo conditions. However, use of polymeric additives may result in unwanted precipitation. Compensating the loss of hydrogen bonds specifically could have the same result in a more controllable manner. It is known, that the cpp value of surfactants (Equation 3) is affected by associated small molecule alcohols, also affecting the geometry (solvation energy) of the micellar assemblies. Similarly, suitable additives or protein stabilizers could be considered to stabilize biomolecular assemblies in vitro.

*Application step*

The application step of hydrophobin fusion design introduces case-sensitive variables to be considered. As has been stated previously, HFBI is an excellent tag for ATPS based processes. Neither the overall hydrophilicity nor the immediate size of the fusion partners evidently prohibit phase partition of the hydrophobin. Development of applications relying on this detergent interaction is thus well grounded. Detergent composition is one of the most important variables in applications utilizing a

two-phase system. The optimal non-ionic detergent should provide aliphatic support for the hydrophobic patches, and at the same time offer sufficient ionic and hydrogen bonds to incorporate the hydrophilic complex. The ATPS systems for hydrophobin fusions could be further enhanced by introducing a pulling force from the detergent phase, for example in the form of mixed micelles or specific interactions to charged amino acid residues. It is also important to ensure that the chosen detergent is tolerated by the fusion partner.

The measured sensitivities of the G-FET sensor demonstrated the suitability of hydrophobin fusions for biofunctionalization in electric devices. The model analytes were selectively measured with high sensitivity. Although the HFBI layer was observed to act as a dielectric in previous experiments, charges could be sensed by the graphene, presumably via holes and cavities in the protein layer. The protein layer is hydrated to some extent, thus allowing mobility of ions to connect the solution environment and graphene surface. Molecular movement near the surface causes displacement of the solution ions and changes in the electrostatic interactions.

The effect of ionic screening by the electric double layer was smaller than was expected. This was assumed to be due to low water confinement and discontinuity of the Debye length (Equation 1) in the biomolecular structures, in accordance with a previous computational study (Stigliano et al. 2013). The phenomenon is closely related to the previously discussed entrapment of water in supramolecular assemblies of amphiphilic molecules (Chandler 2005). Adaptation of hydrophobin fusion technology to environments containing authentic biological samples should be studied further.

Exfoliation and solubilization of carbon nanotubes or graphene by hydrophobin is actually an example of a 3D system composed of a 2D interface. Architectures based on a continuous phase of 2D interfaces ensure the optimal binding interactions of hydrophobins to be employed in 3D systems. In freely associated 3D systems such as the HFBI-ProteinA antibody harvesting method, control over the system is more difficult to achieve. Most importantly, molecule stoichiometry needs to be considered and protein interconnectivity avoided.

The exceptionally large, exposed hydrophobic patch of the hydrophobin HFBI leads to a specific affinity for interfaces. Understanding the mechanisms of hydrophobin function is beneficial for development of hydrophobin fusion technology. However, the detailed mechanism relating the events of surface adsorption and solution behavior are unknown. The design and application of various hydrophobin fusion proteins implied, that certain key factors are associated with molecular behavior. Most importantly, it is the amphiphilic structure, which dictates the final mode of hydrophobin assembly. As a consequence of the interaction of the hydrophobic patches with matching interfaces, critical geometrical restrictions are exerted to the connected fusion partners.

In light of the described energetic and geometrical limitations, it seems plausible, that destabilization of solution multimers of the hydrophobin fusion proteins would lead to an increased concentration of the monomeric form of the fusion protein.

Thus, the fusion protein would actually be more available for adsorption at an available interface. In this view, wild-type hydrophobins and their fusion proteins do not compete equally for interfacial adsorption sites.

Hydrophobin fusion technology shows promise especially in 2D biofunctionalization of interfaces in high-technology applications. To further advance the robustness of the hydrophobin fusion technology, control over surface composition and coverage as well as binding affinity to different solid substrates needs to be mastered. Examination of the design process may help to identify variables, which are significant for the hydrophobin fusion engineering. The findings described in this thesis show, that successful application of hydrophobin fusion technology requires consideration of the final system architecture and molecular environment. Use of more flexible production organisms, smart bioconjugation chemistry, and thorough understanding of related molecular mechanisms and geometrical features at the interface may simplify the design process to create a more functional, iterative practice.

# 5. Conclusions

In conclusion, the work presented in this thesis demonstrates the design and use of protein functionalities for creation of biomolecular assemblies based on self-assembly of class II hydrophobin HFBI. The focus of the research was to evaluate the functionality of the fusion proteins in liquid environment and solid-liquid interfaces in relevant model applications. The results underline the importance of considering protein architecture and stoichiometry in the design process, while also bringing out holistic aspects in the final application stage.

For the hydrophobin to act in its natural function, the affinity of the hydrophobin monomer to interact with another via the hydrophobic patch must be weaker than its affinity for an interface. The solution equilibrium includes exchange of hydrophobin monomers in the oligomeric assemblies, producing solubilized monomers in the process. However, contributions of the hydrophobic effect, i.e., the enthalpic cost of exposing the hydrophobic patch to water, is the same, regardless of the volume of the hydrophilic end. The hydrophilic parts remain in the aqueous environment throughout the process. Thus, the immediate size of the hydrophilic fusion partner does not disturb the functionality of the hydrophobin. However, available configurations of the hydrophilic parts are restricted in the supramolecular assembly. This causes disturbance to the structure of vicinal water molecules, i.e., increases the entropic element of the solvation free energy of the molecular assembly. Accordingly, simultaneous existence of high affinity multimerization and exposure of the hydrophobic patch may result in an unstable, hardly controllable system, as in the case of the HFBI-ProtA antibody complex.

Geometrical issues to consider relate to the fit of the solid substrate and the hydrophobic patch. This effect becomes prominent in nanotechnological applications, but may also affect the outcome of hydrophobin-stabilized liquid based systems. Hydrophobin-derived fusion proteins most applicable at the solid-liquid interface. Introducing a 2D continuous phase in 3D systems may be beneficial for system stability, as well as lessening the multimerization degree of the fusion partner. In conclusion, reflection of interface geometries, solution dynamics and molecule assembly characteristics is necessary throughout the design process. Final application design is a cross-disciplinary effort, which requires understanding throughout the physicochemical fields.

# References


Askolin, S., Nakari-Setälä, T. & Tenkanen, M., 2001. Overproduction, purification, and characterization of the Trichoderma reesei hydrophobin HFBI. *Applied Microbiology and Biotechnology*, 57(1–2), pp.124–130.

Asuri, P. et al., 2006. Water-soluble carbon nanotube-enzyme conjugates as functional biocatalytic formulations. *Biotechnology and Bioengineering*, 95(5), pp.804–811.

Autumn, K. et al., 2002. Evidence for van der Waals adhesion in gecko setae. *Proceedings of the National Academy of Sciences*, 99(19), pp.12252–12256.

Baughman, R.H., Zakhidov, A.A. & de Heer, W.A., 2002. Carbon nanotubes - the route toward applications. *Science*, 297(5582), pp.787–792.

Byrne, B. et al., 2009. Antibody-Based Sensors: Principles, Problems and Potential for Detection of Pathogens and Associated Toxins. *Sensors*, 9(6), pp.4407–4445.

Castro Neto, A.H. et al., 2009. The electronic properties of graphene. *Reviews of Modern Physics*, 81(1), pp.109–162.

Chandler, D., 2005. Interfaces and the driving force of hydrophobic assembly. *Nature*, 437(7059), pp.640–647.

Collén, A. et al., 2002. A novel two-step extraction method with detergent/polymer systems for primary recovery of the fusion protein endoglucanase I–hydrophobin I. *Biochimica et Biophysica Acta (BBA) - General Subjects*, 1569(1–3), pp.139–150.

Collén, A., 2001. *Hydrophobic Fusion Tags. Implications for Bioseparation and Cellular Expression. PhD Thesis.* Lund University, Lund, Sweden.

Deisenhofer, J., 1981. Crystallographic refinement and atomic models of a human Fc fragment and its complex with fragment B of protein A from Staphylococcus aureus at 2.9- and 2.8-.ANG. resolution. *Biochemistry*, 20(9), pp.2361–2370.

Elvin, J.G., Couston, R.G. & van der Walle, C.F., 2013. Therapeutic antibodies: Market considerations, disease targets and bioprocessing. *International Journal of Pharmaceutics*, 440(1), pp.83–98.

Forsgren, A. & Sjöqvist, J., 1966. Forsgren_1966.pdf. *Journal of Immunology*, 97(6), pp.822–827.

Geim, A.K. & Novoselov, K.S., 2007. The rise of graphene. *Nature materials*, 6(3), pp.183–91.

Goddard, E.D., 1989. Surfactants and interfacial phenomena. *Colloids and Surfaces*, 40, p.347.

Green, N.M., 1963. Avidin. *Biochemical Journal*, 89, pp.585–591.

Green, N.M., 1990. Avidin and streptavidin. *Methods in Enzymology*, 184, pp.51–67.

Grunér, M.S. et al., 2012. Self-assembly of Class II Hydrophobins on Polar Surfaces. *Langmuir*, 28(9), pp.4293–4300.

Hakala, T.J. et al., 2012. Adhesion and tribological properties of hydrophobin proteins in aqueous lubrication on stainless steel surfaces. *Rsc Advances*, 2(26), pp.9867–9872.

Hakanpää, J. et al., 2006. Two crystal structures of Trichoderma reesei hydrophobin HFBI--the structure of a protein amphiphile with and without detergent interaction. *Protein science : a publication of the Protein Society*, 15(Ebbole 1997), pp.2129–2140.

Hirsch, A., 2002. Functionalization of single-walled carbon nanotubes. *Angewandte Chemie-International Edition*, 41(11), pp.1853–1859.

Hober, S., Nord, K. & Linhult, M., 2007. Protein A chromatography for antibody purification. *Journal of Chromatography B*, 848(1), pp.40–47.

Holmberg, K. et al., 2002. *Surfactants and Polymers in Aqueous Solution* 2nd ed., West Sussex, England: Wiley Inc.

Hytonen, V.P. et al., 2006. Controlling quaternary structure assembly: Subunit interface engineering and crystal structure of dual chain avidin. *Journal of Molecular Biology*, 359(5), pp.1352–1363.

Iijima, S., 1991. Helical microtubules of graphitic carbon. *Nature*, 354(6348), pp.56–58.

Israelachvili, J., 1991. *Intermolecular & Surface Forces* second., London: Academic Press Inc.

Joensuu, J.J. et al., 2010. Hydrophobin Fusions for High-Level Transient Protein Expression and Purification in Nicotiana benthamiana. *Plant Physiology*, 152(2), pp.622–633.

Khalesi, M., Gebruers, K. & Derdelinckx, G., 2015. Recent Advances in Fungal

Hydrophobin Towards Using in Industry. *The Protein Journal*, 34(4), pp.243–255.

Kisko, K. et al., 2009. Self-Assembled Films of Hydrophobin Proteins HFBI and HFBII Studied in Situ at the Air/Water Interface. *Langmuir*, 25(3), pp.1612–1619.

Kivioja, J.M. et al., 2009. Electrical transport through ordered self-assembled protein monolayer measured by constant force conductive atomic force microscopy. *Applied Physics Letters*, 94(18), pp.1–4.

Krivosheeva, O. et al., 2013. Kinetic and equilibrium aspects of adsorption and desorption of class II hydrophobins HFBI and HFBII at silicon oxynitride/water and air/water interfaces. *Langmuir*, 29(8), pp.2683–2691.

Kuriyan, J., Konforti, B. & Wemmer, D., 2012. *The Molecules of Life* 1st ed., Garland Science.

Laaksonen, P. et al., 2011. Genetic engineering of biomimetic nanocomposites: Diblock proteins, graphene, and nanofibrillated cellulose. *Angewandte Chemie - International Edition*, 50(37), pp.8688–8691.

Laaksonen, P. et al., 2010. Interfacial Engineering by Proteins: Exfoliation and Functionalization of Graphene by Hydrophobins. *Angewandte Chemie-International Edition*, 49(29), pp.4946–4949.

Lee, C. et al., 2008. Measurement of the elastic properties and intrinsic strength of monolayer graphene. *Science*, 321(5887), pp.385–388.

Lienemann, M. et al., 2015. Charge-Based Engineering of Hydrophobin HFBI: Effect on Interfacial Assembly and Interactions. *Biomacromolecules*, 16(4), pp.1283–1292.

Lienemann, M. et al., 2013. Structure-Function Relationships in Hydrophobins: Probing the Role of Charged Side Chains. *Applied and Environmental Microbiology*, 79(18), pp.5533–5538.

Linder, M. et al., 2002. Surface adhesion of fusion proteins containing the hydrophobins HFBI and HFBII from Trichoderma reesei. *Protein science : a publication of the Protein Society*, 11(9), pp.2257–66.

Linder, M. et al., 2001. The hydrophobins HFBI and HFBII from Trichoderma reesei showing efficient interactions with nonionic surfactants in aqueous two-phase systems. *Biomacromolecules*, 2(2), pp.511–517.

Linder, M.B. et al., 2004. Efficient Purification of Recombinant Proteins Using Hydrophobins as Tags in Surfactant-Based Two-Phase Systems.

*Biochemistry*, 43(37), pp.11873–11882.

Linder, M.B., 2009. Hydrophobins: Proteins that self assemble at interfaces. *Current Opinion in Colloid & Interface Science*, 14(5), pp.356–363.

Livnah, O. et al., 1993. Three-dimensional structures of avidin and the avidin-biotin complex. *Proceedings of the National Academy of Sciences*, 90(11), pp.5076–5080.

Loh, K.P. et al., 2010. The chemistry of graphene. *Journal of Materials Chemistry*, 20(12), pp.2277–2289.

Low, D., O'Leary, R. & Pujar, N.S., 2007. Future of antibody purification. *Journal of Chromatography B*, 848(1), pp.48–63.

Lupas, A.N. & Bassler, J., 2016. Coiled Coils – A Model System for the 21st Century. *Trends in Biochemical Sciences*, xx, pp.1–11.

Magarkar, A. et al., 2014. Hydrophobin Film Structure for HFBI and HFBII and Mechanism for Accelerated Film Formation. *PLoS Computational Biology*, 10(7).

Makkar, R.S., Cameotra, S.S. & Banat, I.M., 2011. Advances in utilization of renewable substrates for biosurfactant production. *AMB Express*, 1(1), p.5.

Malho, J.M. et al., 2015. Modular Architecture of Protein Binding Units for Designing Properties of Cellulose Nanomaterials. *Angewandte Chemie - International Edition*, 54(41), pp.12025–12028.

Marchesan, S. & Prato, M., 2015. Under the lens: carbon nanotube and protein interaction at the nanoscale. *Chem. Commun.*, 51(21), pp.4347–4359.

Mayorov, A.S. et al., 2011. Micrometer-Scale Ballistic Transport in Encapsulated Graphene at Room Temperature. *Nano Letters*, 11(6), pp.2396–2399.

McLean, M.D. et al., 2012. Purification of the therapeutic antibody trastuzumab from genetically modified plants using safflower Protein A-oleosin oilbody technology. *Transgenic Research*, 21(6), pp.1291–1301.

Meyer, E.E., Rosenberg, K.J. & Israelachvili, J., 2006. Recent progress in understanding hydrophobic interactions. *Proceedings of the National Academy of Sciences of the United States of America*, 103(43), pp.15739–15746.

Moks, T. et al., 1986. Staphylococcal protein A consists of five IgG-binding domains. *European Journal of Biochemistry*, 156(3), pp.637–643.

Moll, J.R. et al., 2001. Designed heterodimerizing leucine zippers with a range of pIs and stabilities up to 10(-15) M. *Protein Science*, 10(3), pp.649–655.

Monera, O.D., Kay, C.M. & Hodges, R.S., 1994. Electrostatic Interactions Control the Parallel and Antiparallel Orientation of .alpha.-Helical Chains in Two-Stranded .alpha.-Helical Coiled-Coils. *Biochemistry*, 33(13), pp.3862–3871.

Mukherjee, S., Das, P. & Sen, R., 2006. Towards commercial production of microbial surfactants. *Trends in Biotechnology*, 24(11), pp.509–515.

Niemeyer, C.M., 2007. Functional devices from DNA and proteins. *Nano Today*, 2(2), pp.42–52.

Nordlund, H.R. et al., 2004. Construction of a Dual Chain Pseudotetrameric Chicken Avidin by Combining Two Circularly Permuted Avidins. *Journal of Biological Chemistry*, 279(35), pp.36715–36719.

Nordlund, H.R. et al., 2005. Tetravalent single-chain avidin: from subunits to protein domains via circularly permuted avidins. *Biochemical Journal*, 392, pp.485–491.

Novoselov, K., 2007. Graphene: mind the gap. *Nature materials*, 6(10), pp.720–721.

Novoselov, K.S. et al., 2016. 2D materials and van der Waals heterostructures. *Science*, 353(6298), p.461.

Novoselov, K.S. et al., 2012. A roadmap for graphene. *Nature*, 490(7419), pp.192–200.

Novoselov, K.S., 2004. Electric Field Effect in Atomically Thin Carbon Films. *Science*, 306(5696), pp.666–669.

Novoselov, K.S. et al., 2005. Two-dimensional gas of massless Dirac fermions in graphene. *Nature*, 438(7065), pp.197–200.

O'Shea, E. et al., 1989. Preferential heterodimer formation by isolated leucine zippers from fos and jun. *Science*, 245(4918), pp.646–648.

Paananen, A. et al., 2003. Structural hierarchy in molecular films of two class II hydrophobins. *Biochemistry*, 42(18), pp.5253–5258.

Reuter, L.J. et al., 2014. Scale-up of hydrophobin-assisted recombinant protein production in tobacco BY-2 suspension cells. *Plant Biotechnology Journal*, 12(4), pp.402–410.

Riccardi, L. & Mereghetti, P., 2016. Induced Fit in Protein Multimerization : The HFBI

Case. *PLoS Computational Biology*, 12(11), pp.1–20.

Riikonen, J. et al., 2013. Photo-thermal chemical vapor deposition of graphene on copper. *Carbon*, 62, pp.43–50.

Rodahl, M. et al., 1997. Simultaneous frequency and dissipation factor QCM measurements of biomolecular adsorption and cell adhesion. *Faraday Discussions*, 107, pp.229–246.

Schor, M. et al., 2016. The Diverse Structures and Functions of Surfactant Proteins. *Trends in Biochemical Sciences*, 41(7), pp.610–620.

Shukla, A.A. & Thömmes, J., 2010. Recent advances in large-scale production of monoclonal antibodies and related proteins. *Trends in Biotechnology*, 28(5), pp.253–261.

Sjödahl, J., 1977. Structural studies on the four repetitive Fc-binding regions in protein A from Staphylococcus aureus. *European journal of biochemistry / FEBS*, 78(2), pp.471–490.

Stigliano, A.F., Stiglianoa, A.F. & Fernández Stigliano, A., 2013. Breakdown of the Debye polarization ansatz at protein-water interfaces. *Journal of Chemical Physics*, 138(22), p.

Stine, R. et al., 2013. Fabrication, optimization, and use of graphene field effect sensors. *Analytical Chemistry*, 85(2), pp.509–521.

Szilvay, G.R., Nakari-Setälä, T. & Linder, M.B., 2006. Behavior of Trichoderma reesei Hydrophobins in Solution: Interactions, Dynamics, and Multimer Formation. *Biochemistry*, 45(28), pp.8590–8598.

Szilvay, R. et al., 2007. Self-Assembled Hydrophobin Protein Films at the Air - Water Interface: Structural Analysis and Molecular Engineering. *Biochemistry*, 46(1), pp.2345–2354.

Tasis, D. et al., 2006. Chemistry of Carbon Nanotubes. *Chem. Rev.*, (106), pp.1105–1136.

Torkkeli, M. et al., 2002. Aggregation and Self-Assembly of Hydrophobins from Trichoderma reesei: Low-Resolution Structural Models Thioflavin T staining. , 83(October), pp.2240–2247.

Uhlen, M. et al., 1984. Complete sequence of the staphylococcal gene encoding protein A. A gene evolved through multiple duplications. *The Journal of biological chemistry*, 259(3), pp.1695–1702.

Valo, H. et al., 2013. Drug release from nanoparticles embedded in four different

nanofibrillar cellulose aerogels. *European Journal of Pharmaceutical Sciences*, 50(1), pp.69–77.

van der Vegt, W. et al., 1996. A comparison of the surface activity of the fungal hydrophobin SC3p with those of other proteins. *Biophysical Chemistry*, 57(2–3), pp.253–260.

Wang, X.S. et al., 2010. Noncovalently functionalized multi-wall carbon nanotubes in aqueous solution using the hydrophobin HFBI and their electroanalytical application. *Biosensors & bioelectronics*, 26(3), pp.1104–1108.

Wang, Z.F. et al., 2010. Mechanisms of Protein Adhesion on Surface Films of Hydrophobin. *Langmuir*, 26(11), pp.8491–8496.

Wessels, J.G.H., 1994. Developmental Regulation of Fungal Cell-Wall Formation. *Ann. Rev. Phytopathol.*, 32, pp.413–437.

Wösten, H.A.B. & de Vocht, M.L., 2000. Hydrophobins, the fungal coat unravelled. *Biochimica et Biophysica Acta (BBA) - Reviews on Biomembranes*, 1469(2), pp.79–86.

Yang, L., Biswas, M.E. & Chen, P., 2003. Study of binding between protein a and Immunoglobulin G using a surface tension probe. *Biophysical Journal*, 84(1), pp.509–522.

Yang, W.R. et al., 2013. Surface functionalization of carbon nanomaterials by self-assembling hydrophobin proteins. *Biopolymers*, 99(1), pp.84–94.

Young, H. & Freeman, R., 1996. *University Physics* 9th ed., Addison-Wesley Publishing Company, Inc.

Zhang, K., Diehl, M.R. & Tirrell, D.A., 2005. Artificial Polypeptide Scaffold for Protein Immobilization. *Journal of the American Chemical Society*, 127(29), pp.10136–10137.

Zheng, M. et al., 2003. DNA-assisted dispersion and separation of carbon nanotubes. *Nature materials*, 2(5), pp.338–342.

# I

Kurppa, Katri*; Reuter, Lauri*; Ritala, Anneli; Linder, Markus; Joensuu, Jussi. Antibody harvesting with a plant-produced hydrophobin-ProteinA fusion. *Manuscript.*

# ANTIBODY HARVESTING WITH A PLANT-PRODUCED HYDROPHOBIN-PROTEIN A FUSION

Running title: **Antibody capture with HFB-Protein A**

Katri Kurppa[1Δ], Lauri Reuter[1Δ], Anneli Ritala[1], Markus Linder[1,2], Jussi Joensuu[1]*

To be submitted to: *Plant Biotechnology Journal*

[1] VTT Technical Research Institute of Finland Ltd., Tietotie 2, P.O. Box 1000, FI-02044 VTT, Espoo, Finland

[2] Aalto University, Department of Biotechnology and Chemical Technology, Kemistintie 1, FI-00076, Espoo, Finland

*Corresponding author
[Δ] Equal contribution as first authors

Key words**:** antibody, hydrophobin, *Nicotiana benthamiana*, Protein A, purification, tobacco BY-2 suspension cells

Word count: 6776

**Summary**

Purification is a bottleneck and a major cost factor in the production of antibodies. We set out to engineer a bi-functional fusion protein from two building blocks, Protein A and a hydrophobin, aiming at low-cost and scalable antibody capturing in solutions. Immunoglobulin-binding Protein A is widely used in affinity-based purification. The hydrophobin fusion tag, on the other hand, has been shown to enable purification by two-phase separation.

Protein A was fused to two different hydrophobin tags, HFBI or II, and expressed transiently in *Nicotiana benthamiana*. The hydrophobins enhanced accumulation up to 35-fold, yielding up to 25% of total soluble protein. Both fused and non-fused Protein A accumulated in protein bodies. Hence the increased yield could not be attributed to HFB-induced protein body formation. We also demonstrated production of HFBI-Protein A fusion protein in tobacco BY-2 suspension cells in 30 l scale, with a yield of 35 mg/l.

Efficient partitioning to the surfactant phase confirmed that the fusion proteins retained the amphipathic properties of the hydrophobin block. The reversible antibody binding capacity of the Protein A block was found to be similar to that of non-fused Protein A. The best-performing fusion protein was tested in capturing antibodies from plant leaf extract with two phase separation. The fusion protein was able to carry Rituximab antibodies to the surfactant phase and subsequently release them back to the aqueous phase after a change in pH. This report demonstrates the interesting potential of hydrophobin fusion proteins for novel applications, such as harvesting antibodies in solutions.

## Introduction

Antibodies are essential in modern medicine as diagnostic agents and in targeted drug delivery. Being the fastest growing area of the pharmaceutical industry, monoclonal antibodies (mAbs) are estimated to reach a total market size of 125 billion US$ by 2020 (Ecker *et al.,* 2015). MAbs are mainly produced in animal cell cultures, where they are secreted to the culture media. The industrial standard for harvesting mAbs involves an initial Protein A-based affinity chromatography step. Despite their widespread use, chromatographic methods suffer from difficulties in scalability. The system relies on batch operation, and transfer to continuous mode is not possible. It is a multistep, labour-intensive process that represents a major part of the overall production costs. Alternative procedures include two-phase extraction using conventional salt-polymer systems, for example polyethylene glycol (Azevedo *et al.,* 2009). The drawback of these rather simple two-phase systems is often poor reproducibility due to sensitivity to e.g. temperature, contaminants or salt concentration (Collen *et al*., 2002).

Here we describe a novel bi-functional fusion protein, produced in plants, which may enable a novel, low cost and easily scalable strategy for antibody harvesting in solutions. Our approach is inspired by two proteins with specific properties: *Trichoderma reesei* hydrophobins (HFBs) and *Staphylococcus aureus* Protein A.

HFBs are small globular proteins which display extreme surface activity due to their unique amphipathic structure (Linder, 2009; Wessels, 1994; Wosten and Scholtmeijer, 2015). They are found exclusively in filamentous fungi, where they fulfil a broad range of biological functions. Secreted HFBs facilitate penetration of water-air interfaces by decreasing surface tension, and coat the hypha and spores thereby decreasing wettability,

improving dispersion and providing surface adhesion. The versatile biological roles of HFBs have generated a multitude of potential uses in biotechnology, from structure-enhancing food additives to coating of sensors, nanoparticles and medical instruments (Wosten and Scholtmeijer, 2015).

HFBs are grouped into two classes according to their hydropathy plots. In this work, we focus on the class II hydrophobins HFBI and HFBII. HFBs show a distinct structure comprising a hydrophobic patch at one end of the molecule and a hydrophilic surface at the other (Hakanpää *et al.,*2006a; Hakanpää *et al.,* 2006b). Due to this unique structure, the hydrophobins self-assemble at liquid-liquid, liquid-solid or liquid-air interfaces to form monolayers (Linder, 2009; Liner *et al.,* 2002; Szilvay *et al.,*2007). Their amphipathic nature also allows hydrophobins to interact with small molecule surfactants. This property is commonly used in the purification of hydrophobins and hydrophobin fusion proteins by aqueous two-phase separation (ATPS) (Collen *et al.,* 2002; Joensuu *et al.,* 2010; Linder *et al.,* 2001).

Protein A is an antibody-binding protein widely used in affinity chromatography during recent decades. It reversibly binds antibodies of the IgG class (IgG1, IgG2, IgG4, IgG3). Based on the number of binding sites, a Protein A molecule can bind up to five IgG molecules (Uhlen *et al.,* 1984). However, experimental data suggests that the ratio of Protein A to IgG is closer to 1:2 (Yang *et al.,* 2003). In most applications the Protein A is chemically bound to a solid chromatography matrix. The antibodies are released from Protein A by decreasing the pH.

We set out to engineer a fusion protein combining two active blocks, HFB and the immunoglobulin binding domain of Protein A, in the same polypeptide chain. We

expected the novel bi-functional protein to bind mAbs effectively in solution, but also to be separated in a water-surfactant two-phase extraction system. Hence, the fusion protein may be used to capture antibodies from solution and concentrate them to the surfactant phase. The phase separation can be performed in a single vessel, by addition of the antibody-capturing fusion protein and a surfactant. The whole process requires only liquid handling and is therefore easily scalable and avoids the need for complex equipment. A similar two-phase system utilizing the Protein A – IgG interaction was recently reported by McLean *et al.* (2012). Whereas their two-phase system was formed intrinsically by an oleosin-tag fused to the Protein A moiety, we chose a strategy utilizing external two-phase systems based on non-ionic surfactant to allow case-sensitive optimization of purification conditions in a more flexible manner. Moreover, the hydrophobin-tag unit can be cleaved or modified without sacrificing surface-active functionality. Bound antibodies can also be guided to chosen liquid-solid interfaces via hydrophobin self-assembly.

HFB-fusion proteins have been produced in filamentous fungi (Linder *et al.,* 2004; Mustalahti *et al*., 2013), insect cell cultures (Lahtinen *et al*., 2008), plants (Gutiérrez *et al*., 2013; Jacquet *et al.,* 2014; Joensuu *et al*., 2010; Phan *et al*., 2014; Pereira *et al*., 2014; Saberianfar *et al*., 2015) and in plant cell cultures (Reuter *et al*., 2014). Whereas production of HFB-fusion proteins has been challenging in some other hosts, plants have shown to be an especially suitable production platform. The HFB-fusion strategy has, in some cases, significantly enhanced accumulation of the recombinant proteins (Joensuu *et al.,* 2010; Jacquet *et al.,* 2014). This effect has been attributed to HFB-induced formation of protein bodies in the host cells (Conley *et al.,* 2011; Joensuu *et al.,* 2010). In plants the fusion proteins are not only accumulated in high yields, but are also correctly folded. In

addition, plants contain very few native proteins that would be co-purified in ATPS lowering the product purity (Joensuu *et al.,* 2010; Reuter *et al.,* 2014). Furthermore, field grown transgenic plants may provide an ideal low-cost production platform for commodity proteins aimed at biotechnological applications outside the pharma industry (Fischer *et al.,* 2013). However, contained production might be necessary for some applications, and regulatory issues may apply. Both transient expression systems and plant cell cultures may be contained and provide adherence to cGMP requirements (Fischer *et al.,* 2012; Ritala *et al.,* 2014). Considering the downstream processing, suspension cell cultures may provide better overall cost efficiency.

Our goal in this study was to demonstrate a proof of principle for in-solution antibody harvesting using a novel bi-functional fusion protein. We also evaluated production of the fusion proteins both in *Nicotiana benthamiana* plants and in tobacco BY-2 suspension cells.

**Results**

*Screening for a hydrophobin fusion strategy*

We used agro-infiltrated *Nicotiana benthamiana* plants to screen for the best hydrophobin fusion strategy. Protein A was constructed in the same polypeptide chain with HFBI or HFBII in both N- and C-terminal orientations (Figure 1a and Figure S1).The yield of both N- and C-terminal HFBI fusions reached 1.7±0.3 and 1.3±0.5 mg/g of fresh leaf material (mean±SE, n=6) (Figure 1b). The HFBII-Protein A accumulated better than the HFBI fusions, 2.4±0.6 mg/g fresh leaf material or 24.3±6.9% of TSP. This represented an approximately 35-fold increase in yield in comparison to non-fused Protein A. However, the yield of Protein A-HFBII remained on a similar level to that of the non-fused Protein

A. Due to consistent expression levels, we used only the N-terminal fusions, HFBI-Protein A and HFBII-Protein A, in further experiments.

*Subcellular localization*

We studied the subcellular localization of the ER-targeted recombinant proteins by immunofluorescent microscopy of protoplasts prepared from agro-infiltrated *N. benthamiana* leaves (Figure 2). GFP-HFBI fusion protein, which is known to accumulate in protein bodies (Joensuu *et al.,* 2010) served as a positive control. The GFP-HFBI-induced protein bodies were visible both in intact leafs (not shown) and in the fixed protoplasts (Figure 2). The protein bodies were visualized equally well by the GFP as by the signal derived from the fluorescent probe binding to c-Myc tag. Protein A, both fused and non-fused, aggregated similarly into protein body-like structures. We observed no apparent difference between the constructs. However, the bodies were less abundant and slightly more scattered than the GFP-HFBI induced protein bodies.

*Aqueous two-phase separation*

Next, we examined the amphipathic properties of the HFB blocks by performing ATPS using two fusion constructs, HFBI-Protein A and HFBII-Protein A (Figure 3). The partition coefficient ($k$) describes the ratio of the protein concentration between surfactant phase and residue. Both HFBI-Protein A and HFBII-Protein A displayed regular hydrophobin-like partitioning in the two-phase system resulting in $k$-values of 4.8±0.9 and 2.4±0.6, respectively (mean±SD, n=3), whereas the non-fused Protein A did not partition into the surfactant ($k$=0.4±0.1). The overall recovery rate of HFBI-Protein A (62±5%) was significantly better than that of HFBII-Protein A (47±4%) or non-fused Protein A (25±1%). Volumes of the phases are given in Figure S2.

*Antibody binding capacity of the hydrophobin-Protein A fusion proteins*

Having confirmed that the fusion proteins could be separated in ATPS, we set out to study the antibody binding capacity of the Protein A block. Antibody binding was measured using a quartz crystal microbalance with dissipation monitoring (QCM-D). The QCM-D technique measures the change in oscillation frequency as a substance is bound to the surface of a quartz crystal oscillating at its resonance frequency. The frequency change is related to the mass of the bound thin layer via the Sauerbrey equation (Höök *et al.,* 2001). The surface-bound layer dampens the oscillation frequency of the freely oscillating crystal. This effect is described by the dissipation factor and depicts the structure of the bound layer. Commercially available Protein A (Sigma Aldrich, USA) served as a reference for HFBI-Protein A and HFBII-Protein A. All three proteins formed reproducible and stable thin layers on the polystyrene surface (Figure 4b, bottom bars). In order to evaluate the IgG binding capacity of the fusion proteins, a solution of the Rituximab antibody was applied to the protein layers. Addition of the antibody resulted in a mass increase that was similar in the case of all three proteins (Figure 4b, top bars). The molar ratios of Rituximab bound to the immobilized fusion proteins were estimated on the basis of the Sauerbrey masses obtained from the QCM-D data. One mole of immobilized HFBI-Protein A bound 1.5±0.3 (mean ± SD, n=3) moles of Rituximab. The corresponding figure for HFBII-Protein A was slightly lower, 1.2±0.5. The molar ratio of the commercial Protein A to Rituximab was 1.2±0.3. No specific antibody binding was observed on layers of non-fused HFBI (data not shown) or BSA (Figure S3). The results confirmed that both fusion proteins retained the immunoglobulin-binding capacity of the Protein A block.

In order to demonstrate the release of antibodies and regeneration of the antibody-binding layer, we performed two successive rounds of IgG binding and release using commercial IgG λ antibodies. Release of the bound IgG λ from the HFBI-Protein A and HFBII-Protein A layers was accomplished by decreasing the pH by rinsing the layer with acidic buffer (Figure 4a). When glycine buffer at pH 2.2 was introduced to the surface-bound HFB-Protein A/IgG λ complex, the mass decreased instantly. The released mass corresponded to the amount of antibody initially bound. After elevating the pH to 8 the layer was capable of re-binding the IgG λ without a significant decrease with respect to the initial amount. We also noted that the HFB-Protein A layers remained stable and capable of binding IgG λ after overnight incubation in buffer (data not shown).

*Antibody capture from plant leaf extract with hydrophobin-Protein A fusion protein*

After confirming the bi-functionality of the fusion proteins, the IgG binding capacity of the Protein A block and the amphipathic properties of the HFB block, we proceeded to demonstrate the principle of antibody capture in ATPS (Figure 5a). In this experiment we used only HFBI-Protein A, as it outperformed HFBII-Protein A in the initial ATPS and IgG binding experiments. We spiked *N. benthamiana* leaf extract with Rituximab IgG and HFBI-Protein A, either separately or both together. After establishing a two-phase system, the residual aqueous phase was removed and acidic buffer added to release the antibodies from the Protein A block and the surfactant phase.

Most of native plant proteins remained in the aqueous residue phase (figure 5 b, lane 2) and only little background was observed in surfactant phase (lane 3). The acidic buffer (lane 4) contains purified antibody. With HFBI-Protein A 28±1% (mean±SD, n=3) of the

antibody was recovered while the recovery rate without the fusion protein was significantly lower, 12±2%. Volumes of the phases are given in Table S1.

Binding to IgG had no effect to the separation of the HFBI-Protein A into the surfactant phase: there was no significant difference in recovery rates in presence or absence of the antibody (figure 5 c). Recovery of the fusion protein after release of the antibody and second ATPS was poor, only a fifth of the initial amount (figure 5c). This could be partly due to degradation in acidic conditions as shown on the SDS-PAGE (figure 5b, lane 5).

*Contained protein production in BY-2 suspension cells*

Having established the good expression levels in *N. benthamiana* and demonstrated the functionality of the HFBI-Protein A, we decided to evaluate the possibility to produce the fusion proteins in transgenic BY-2 cells. After preliminary screening of callus lines, protein accumulation was quantified for the 10 best clones expressing Protein A, HFBI-Protein A and HFBII-Protein A (Figure 6). Non-fused Protein A yielded on average approximately 2 µg/g of fresh callus, whereas both HFBI and HFBII fusions boosted the average accumulation approximately tenfold to 20 to 30 µg/g fresh callus (Figures 6a and b). It should be noted however, that the accumulation levels between the best 10 clones of each line showed considerable variation (Figure 6c). This is most probably due to random insertion sites in the genome and effect of the location to the transcriptional activity.

Based on favourable growth characteristics and homogeneity of the callus,we selected a clone expressing HFBI-Protein A to be grown in suspension culture in shake flasks and subsequently in a stirred tank bioreactor in 30 l scale. The accumulation of biomass (dry weight) in the bioreactor was comparable to that in shake flasks (Figure 7a). The yield of

HFBI-Protein A reached 30±6 mg/l (mean±SD, n=3) and 36±3 mg/l in shake flasks and bioreactor, respectively (Figure 7c). In order to establish a streamlined downstream process suitable for large scale production, the whole culture suspension was homogenized in a high pressure homogenizer and clarified by centrifugation. The clarified extract was directly applied to two phase separation with 2% surfactant, resulting in partially purified protein extract with HFBI-Protein A concentrated to 44±2 mg/l with recovery rate of 49±10% (mean±SD, n=3). Thus the total yield after first purification was approximately 18 mg HFBI-Protein per litre of culture volume.

**Discussion**

Monoclonal antibodies have a key role in modern medicine, research and diagnostics. In many cases however, the high costs of production are limiting their use. The production cost becomes an issue especially now as the first generic antibody drugs are entering the market. Harvesting and initial purification of antibodies using chromatographic methods poses a major bottle-neck and represents a large part of the overall production cost (Farid, 2007; Raven *et al.*, 2015). The aim of this study was to show that the use of a HFB tag can be broadened to include not only purification of fusion proteins themselves, but also of non-covalently bound target molecules, such as antibodies. We constructed a bi-functional fusion protein from two blocks: Protein A and either HFBI or HFBII. The fusion proteins were produced in *Nicotiana benthamiana* plants and in BY-2 suspension cells. The best performing fusion protein was finally tested for capturing Rituximab antibodies from solution.

HFB-fused Protein A reached excellent yields in *N. benthamiana.* Both N-terminal HFB fusion-tags improved accumulation in comparison to non-fused Protein A up to 35 fold. We observed the same trend later in BY-2 calli, although the accumulation levels varied

between the clones. HFBI fused to either the N- or C-terminus of the Protein A improved the accumulation to similar levels in *N. benthamiana*. HFBII, however, enhanced the accumulation of Protein A only as an N-terminal fusion, whereas the C-terminal fusion accumulated to levels similar to those observed with non-fused Protein A. The N-terminus of the HFBII, before the first disulphide bridge, is four amino acids shorter than that of HFBI (Sunde *et al.,* 2008). This may cause a steric hindrance for correct folding of the Protein A-HFBII and thus limit its accumulation. The HFBI fusion has previously been reported to enhance the accumulation of some fusion proteins in plants (Gutiérrez *et al.,* 2013; Jacquet *et al.,* 2014; Joensuu *et al.,* 2010). However, this effect has not been consistent and several studies have shown no improvement in yields (Pereira *et al.,* 2014; Phan *et al.,* 2014). This is the first report on improved product accumulation in BY-2 cells using a HFB tag.

The yield-enhancing effect of HFB fusion tags has been attributed to the formation of protein bodies (Conley *et al.,* 2011; Joensuu *et al.,* 2010). We examined the sub-cellular localization of the fusion proteins by immunofluorescent confocal microscopy of protoplasts prepared from agro-infiltrated *N. benthamiana* leaves. Interestingly, we found that all Protein A constructs accumulated in protein body-like structures, regardless of the HFB fusion. When compared to GFP-HFBI-induced protein bodies, the Protein A induced bodies appeared to be less abundant, but were similar in size. We observed no apparent differences in localization of fused or non-fused Protein A. Previous reports have suggested that protein bodies would form independently of the presence of HFBs when the recombinant proteins accumulate in levels higher than 0.2% of TSP (Gutiérrez *et al.,* 2013; Saberianfar *et al.,* 2015). In our experiments the yields of all recombinant proteins exceeded that threshold. Thus the results here support the conclusions of the previous

studies that formation of protein body-like structures may indeed be largely a concentration-dependent phenomenon. However, in our experiment even the ca. 20-fold difference in accumulation levels of fused and non-fused Protein A did not result in apparent differences in number or size of the protein bodies. Therefore the formation of protein bodies alone may not be the only reason for increased accumulation. This challenges the previous assumption and leaves open the question of other possible yield-increasing mechanisms of the HFB fusion. However, this question was outside the scope of this study.

In the future, transgenic plants grown in the field may provide an ideal low-cost production platform for HFBI-Protein A and other commodity proteins. However, contained production might be a necessity for some applications, especially in the case of pharmaceutical targets (Fischer *et al.,* 2012; Ritala *et al.,* 2014). In comparison to *N. benthamiana*-based transient production systems, plant suspension cells may prove to be a useful alternative. As demonstrated here and in previous studies, BY-2 cell lines can be propagated in conventional industrial scale bioreactors and the downstream processing is readily scalable (Raven *et al.,* 2015; Reuter *et al.,* 2014). Low productivity is nevertheless an issue. Yields in plant cell cultures typically vary from 0.005 to 200 mg/l and a yield in range of 10 mg/l is generally considered satisfactory for starting commercial product development (Hellwig *et al.,* 2004). Thus the intrinsic productivity of the suspension culture here was on a good level (36 mg/l). Nevertheless, an approximate calculation indicates that the 30 litre culture volume correlated in yield to only ca. 40 *N. benthamiana* plants. However, it should be noted that the yield of HFBI-Protein A in transient expression was very high, whereas the potential to increase productivity of the BY-2 suspension culture remains vast. We have previously reported tenfold increase in

productivity with a stable model protein GFP-HFBI in BY-2 suspension cells (Reuter *et al.,* 2014). Several means for improving the productivity of BY-2 suspension cells have been published recently, including improved culture media (Holland *et al.,* 2010), FACS-based clone screening (Kirchhoff *et al.,* 2012), protease knockout lines (Mandal *et al.,* 2014) and development of culture systems (Raven *et al.,* 2015). However, improving the yield in the BY-2 suspension cells was not the aim of this study.

We expected the fusion proteins to exhibit two functions. First, they should demonstrate the amphipathic properties of hydrophobins and be efficiently separated into a surfactant phase from aqueous solution. Second, they should reversibly bind immunoglobulins. The initial ATPS experiment showed that both HFBI-Protein A and HFBII-Protein A partitioned well to surfactant phase. The HFBI-Protein A, however, partitioned slightly better than HFBII-Protein A (Figure 3).In order to examine the antibody binding capacity of the fusion proteins, we used a quartz crystal microbalance with dissipation monitoring (QCM-D). Both fusion proteins bound IgG with similar efficiency to that of commercial Protein A. According to the literature, the wild type Protein A could theoretically bind to five immunoglobulins (Uhlen *et al.,* 1984), but the experimental data, as well as information from chemical providers, suggest that the real rate is close to 1:2. Although this potential rate was not reached in this experiment, we conclude that the HFB block does not hinder the antibody binding capacity of the fusion proteins. The fusion proteins also retained the capability of Protein A to repeated rounds of antibody binding and release by adjusting the pH. Thus the fusion protein could be potentially re-used in a recyclable system, thus lowering the purification costs.

Having separately confirmed the two functions of the fusion protein, we put the HFBI-Protein A to a final test to see whether it could be used to harvest antibodies from plant

leaf extract. The ATPS experiments demonstrated that the antibody was bound by the Protein A block and carried to the surfactant phase by the HFB block of the fusion protein. Furthermore, the antibody could be recovered back to the aqueous phase by decreasing the pH. This would enable recycling of the HFBI-Protein A for another round of harvesting, if issues with degradation and low recovery can be solved. Use of other variants of Protein A may allow milder elution conditions and better stability in comparison to the wild type protein used here (Pabst, *et al.,* 2014). The recovery rate of the antibody was clearly lower than would have been expected on the basis of separation of HFB-Protein A alone. The vastly larger size and relatively hydrophilic nature of the HFBI-Protein A/IgG complex in comparison to the smaller and sufficiently amphipathic fusion protein alone may have hindered the separation of the complex. However, the presence of the IgG did not influence the recovery of HFB-Protein A. This suggests that it is the formation of the complex, or the binding of Protein A block to the antibody, rather than the separation efficiency of the fusion protein that limits the recovery rate of IgG. Binding of the fusion protein to the IgG could also have been hindered by multimerization of the fusion protein due to self-assembly tendency of the HFB block (Linder *et al.,* 2002). Further work to improve the affinity of the fusion protein and the purification conditions is ongoing.

A fraction of the antibody (12%) was recovered from the ATPS also without HFBI-Protein A. Some of the antibody may have migrated to the surfactant phase due non-specific hydrophobic interactions with the surfactant or passive distribution between the phases. Similarly the antibody may have migrated back to the acidic buffer. Nevertheless, the difference to recovery rate using HFB-Protein A was sufficient for proof of concept.

Whereas the experiments yielded merely a qualitative demonstration of the phenomenon, further optimization of the process could result in a feasible, recyclable antibody purification system. Options for tuning and optimization of the system are versatile with respect to choice of surfactant, additives and buffer composition.

This report makes a case for novel applications of HFBs beyond their use as a fusion tag simply to aid production and purification of recombinant proteins. The bi-functional fusion protein, inspired by the unique properties of the HFBs, may open novel applications for antibody harvesting and purification. However, the applications are not limited to that. Recently the surface active and self-assembling properties of HFBs and HFB-fusion proteins have been utilized for example in functional coatings of nanoparticles (Sarparanta *et al.,* 2012) and surfaces (Kurppa *et al.,* 2014). With the emerging interest in material technology, HFBs can be seen as very interesting building blocks for a host of novel fusion proteins.

**Experimental procedures**

*Construct design*

A codon optimized coding sequence for the immunoglobulin binding domain (amino acids 27-325) of *Staphylococcus aureus* Protein A (accession 1314205A) was synthesised at Genscript (USA). Four potential N-glycosylation sites were removed (N to Q) (Figure S1). The coding sequence was connected to *HFBI* (accession XM_006964119.1) or *HFBII* (accession P79073) of *Trichoderma reesei* by a $(GGGS)_3$ linker as described in Figure 1. The sequence for HFBII was codon optimized. The constructs were assembled and placed in a plant binary expression vector pCaMterX (Harris and Gleddie. 2001) under the control of the dual-enhancer cauliflower mosaic virus 35S promoter (Kay *et al.,*

1987), tcup translational enhancer (Wu *et al*., 2001) and the soybean (*Glycine max*) vspB (Mason *et al.,* 1988) terminator using Golden Gate cloning (Engler *et al.,* 2009). The vector incorporates a c-Myc-tag and a signal sequence for secretory pathway (Prb1) in the N-terminus and StrepII-tag and ER-retention signal (KDEL) in the C-terminus of the open reading frame. See Figure S1 for complete nucleotide sequence. The expression vectors were transformed into *Agrobacterium tumefaciens* strain EHA105 (Hood *et al.,* 1993).

*Transient expression in Nicotiana benthamiana plants, tissue sampling and protein extraction*

*A. tumefaciens* cultures were grown in liquid LB-media overnight. The optical density at 600 nm was adjusted to 0.8 with infiltration buffer (1mM MES, 1mM $MgSO_4$). The suspension was mixed with (ratio 2:1) a suspension of *Agrobacterium* carrying an expression vector for p19 (Silhavy *et al.,* 2002). Leaves from six different 5 to 6 weeks old *N. benthamiana* plants were infiltrated using a syringe and sampled six days post infiltration (dpi) by collecting four leaf discs (Ø 7.1 mm) for each construct.

The leaf discs were stored frozen at -80 C and homogenized using a Retsch mill (MM301, Haan, Germany). Ice-cold extraction buffer (phosphate buffered saline, PBS;137 mM NaCl, 2.7 mM KCl, 8.1 mM Na2HPO4, 1.8 mM KH2PO4 , 2 % sodium ascorbate, 1 mM EDTA, 1 mM PMSF, 1.25 ug/ml leupeptin pH 7.4) was added (300 ul) and the leaf powder was mixed to a slurry. The protein extract was clarified by centrifugation at 16 873 **g** for 2x5 min at +4 ºC; Eppendorf 5418R, Germany). The replicates were either analysed separately to obtain data for statistical analysis or pooled together to show representative sample on SDS-PAGE and western blot.

*Protoplast preparation and imaging*

Agro-infiltrated leaves (6 dpi) were cut into thin strips and digested in enzyme solution (1.5% cellulaseR10 (Serva Germany), 0.4% macerozymeR10 (Serva, Germany), 0.4 M mannitol, 20 mM KCl, 20 mM MES (pH 5.7), 10 mM $CaCl_2$, 5 mM β-mercaptoethanol) in the dark at RT overnight. Protoplasts were sieved through a 100 µm mesh and centrifuged for 10 min at 60 **g** at 4 $^{o}$C (Eppendorf 5810R). After washing twice with WI buffer (0.5 M mannitol, 4 mM MES (pH 5.7), 20 mM KCl), the protoplasts were fixed in 4% paraformaldehyde (Sigma-Aldrich, USA) in WI for 1 hour at RT. The membranes were permeated by incubation in 3% IGEPAL CA-630 (Sigma-Aldrich) and 10% DMSO (Merck, Germany) in PBS for 5 min at RT. Non-specific binding was blocked by incubation in 2% BSA (Sigma-Aldrich) in PBS for 1 hour at RT. Primary antibody against the c-Myc tag (mouse, A00864, GenScript, USA) was applied in PBS (1:100) and incubated at 4 $^{o}$C overnight. Secondary antibody, conjugated with Alexafluor®555 (goat anti mouse, A21422, Life Technologies, USA), was applied in PBS (1:100) and incubated for 2 hours at 38 $^{o}$C. Between each step the protoplasts were washed 3x with PBS.

Z-stack images were acquired with a Zeiss LSM 710 laser scanning confocal microscope (Carl Zeiss, Germany) equipped with a 63X water immersion objective. Excitation with a 488-nm agron laser was used for GFP and fluorescence was detected at 495-550 nm. Alexafluor®555 was excited with a 543-nm HeNe laser and fluorescence was detected at 550-630 nm.

*ATPS and protein purification*

Proteins were extracted for purification by homogenizing snap-frozen agro-infiltrated leaves in cold extraction buffer (4x buffer volume/leaf weight). The homogenate was

clarified by centrifugation (10 min at 3220 **g** at 4 $^{o}$C; Eppendorf 5810R). To precipitate host cell proteins, particularly Rubisco, the supernatant was set up on magnetic stirrer plate and the pH was adjusted to 4.8 by adding HCl. After two minutes the supernatant was tittered back to pH 7.2 with NaOH and clarified with a second centrifugation step. For the ATPS, the supernatant was warmed to 24$^{o}$C and mixed with Triton X-114 (6% w/v, Sigma Aldrich, USA). After mixing the phases were allowed to separate in a separation funnel. The lower (detergent-rich) phase was collected and washed with isobutanol (Sigma Aldrich, USA; 10-fold volume with respect to detergent mass). The aqueous phase was collected and the buffer was changed to 100 mM Tris-HCl, 150 mM NaCl and 1 mM EDTA (pH 8.0) with 10DG gel filtration columns (Biorad, USA). Finally the extract was purified by affinity chromatography using a Streptactin macroprep column according to the manufacturers' protocol (IBA, Germany)

*Transformation and maintenance of BY-2 cell cultures*

Transformation of the BY-2 cells was performed as described earlier (De Sutter *et al.,* 2005). After two passages on selective media, 48 two weeks old calli were screened for product accumulation. Ten lines were selected for further experiments. After 3 weeks the lines were sampled again for quantitative analysis. The lines were further maintained by sub-culturing at 3 week intervals on modified MS media (Nagata and Kumagai, 1999) supplemented with 50 ppm kanamycin. Three lines with good expression levels of HFBI-Protein A were grown in suspension cultures of which one was selected for scaling-up according to product accumulation and growth characteristics. Suspension cultures were maintained in liquid modified MS media supplemented with 50 ppm kanamycin and sub-cultured weekly.

*Bioreactor cultivation*

Bioreactor (New Brunswick Scientific IF 40) cultivation was conducted in a total culture volume of 30 l in batch mode by inoculating at 5% (v/v) with a 7 days old suspension from shake flask cultures. The medium, without antibiotics, was prepared and sterilized in the bioreactor. Cultivation was carried out at 28ºC. Dissolved oxygen (DO) was controlled by stirring speed, airflow and vessel overpressure to maintain DO concentration above 20%. The pH was monitored, but not controlled. As a control, the same line was propagated in 50 ml volume in shake flasks.

The fresh weight was determined by sampling 10.0 ml of culture suspension in a conical tube and weighing the cell pellet after centrifugation for 10 min at 3220 **g** (Eppendorf 5810R). The pellet was freeze dried to obtain dry weight.

*Protein extraction from BY-2*

Callus samples were stored at -20 ºC. For protein extraction ice-cold buffer (PBS, 1mM EDTA) was added 1:2 v/w to callus samples thawed on ice and subsequently homogenized using the Retsch mill. For protein extraction from freeze dried cell material from suspension cultures, extraction buffer was added to powdered cell material (40:1 v/w) and homogenized using the Retsch mill. The protein extracts were clarified by centrifugation for 10 min at 21130 **g** at 4 ºC (Eppendorf 5424R).

For the scaled up downstream process 10x extraction buffer (10x PBS, 10mM EDTA) was added 1:10 to cooled (+4ºC) cell suspension. The broth was homogenized in a high pressure homogenizer (Rannie LAB 12.15 H, Maskinfabriken Rannie A/S, Denmark) two times at 500 to 600 bar and clarified by centrifugation in 2 litre bottles (Sorvall

RC12BP, *ca*. 4000 **g**, 15 min, RT). The ATPS was done in a 20 l glass vessel with 2 % w/v Triton X-114.

*Protein Analysis*

Concentration of TSP was measured using the Bradford analysis (1976) with Bio-Rad reagent (Bio-Rad, USA). Protein separation was performed by SDS-PAGE on Bio-Rad Criterion-TGX and Mini-PROTEAN precast gels and stained using GelCode® Blue Stain Reagent (Thermo Scientific, USA). Protein quantifications were performed either from SDS-PAGE or by western blot analysis after transferring proteins on nitrocellulose membrane using the Trans-Blot® Turbo™ system (Biorad, USA). Proteins were visualized with anti-c-Myc tag primary antibody (rabbit, A00172, GeneScript) and a secondary antibody for detection (anti-rabbit-AP, 170-6518, BioRad) For quantification (Figure 1d) and work in BY-2 a fluorescently labelled secondary antibody (goat anti-rabbit, IR Dye® 680RD, LI-COR Biosciences, Germany) was used. Detection was done with Odyssey CLX densitometer (LI-COR Biosciences, Germany) and Image Studio 2.1 software. Protein quantities were assessed against known concentrations of purified HFBI-Protein A or commercial Rituximab (Oriola, Finland).

*QCM-D*

Protein adsorption was measured by QCM-D (E4 Biolin Scientific). Polystyrene crystals (Biolin Scientific) were cleaned according to supplier's protocol. Protein solutions were diluted in buffer M (0.1 M sodium phosphate, pH 7) and pumped for 5 min. Adsorbed surfaces were stabilized 45-60 min and rinsed with buffer M.

Protein samples were diluted as follows: HFB-Protein A 2 µM, IgG1 λ antibodies 0.05 mg/ml, 0.3 µM (Sigma Aldrich, USA). In Figure 4 a 1/3 molar equivalents of wild type

HFBI was used together with HFBI-Protein A to enhance surface packing. Antibodies were released by rinsing with glycine-HCl buffer (pH 2.2) for 5 min, followed by buffer M (pH 8).

Three replicate binding experiments were conducted (Fig. 4b). HFBI-Protein A, HFBII-Protein A and commercial Protein A (Sigma Aldrich, USA) were diluted to 0.1 mg/ml (ca. 2 μM). Rituximab IgG was added (82 nM, 0.01 mg/ml) to the adsorbed protein surfaces for 5-7 min. The values for bound mass were obtained at the buffer rinsing steps by averaging the data over 100 time points (260 s). The bound mass Δm was calculated using the Sauerbrey equation $\Delta m = -C \cdot \Delta f / n_5$, where C = 17.7 $ngHz^{-1}cm^{-2}$ for a 5 MHz quartz crystal and $n_3 = 3$, the overtone number. Dissipation values were used to examine the viscoelastic properties of the protein layers. D-values are given by $D = E_{lost}/2\pi \cdot E_{stored}$. Molar ratios were calculated using the Saurbrey mass values and molecular weights of 44 kDa (HFBI-Protein A and HFBII-Protein A) and 50 kDa (commercial Protein A).

*Antibody capture by two-phase extraction*

HFBI-Protein A (0.1 mg/ml) and Rituximab (0.2 mg/ml) were mixed with *N. benthamiana* leaf extract, incubated at RT for 45min and mixed with Triton X-114 (4% w/v). The total volume was 1.8 ml. Phases were allowed to separate at RT for 2 h and centrifuged at 16 873 **g** for 2 min (Eppendorf 5418R, Germany). The residue phase was removed. 1x volume acidic buffer (0.1M glycine-HCl, pH 2.3) was mixed into the surfactant phase and incubated for 5 min. After 2 min centrifugation at 16 873 **g** (Eppendorf 5418R) the aqueous top phase (containing the released antibodies) was recovered and neutralized by adding 70μl 1M Tris-HCl (pH 8.5). Prior to the analysis on

SDS-PAGE gels the phases containing surfactant were extracted with isobutanol and centrifuged.

*Statistical analysis*

The data was analysed

Statistical analyses were done with SPSS Statistic 22.0 (IBM, Armonk, NY) using Two-tailed Student's independent samples T test for two samples and one way ANOVA test followed by Tukey HSD for three or more samples, with significance level of 95%.

**Acknowledgements**

We thank the Academy of Finland, Centres of Excellence Programme (2014-2019) and Grant 252442 for the support. Also the support from Eurostars project E!5320 is acknowledged. We thank Tuuli Teikari, Juha Tähtiharju, Riitta Suihkonen and Karita Viita-aho for assistance with protein production and purification.

**References**

Azevedo, A.M., Rosa, P.A.J., Ferreira, I.F. and Aires-Barros, M.R. (2009) Chromatography-free recovery of biopharmaceuticals through aqueous two-phase processing. *Trends in Biotechnology,* **27**, 240-247.

Bradford, M.M. (1976) A rapid and sensitive method for the quantitation of microgram quantities of protein utilizing the principle of protein-dye binding. *Anal. Biochem.,* **72**, 248-254.

Collén, A., Persson, J., Linder, M., Nakari-Setälä, T., Penttilä, M., Tjerneld, F., Sivars, U. (2002) A novel two-step extraction method with detergent/polymer systems for primary recovery of the fusion protein endoglucanase I–hydrophobin I. *Biochimica et Biophysica Acta*, **1569**, 139-150

Conley, A.J., Joensuu, J.J., Richman, A. and Menassa, R. (2011) Protein body-inducing fusions for high-level production and purification of recombinant proteins in plants. *Plant Biotechnology Journal,* **9**, 419-433.

De Sutter, V., Vanderhaeghen, R., Tilleman, S., Lammertyn, F., Vanhoutte, I., Karimi, M., Inzé, D., Goossens, A. and Hilson, P. (2005) Exploration of jasmonate signalling via automated and standardized transient expression assays in tobacco cells. *Plant Journal,* **44**, 1065-1076.

Ecker, D.M., Jones, S.D. and Levine, H.L. (2015) The therapeutic monoclonal antibody market. *mAbs,* **7**, 9-14.

Engler, C., Gruetzner, R., Kandzia, R. and Marillonnet, S. (2009) Golden gate shuffling: A one-pot DNA shuffling method based on type ils restriction enzymes. *PLoS ONE,* **4**.

Farid, S. (2007) Process economics of industrial monoclonal antibody manufacture. *Joural of Chromatography B,* **848**, 8-18

Fischer, R., Schillberg, S., Buyel, J.F. and Twyman, R.M. (2013) Commercial aspects of pharmaceutical protein production in plants. *Curr. Pharm. Des.,* **19**, 5471-5477.

Fischer, R., Schillberg, S., Hellwig, S., Twyman, R.M. and Drossard, J. (2012) GMP issues for recombinant plant-derived pharmaceutical proteins. *Biotechnol. Adv.,* **30**, 434-439.

Gutiérrez, S.P., Saberianfar, R., Kohalmi, S.E. and Menassa, R. (2013) Protein body formation in stable transgenic tobacco expressing elastin-like polypeptide and hydrophobin fusion proteins. *BMC Biotechnology,* **13**.

Hakanpää, J., Linder, M., Popov, A., Schmidt, A., Rouvinen, J. (2006a) Hydrophobin HFBII in detail: ultrahigh-resolution structure at 0.75Å. *Acta Cryst,* **62**, 356-367

Hakanpää, J., Szilvay, G.R., Kaljunen, H., Maksimainen, M., Linder, M., Rouvinen, J. (2006b) Two crystal structures of Trichoderma reesei hydrophobin HFBI—The structure of a protein amphiphile with and without detergent interaction. *Protein Science,* **15**, 2129-2140

Harris, L.J. and Gleddie, S.C. (2001) A modified Rp13 gene from rice confers tolerance of the Fusarium graminearum mycotoxin deoxynivalenol to transgenic tobacco. *Physiol. Mol. Plant Pathol.,* **58**, 173-181.

Hellwig, S., Drossard, J., Twyman, R.M., Fischer, R. (2004) Plant cell cultures for the production of recombinant proteins. *Nature biotechnology,* **22**, 1415-1422

Holland, T., Sack, M., Rademacher, T., Schmale, K., Altmann, F., Stadlmann, J., Fischer, R. and Hellwig, S. (2010) Optimal nitrogen supply as a key to increased and sustained production of a monoclonal full-size antibody in BY-2 suspension culture. *Biotechnol. Bioeng.,* **107**, 278-289.

Hood EE, Gelvin SB, Melchers LS, Hoekema A (1993) New Agrobacterium helper plasmids for gene transfer to plants. *Transgenic Res.,* **2**, 208–218

Höök, F., Kasemo, B., Nylander, T., Fant, C., Sott, K. and Elwing, H. (2001) Variations in coupled water, viscoelastic properties, and film thickness of a Mefp-1 protein film during adsorption and cross-linking: A quartz crystal microbalance with dissipation monitoring, ellipsometry, and surface plasmon resonance study. *Anal. Chem.,* **73**, 5796-5804.

Jacquet, N., Navarre, C., Desmecht, D. and Boutry, M. (2014) Hydrophobin fusion of an influenza virus hemagglutinin allows high transient expression in Nicotiana benthamiana, easy purification and immune response with neutralizing activity. *PLoS ONE,* **9**.

Joensuu, J.J., Conley, A.J., Lienemann, M., Brandle, J.E., Linder, M.B. and Menassa, R. (2010) Hydrophobin Fusions for High-Level Transient Protein Expression and Purification in Nicotiana benthamiana. *Plant Physiol.,* **152**, 622-633.

Kay, R., Chan, A., Daly, M. and McPherson, J. (1987) Duplication of CaMV 35S promoter sequences creates a strong enhancer for plant genes. *Science,* **236**, 1299-1302.

Kirchhoff, J., Raven, N., Boes, A., Roberts, J.L., Russell, S., Treffenfeldt, W., Fischer, R., Schinkel, H., Schiermeyer, A. and Schillberg, S. (2012) Monoclonal tobacco cell lines with enhanced recombinant protein yields can be generated from heterogeneous cell suspension cultures by flow sorting. *Plant Biotechnology Journal,* **10**, 936-944.

Kurppa, K., Hytönen, V. P., Nakari-Setälä, T., Kulomaa, M.S., Linder, M.B. (2014) Molecular engineering of avidin and hydrophobin for functional self-assembling interfaces. *Colloids and Surfaces B: Biointerphases*, **120**, 102-109

Lahtinen, T., Linder, M.B., Nakari-Setälä, T. and Oker-Blom, C. (2008) Hydrophobin (HFBI): a potential fusion partner for one-step purification of recombinant proteins from insect cells. *Protein Expr. Purif.* **59**, 18–24.

Linder, M., Selber, K., Nakari-Setälä, T., Qiao, M., Kula, M-R., Penttilä, M. (2001) The hydrophobins HFBI and HFBII from Trichoderma reesei showing efficient interactions with nonionic surfactants in aqueous two-phase systems. *Biomacromolecules*, **2**, 511-517

Linder, M., Szilvay, G.R., Nakari-Setälä, T., Söderlund, H., Penttilä, M. (2002) Surface adhesion of fusion proteins containing the hydrophobins HFBI and HFBII from Trichoderma reesei. *Protein Sci.,* **9**, 2257-2266

Linder, M.B., Qiao, M., Laumen, F., Selber, K., Hyytiä, T., Nakari-Setälä, T. and Penttilä, M.E. (2004) Efficient purification of recombinant proteins using hydrophobins as tags in surfactant-based two-phase systems. *Biochemistry*, **43**, 11873–11882.

Linder, M.B. (2009) Hydrophobins: Proteins that self assemble at interfaces. *Current Opinion in Colloid & Interface Science,* **14**, 356-363.

Mandal, M.K., Fischer, R., Schillberg, S. and Schiermeyer, A. (2014) Inhibition of protease activity by antisense RNA improves recombinant protein production in Nicotiana tabacum cv. Bright Yellow 2 (BY-2) suspension cells. *Biotechnology Journal,* **9**, 1065-1073.

Mason, H.S., Guerrero, F.D., Boyer, J.S. and Mullet, J.E. (1988) Proteins homologous to leaf glycoproteins are abundant in stems of dark-grown soybean seedlings. Analysis of proteins and cDNAs. *Plant Mol. Biol.,* **11**, 845-856.

McLean, M.D., Chen, R.J., Yu, D.Q., Mah, K.Z., Teat, J., Wang, H.F., Zaplachinski, S., Boothe, J. and Hall, J.C. (2012) Purification of the therapeutic antibody trastuzumab from genetically modified plants using safflower Protein A-oleosin oilbody technology. *Transgenic Research,* **21**, 1291-1301.

Mustalahti, E., Saloheimo, M. and Joensuu, J.J. (2013) Intracellular protein production in Trichoderma reesei (Hypocrea jecorina) with hydrophobin fusion technology. *New Biotechnol*. **30**, 262–268.

Nagata, T. and Kumagai, F. (1999) Plant cell biology through the window of the highly synchronized tobacco BY-2 cell line. *Methods in Cell Science,* **21**, 123-127.

Pabst, T.M., Palmgren, R., Forss, A., Vasic, J., Fonseca, M., Thompson, C., Wang, W.K., Wang, X., Hunter, A. (2014) Engineering of novel Staphylococcal Protein A ligands to enable milder elution pH and high dynamic binding capacity. *Journal of Chromatography A*, **1362**, 180-185

Pereira, E., Kolotilin, I., Conley, A. and Menassa, R. (2014) Production and characterization of in planta transiently produced polygalacturanase from Aspergillus niger and its fusions with hydrophobin or ELP tags. *BMC Biotechnology,* **14**, 59.

Phan, H.T., Hause, B., Hause, G., Arcalis, E., Stoger, E., Maresch, D., Altmann, F., Joensuu, J. and Conrad, U. (2014) Influence of elastin-like polypeptide and hydrophobin on recombinant hemagglutinin accumulations in transgenic tobacco plants. *PLoS ONE,* **9**.

Raven, N., Rasche, S., Kuehn, C., Anderlei, T., Klöckner, W., Schuster, F., Henquet, M., Bosch, D., Büchs, J., Fischer, R. and Schillberg, S. (2015) Scaled-up manufacturing of recombinant antibodies produced by plant cells in a 200-L orbitally-shaken disposable bioreactor. *Biotechnol. Bioeng.,* **112**, 308-321.

Reuter, L.J., Bailey, M.J., Joensuu, J.J. and Ritala, A. (2014) Scale-up of hydrophobin-assisted recombinant protein production in tobacco BY-2 suspension cells. *Plant Biotechnology Journal,* **12**, 402-410.

Ritala, A., Häkkinen, S. and Schillberg, S. (2014) Molecular pharming in plants and plant cell cultures: a great future ahead? *Pharm. Bioprocess.,* **2 (3)**, 223-223-226.

Saberianfar, R., Joensuu, J.J., Conley, A.J. and Menassa, R. (2015) Protein body formation in leaves of Nicotiana benthamiana: a concentration-dependent mechanism influenced by the presence of fusion tags. *Plant Biotechnology Journal,* n/a-n/a.

Sarparanta, M., Bimbo, L.M., Rytkoänen, J., Mäkilä, E., Laaksonen, T.J., Laaksonen, P., Nyman, M., Salonen, J., Linder, M.B., Hirvonen, J., Santos, H.A. and Airaksinen, A.J. (2012) Intravenous delivery of hydrophobin-functionalized porous silicon nanoparticles: Stability, plasma protein adsorption and biodistribution. *Molecular Pharmaceutics,* **9**, 654-663.

Silhavy, D., Molnar, A., Lucioli, A., Szittya, G., Hornyik, C., Tavazza, M. and Burgyan, J. (2002) A viral protein suppresses RNA silencing and binds silencing-generated, 21- to 25-nucleotide double-stranded RNAs. *EMBO J.,* **21**, 3070-3080.

Szilvay G.R., Paananen, A., Laurikainen, K., Vuorimaa, E., Lemmetyinen, H., Peltonen, J., Linder, M.B. (2007) Self-assembled hydrophobin protein films at the air-water interface: structural analysis and molecular engineering. *Biochemistry*, **46**, 2345-2354

Sunde, M., Kwan, A.H.Y., Templeton, M.D., Beever, R.E. and Mackay, J.P. (2008) Structural analysis of hydrophobins. *Micron,* **39**, 773-784.

Uhlen, M., Guss, B., Nilsson, B., Gatenbeck, S., Philipson, L. and Lindberg, M. (1984) Complete sequence of the staphylococcal gene encoding protein A. A gene evolved through multiple duplications. *The Journal of biological chemistry,* **259**, 1695-702.

Wessels, J.G.H. (1994) Developmental Regulation of Fungal Cell-Wall Formation. *Ann. Rev. Phytopathol.,* **32**, 413-437.

Wosten, H.A.B. and Scholtmeijer, K. (2015) Applications of hydrophobins: current state and perspectives. *Applied Microbiology and Biotechnology,* **99**, 1587-1597.

Wu, K., Malik, K., Tian, L., Hu, M., Martin, T., Foster, E., Brown, D., Miki, B. (2001) Enhancers and core promoter elements are essential for the activity of a cryptic gene activation sequence from tobacco, tCUP. *Mol Genet Genomics,* **265**, 763–770

Yang, L., Biswas, M.E., Chen, P. (2003). Study of binding between protein A and immunoglobulin G using a surface tension probe. *Biphys J.*, **84**, 509-522.

## Figures

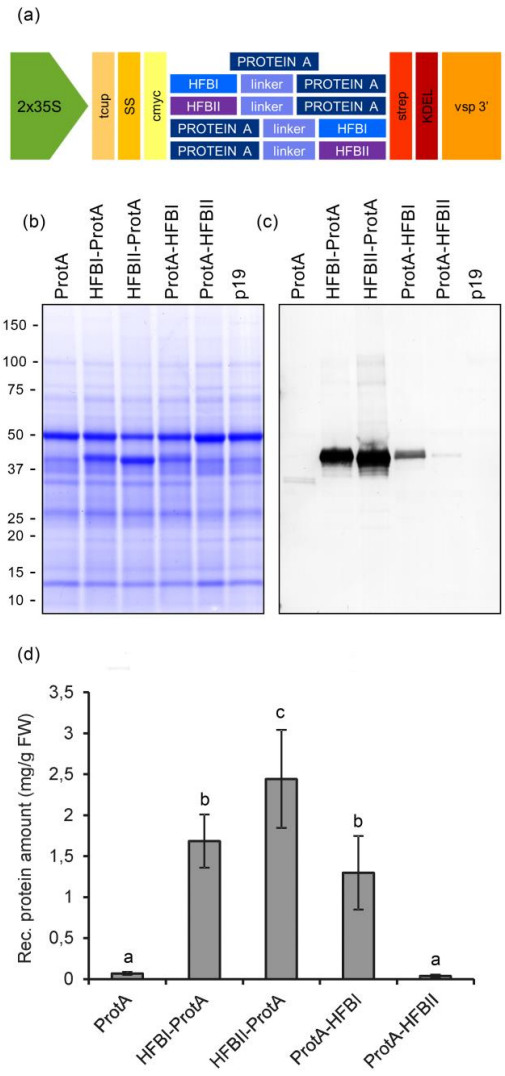


**Figure 1.** Transient expression of Protein A and HFB-fusions in *N. benthamiana.* a) Schematic presentation of gene constructs of Protein A and fusions with HFBI or HFBII. b) Pooled samples analyzed on Coomassie stained SDS-PAGE and c) on western blot. d) Recombinant protein yields analyzed as band intensities from western blots. Error bars indicate standard error of mean (n=6). The letters indicate significant difference ($p$<0.05).

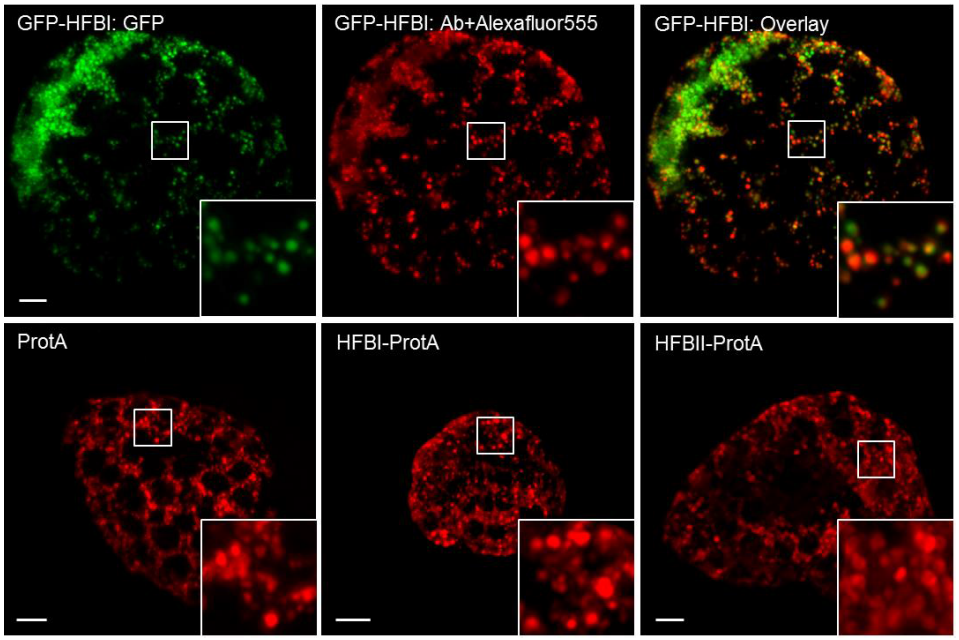


**Figure 2.** Immunostained confocal microscopy images of *N. benthamiana* protoplasts showing subcellular localization of recombinant proteins. Upper panel: GFP-HFBI was used as a positive control. On the left, GFP-derived signal shows a typical morphology of HFBI-induced protein bodies. In the midle, the same cell immunostained with anti-c-Myc primary antibody and Alexafluor®555 conjugated secondary antibody. On the right, an overlay image. No signal was detected from the same sample treated without the primary antibody. Lower panel: representative images of protoplasts expressing Protein A (left), HFBI-Protein A (middle) and HFBII-Protein A (right). Protein body-like structures, similar in size and shape, can be seen in all samples. All images are maximum intensity projections of z-stack images. Scalebars indicate 5µm.

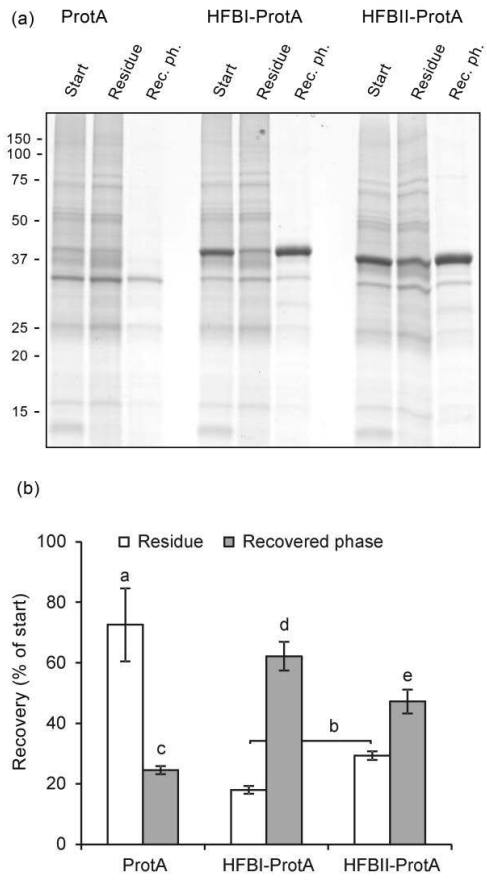


**Figure 3.** Fusion proteins retain the amphipathic properties of the HFB block. a) A Coomassie stained SDS-PAGE of pooled samples from three replicates shows that both fusion proteins partitioned to the surfactant and were found in recovered phase, whereas the non-fused Proten A remained mainly in the residue as did most native plant proteins. Equal volumes of samples were loaded on gel. Fraction volumes are presented in Figure S2. b) Recovery rate of the proteins in residue and in the recovered phase analyzed on a western blot. Letters indicate significant difference ($n$=3, $p$<0.05). Error bars indicate standard deviation.

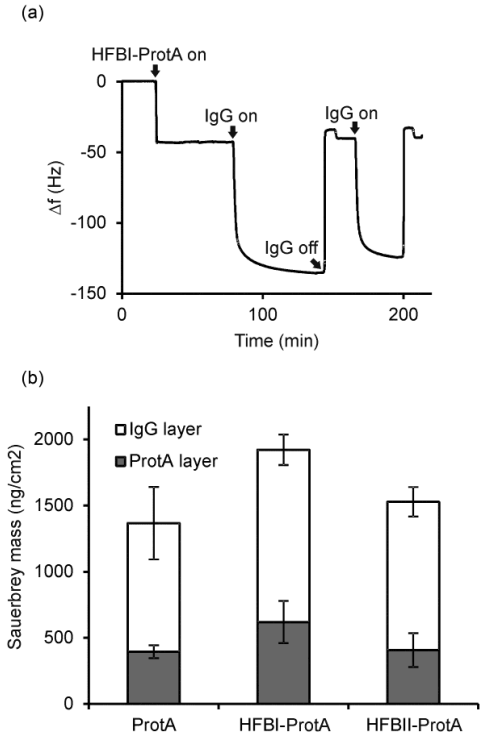


**Figure 4.** Fusion proteins retain the reversible antibody binding capacity of the Protein A block. a) The QCM-D experiment showed reversible antibody binding to the HFBI-Protein A layer, represented as a function of time and oscillation frequency. Protein binding reduced the oscillation frequency of the polystyrene-coated quartz crystal. The curve shows binding of HFBI-Protein A (20 min time point) and of IgG (80 min), and release of IgG by decreasing buffer pH to 2.2 (140 min). The procedure was repeated twice. b) A similar experiment shows that surface-bound Protein A, HFBI-Protein A and HFBII-Protein A (grey bars) all bind Rituximab with similar capacities (white bars). The error bars indicate standard deviation between repeated measurements.

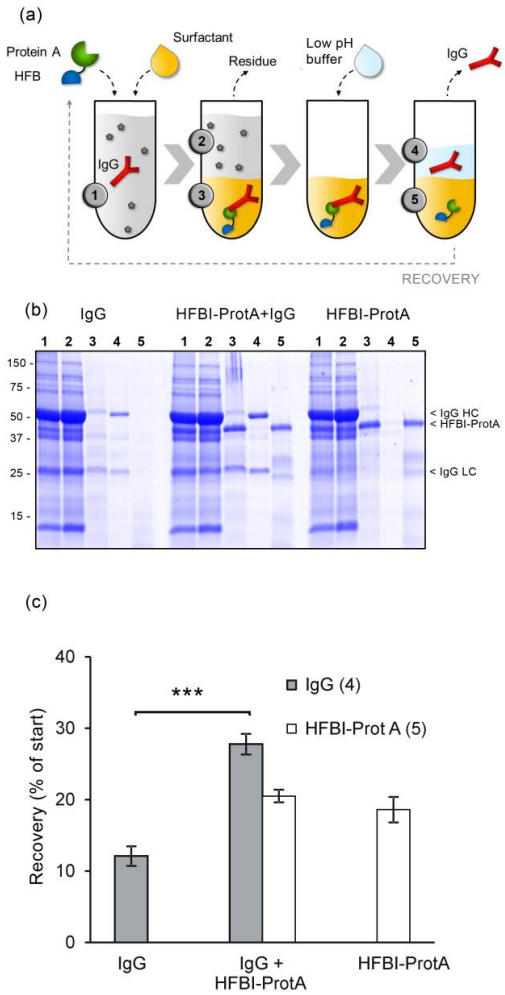


**Figure 5.** The HFBI-Protein A fusion protein can capture antibodies in solutions. a) The concept of the in-solution antibody harvesting. The Protein A block (green) binds to the IgG (red) when added to the antibody-containing plant leaf extract (1). Addition of a surfactant (tan) results in a two-phase system. The HFB block (blue) guides the HFBI-Protein A/IgG complex to the surfactant phase. The aqueous residue (2) is discarded. The IgG is released by addition of acidic buffer and recovered from the aqueous phase (4). The HFBI-Protein A carrier remains in the surfactant phase (5) and can be recycled for a new round of antibody harvesting. b) SDS-PAGE showing the partition of the IgG in ATPS with the HFBI-Protein A (middle) and without (left) and HFBI-Protein A alone (right). Lane numbering corresponds to the illustration on top (a). Volumes of the collected phases are given in Table S4. c) Overall recovery of IgG and HFBI-Protein A. The error bars represent standard deviation of the mean ($n$=3). The asterisks indicate significant difference ($p$>0.001).

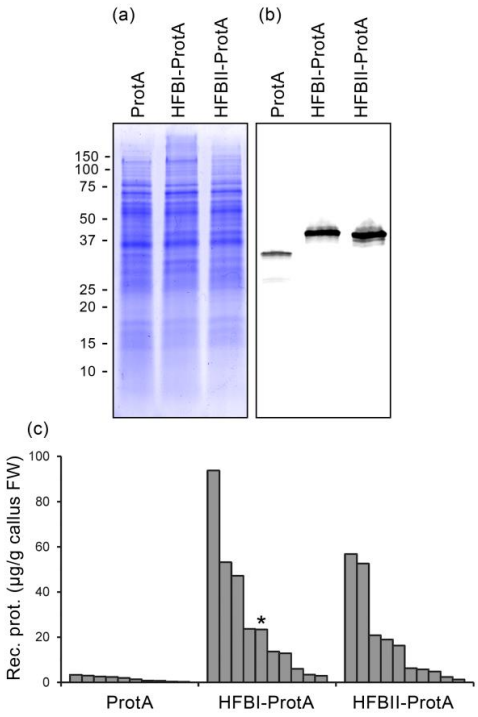


**Figure 6.** Accumulation of Protein A, HFBI-Protein A and HFBII-Protein A in tobacco BY-2 cell cultures. a) A Coomassie stained SDS-PAGE and b) a western blot illustrating the accumulation of the recombinant proteins in samples pooled from 10 callus clones for each construct. The western blot is visualised using anti-c-Myc antibodies. c) Amount of recombinant proteins in the 10 best callus clones for each construct determined from western blots. The line used to initiate a suspension culture is indicated with an asterisk.

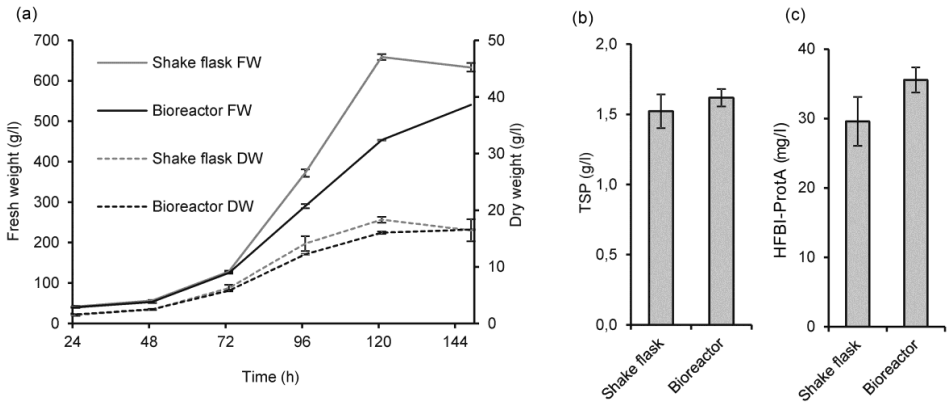


**Figure 7.** HFBI-Protein A producing BY-2 suspension cell culture propagated in 30 litre culture volume. a) Accumulation of dry mass was similar in shake flasks and in the bioreactor. The error bars represent standard deviation between three biological replicates in shake flasks and three technical replicates in the bioreactor. b) The accumulation of total soluble protein, analysed by Bradford-assay, and c) the recombinant protein, analysed from western blots, was comparable in the bioreactor and shake flask cultivations. The error bars represent standard deviation between three technical replicates.

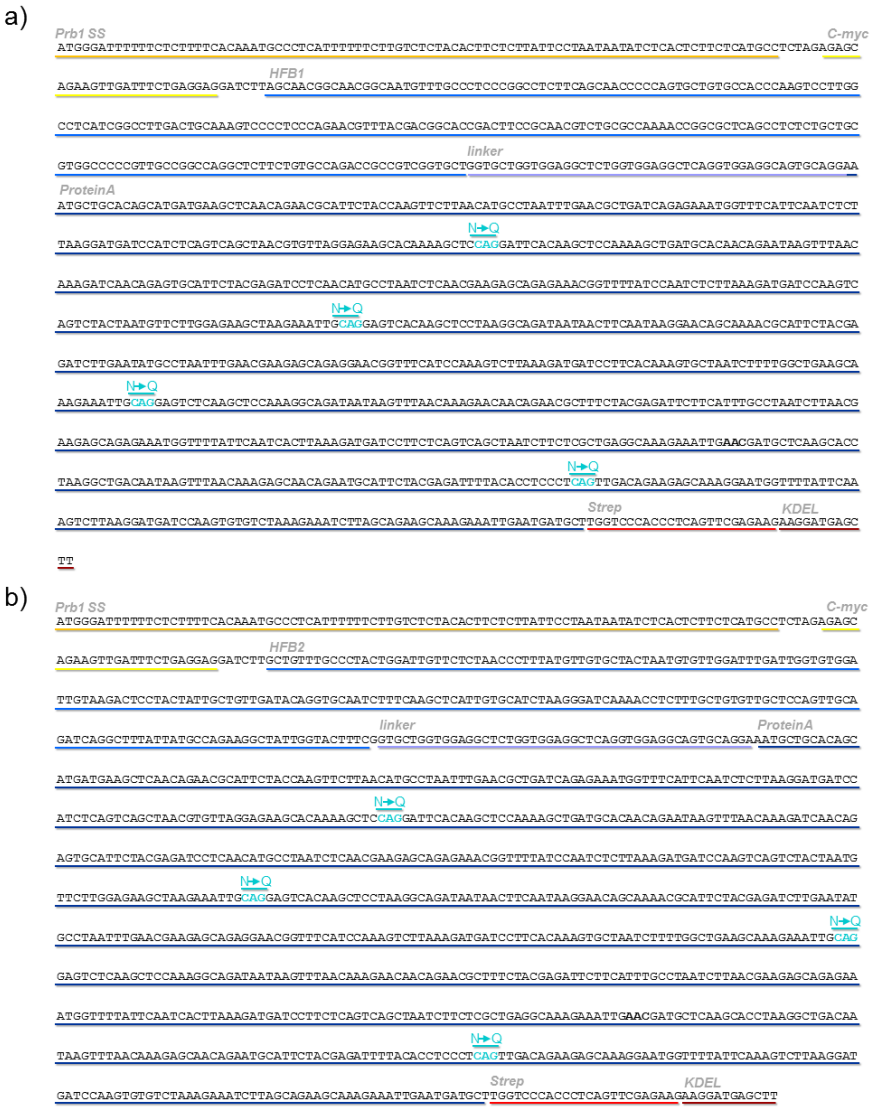


**Figure S1.** Nucleotide sequences of expression cassettes for a) HFBI-ProteinA and b) HFBII-ProteinA. Genes for HFB, linker and ProteinA were cloned in the vector between BsaI restriction sites using Golden gate assembly. The gene of interest is placed under control of double the 35S promoter and the vsp terminator. A Pr1b signal sequence (MGFFLFSQMPSFFLVSTLLLFLIISHSSSHASR) directs the protein to secretory pathway and a KDEL-signal retains it in the ER. The vector also introduces a codon optimized C-myc-tag (GAGCAGAAGTTGATTTCTGAGGAGGATCTT) in the N-terminus and a codon optimized StrepII-tag (TGGTCCCACCCTCAGTTCGAGAAG) in the C-terminus of the amino acid sequence.

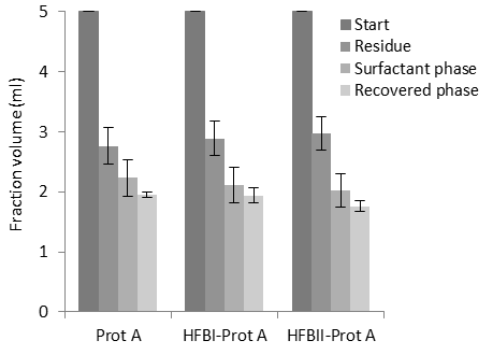


**Figure S2.** Volumes of fraction recovered from ATPS in Figure 3. Error bars indicate standard deviation (n=3).

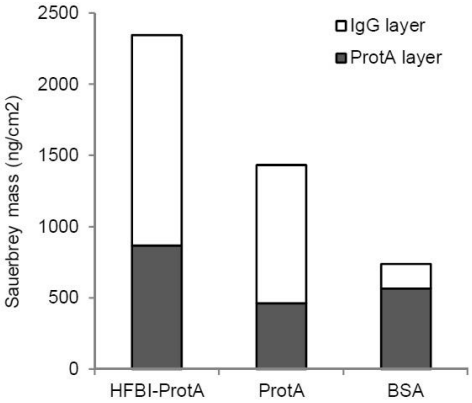


**Figure S3.** QCM-D experiment showing antibody binding to HFBI-Protein A layer, Protein A layer and BSA as negative control.

**Table S1.** Volumes of fractions recovered from ATPS in Figure 5b. Mean± (n=3). Numbers in brackets refer to labelling in figure 5b.

| | start (1) (ml) | residue (2) (ml) | surfactant phase (3) (ml) | acid phase (4) (ml) |
|---|---|---|---|---|
| **IgG** | 1.86±0.02 | 1.05±0.03 | 0.81±0.03 | 0.96±0.05 |
| **HFBI-ProtA+IgG** | 1.85±0.02 | 1.03±0.04 | 0.83±0.02 | 0.98±0.05 |
| **HFBI-ProtA** | 1.86±0.03 | 1.00±0.01 | 0.86±0.01 | 1.07±0.01 |

# II

Kurppa, Katri; Jiang, Hua; Szilvay, Geza, R.; Nasibulin, Albert, G.; Kauppinen, Esko, I.; Linder, Markus. 2007. Controlled Hybrid Nanostructures through Protein-Mediated Functionalization of Carbon Nanotubes. Wiley-VCH Verlag GMBH. Angewandte Chemie International Edition, volume 46, issue 34, pages 6446-6449. ISSN: 1433-7851. DOI:10.1002/anie.200702298.

Nanobiohybrids

DOI: 10.1002/anie.200702298

# Controlled Hybrid Nanostructures through Protein-Mediated Noncovalent Functionalization of Carbon Nanotubes**

*Katri Kurppa,* Hua Jiang, Géza R. Szilvay, Albert G. Nasibulin, Esko I. Kauppinen, and Markus B. Linder*

Metallic nanoparticles (NPs) exhibit interesting electronic and optical properties, especially as organized assemblies.[1–3] Controlled positioning of NPs in nanoarchitectures is essential as the interdistances of neighboring NPs are critical for their collective properties.[4] Also single-walled carbon nanotubes (SWNTs) have many attractive properties for use in nanotechnology.[5] Hierarchically controlled functionalization of the nanotube sidewalls with different NPs is a relevant goal that can lead to new ways of exploiting these properties.[6] Creation of such hybrid structures with control over particle positioning presents a challenging task.[7–11]

NP arrangement in arrays is presently carried out mainly by laborious top-down methods.[12] A more feasible approach to large-scale production of defined nanostructures is bottom-up self-assembly. For this purpose, nature's pool of biomolecules provides us with a diverse toolbox.[3,13–15] Organized arrays of NPs have been created by DNA self-assembly.[1] However, control in structures that demand higher hierarchy is poor with flexible, unordered molecules as templates. More-precise structures can be achieved by using proteins, which self-assemble by interactions based on three-dimensional molecular recognition.[16] Proteins also often have a rigid, defined structure that is in a size scale that is compatible with many nanostructures. The dimensions achieved by protein self-assembly are in principle much smaller than those in DNA-based architectures. Proteins can also be precisely modified by genetic engineering to yield even more specificity in nanostructure design.

Hydrophobins are small, amphiphilic proteins found in filamentous fungi.[17] Their natural function is to adhere to surfaces and function as surfactants. Herein we show that the functional property of a hydrophobin called HFBI can be utilized for controlled functionalization of carbon nanotubes. These features allowed the formation of new protein–nanotube composite structures in which the nanotubes are embedded in protein films. The protein–carbon nanotube interaction was further used to create hybrid structures of carbon nanotubes and regularly spaced gold nanoparticles (AuNPs), named the nano$^3$ hybrid.

We studied the solubilization and functionalization phenomena of SWNTs by using two different SWNTs. Initial solubilization studies were carried out with more-abundant commercially available SWNTs produced by arc discharge. For functionalization studies, we used as-produced SWNTs (see the Supporting Information).[18,19] Two different hydrophobin proteins were used, the naturally occurring (wild type) HFBI, a class II hydrophobin from *Trichoderma reesei*, and its genetically engineered variant named NCysHFBI.[20] The structure of HFBI is amphiphilic due to a patch of aliphatic hydrophobic side chains as shown in Figure 1 a.[21] This feature causes HFBI to be very surface active and to bind to hydrophobic surfaces such as graphite.[22] At the air–water interface, HFBI forms highly elastic films that are one

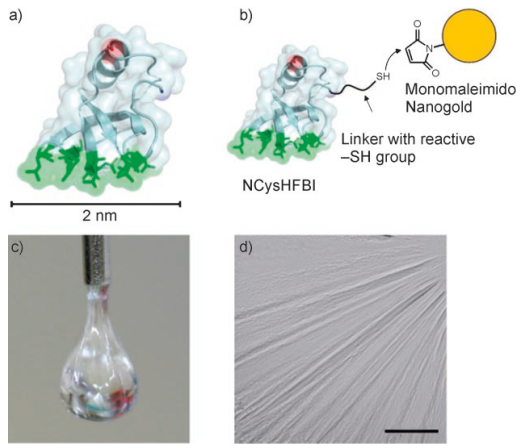


***Figure 1.*** a) HFBI has a compact structure with a large hydrophobic patch (shown in green, side view) as part of an otherwise polar surface. b) A schematic representation of the conjugation of monomaleimido nanogold NPs to NCysHFBI. c) Self-assembly of HFBI leads to the formation of elastic monomolecular films at the surface containing the protein, for example water drops. d) Stretch marks seen on a microscope image of the drop surface illustrate the elasticity and coherence of the film. The scale bar is 50 μm.

[*] K. Kurppa, Dr. H. Jiang, G. R. Szilvay, Prof. E. I. Kauppinen, Dr. M. B. Linder
VTT Biotechnology
VTT Technical Research Centre of Finland
Tietotie 2, P.O. Box 1000, 02044 Espoo (Finland)
Fax: (+358) 20-722-7071
E-mail: katri.kurppa@vtt.fi
Dr. A. G. Nasibulin, Prof. E. I. Kauppinen
Nano Materials Group
Laboratory of Physics and Centre for New Materials
Helsinki University of Technology
Biologinkuja 7, P.O. Box 1000, 02044 Espoo (Finland)

[**] We thank Anton Anisimov for preparation of single-walled nanotube samples and Riitta Suihkonen for technical assistance. This work was supported by the Academy of Finland (grants No. 118519 and 118445).

Supporting information for this article is available on the WWW under http://www.angewandte.org or from the author.

molecule thick and in which the protein molecules have self-assembled in a distinct, highly ordered hexagonal pattern.[22,23] The structure of HFBI is cross-linked by intramolecular disulphide bonds making it very rigid, compact, and stable. NCysHFBI was modified from the wild-type HFBI by linking a stretch of 13 amino acids to its amino terminus (Figure 1b). At the end of the added stretch is a Cys amino acid residue, which has a free reactive -SH group. The -SH groups of different molecules form intermolecular disulphide bonds, resulting in covalently linked dimers $(NCysHFBI)_2$. The intermolecular disulphide can selectively be reduced by dithiotreitol to yield monomeric NCysHFBI with a free -SH group for further conjugation reactions.

The protein–SWNT samples were prepared by adding the aqueous protein solution to a known amount of SWNTs, followed by ultrasonication and centrifugation. HFBI proved to be an extremely capable solubilizing agent for SWNTs. For comparison of the solubilization capability, we performed the same procedures with a formerly reported example, bovine serum albumin (BSA).[24] Previous reports show that as much as 10 mg mL$^{-1}$ (0.15 mM) BSA is needed to solubilize 50 μg mL$^{-1}$ SWNTs.[24] By using HFBI, efficient solubilization of 200 μg mL$^{-1}$ SWNTs was achieved with a concentration as low as 0.25 mg mL$^{-1}$ (0.03 mM). Use of the same concentration of BSA yielded negligible solubilization. The dimeric $(NCysHFBI)_2$ was as efficient as wild-type HFBI. The transmittance values calculated from measured absorbance at 550 nm were 28% and 96% for HFBI-SWNT and BSA-SWNT solutions, respectively (Figure 2). Centrifuged solutions of the hydrophobin–SWNT conjugates were stable for months at room temperature and could be diluted and otherwise handled in a normal manner.

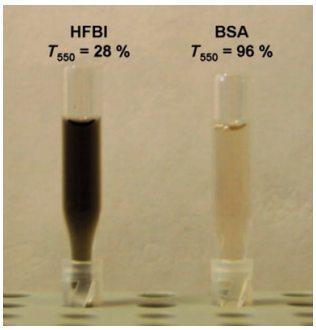


***Figure 2.*** Solutions of SWNTs solubilized by HFBI (left) and BSA (right). The color and transmittance, $T_{550}$, of the centrifuged supernatants represent the amounts of SWNTs in the solution.

Optical characterization of hydrophobin–SWNT conjugates by UV/Vis spectroscopy displays Van Hove peaks that are characteristic of solubilized SWNTs (Figure 3a).[25,26] Broad peaks in the spectra most likely imply the prevalence of bundled carbon nanotubes in the solution.[25] This is possibly a consequence of the rigid, relatively large structure of the protein that prohibits the peeling of individual tubes from the tight bundles formed in the synthesis reactor. No large differences were observed in the spectra of HFBI–SWNT or $(NCysHFBI)_2$–SWNT conjugates. CD spectroscopy measurements showed identical spectra for HFBI, HFBI—SWNT, and NCysHFBI–SWNT (Figure 3b). This shows that neither the interaction between HFBI and SWNTs nor the ultrasonication treatment cause changes in the protein structure.

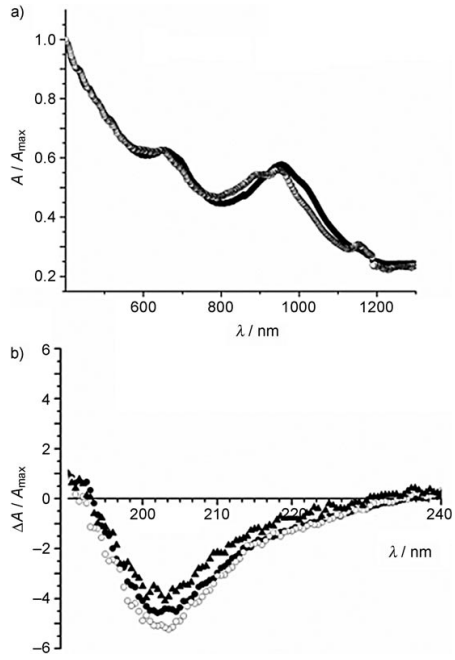


***Figure 3.*** a) UV/Vis spectra of NCysHFBI–SWNT and HFBI–SWNT. b) The CD spectra of HFBI–SWNT, NCysHFBI–SWNT, and HFBI are identical. ● = HFBI–SWNT, ○ = NCysHFBI–SWNT, ▲ = HFBI.

We analyzed the HFBI- and $(NCysHFBI)_2$-functionalized SWNTs by TEM (Figure 4). HFBI–SWNT and $(NCysHFBI)_2$–SWNT samples were prepared by drop-casting the sample solution on TEM grids covered with a holey carbon film. The hydrophobins showed the interesting property of forming thin films spanning the entire carbon film of the grid. SWNTs were embedded in this protein film as individual tubes or bundles. As the protein film also covered the holes of the carbon film, SWNTs were also seen as only supported by the protein film. (Figure 4a and b) Imaging was conducted without staining or protection of the samples. Beam damage was evident after prolonged imaging of a single area of the protein film, causing the formation of rapidly enlarging holes in the protein film. Films prepared from the dimeric $(NCysHFBI)_2$ were more stable in this respect than wild-type HFBI films. This could be due to the additional covalent disulphide bond between NCysHFBI monomers that rigidifies the structure.

The interaction between NCysHFBI and SWNTs was used to create novel hybrid nanostructures of carbon nanotubes, AuNPs, and protein molecules. The single reactive -SH

  

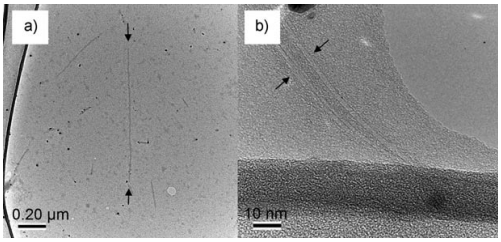


***Figure 4.*** TEM images imaged at 80 kV. a) The $(NCysHFBI)_2$ film suspended over the holey carbon film with SWNTs embedded within. The two arrows indicate the ends of one of the SWNTs. The dark spots are catalyst particles. The edge of the holey carbon film is seen on the left side of the image. b) SWNTs (in the area between the arrows) in the protein film. A hole in the $(NCysHFBI)_2$ film is seen in the upper right corner and the edge of the holey carbon film as a darker area at the lower part of the image.

group of NCysHFBI allows stoichiometric conjugation of other functional groups to only one site of the protein. We used a commercially available monomaleimido nanogold labeling reagent (Nanoprobes, Inc.) to label the single -SH group of the NCysHFBI molecule with a single AuNP. The AuNPs are discrete gold particles of 1.4 nm in diameter and consist of 55–75 gold atoms. A schematic representation of the AuNP–NCysHFBI conjugation is presented in Figure 1b. The AuNP–NCysHFBI conjugate was purified by chromatography and then used to solubilize SWNTs. After sonication and centrifugation, the pelleted hybrid structures of NCysHFBI–AuNPs and SWNTs, named nano$^3$ hybrids, were resuspended into a solution of unmodified NCysHFBI to ensure a protein excess, which was needed for film formation.

Transmission electron microscopy showed that NCysHFBI–AuNPs bound exclusively along the carbon nanotubes (Figure 5a). Only a few stray gold particles were visible in the surrounding NCysHFBI film. Interestingly, the AuNPs were evenly spaced along the SWNTs. Measuring 58 interparticle distances from several images and samples, the average distance between gold particles was found to be $(2.6 \pm 0.4)$ nm (Figure 5b). A schematic representation of the nano$^3$ hybrid is shown in Figure 5c. To verify that the positioning of AuNPs was due to the protein conjugation, a control experiment was made. When SWNTs were solubilized in a mixture of nonconjugated NCysHFBI and free AuNPs, the TEM images showed a random distribution of AuNPs in the protein film (see the Supporting Information and Figure 1). Solutions of Au-functionalized NCysHFBI and SWNTs suspended in a solution of excess NCysHFBI were stored up to a week at $+4\,^{\circ}C$. Even then, only some individual gold particles were observed in the protein film surrounding the functionalized SWNTs. This finding is well descriptive of the high affinity and specificity of the HFBI–SWNT interaction.

Our results demonstrate the self-assembly of three different nanoscale building blocks to form a new type of hybrid material. Functionalization of SWNTs with AuNP–NCysHFBI resulted in novel hybrid nanostructures in which a one-dimensional regular array of AuNPs is bound to the

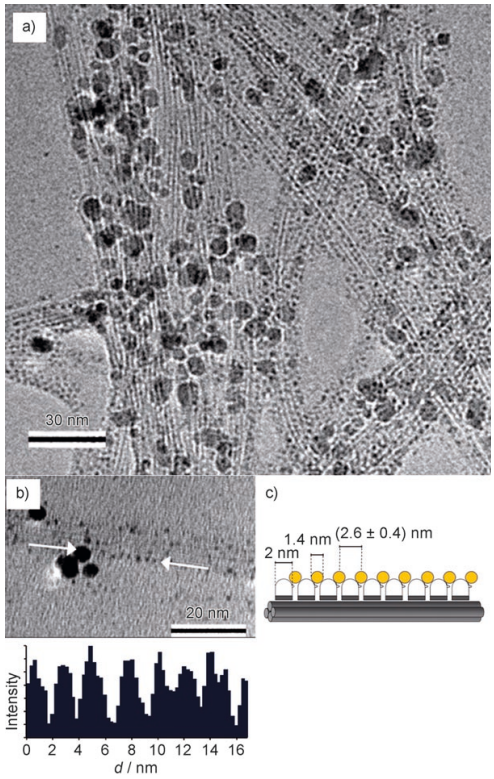


***Figure 5.*** TEM images imaged at 200 kV (a) or 80 kV (b). a) Nano$^3$ hybrids embedded in a $(NCysHFBI)_2$ film. b) An example of a stretch of aligned NPs that was used for calculating particle distances. The intensity profile shown underneath the TEM image was calculated from the row of AuNPs between the arrow heads. c) A schematic view of the nano$^3$ hybrid displaying the diameters of the protein (2 nm) and the AuNPs (1.4 nm) and the interdistances of the AuNPs $((2.6 \pm 0.4)$ nm).

carbon nanotube sidewalls. These nano$^3$ hybrid structures as well as the HFBI–SWNT composite films are prime examples of the structural control that can be achieved with self-assembling proteins. Because HFBI is structurally rigid and was engineered to bind only one AuNP per HFBI molecule, the spacing of the AuNPs on the SWNTs followed the size of the protein, distributing the NPs evenly at a distance of 2.6 nm. Owing to the relatively long 13 amino acid linker connecting the AuNP and the protein, the specific location of the NP with respect to the SWNT cannot be exactly defined. The regular arrangement of AuNPs, however, suggests that the interaction between the HFBI moiety and the SWNT surface is spatially oriented and occurs through a specific location on the protein, presumably the hydrophobic patch.

In conclusion, we have shown efficient solubilization and functionalization of SWNTs by HFBI and an engineered variant NCysHFBI. This interaction allowed the formation of novel protein–SWNT composite films as well as hybrid nanostructures of carbon nanotubes and AuNPs, the

  

nano[3] hybrids. In these hybrid structures, AuNPs were organized on carbon nanotube sidewalls in 1D arrays with a spacing of 2.6 nm, which implies underlying protein organization. Our results differ from previous examples of biomolecule-mediated positioning of NPs in that more structural levels were achieved by combining different types of materials. We show that rational use of proteins can lead to integration of different nanoscale objects in an ordered and hierarchical manner. This opens a route for combining their optical and electronic functions in new ways and can form a valuable addition to the toolbox of biomolecules that are finding use in nanotechnology.

Received: May 24, 2007
Published online: July 25, 2007

**Keywords:** carbon nanotubes · hydrophobin · nanoparticles · nanostructures · self-assembly

[1] J. Zhang, Y. Liu, Y. Ke, H. Yan, *Nano Lett.* **2006**, *6*, 248 – 251.
[2] M.-C. Daniel, D. Astruc, *Chem. Rev.* **2004**, *104*, 293 – 346.
[3] E. Katz, I. Willner, *Angew. Chem.* **2004**, *116*, 6166 – 6235; *Angew. Chem. Int. Ed.* **2004**, *43*, 6042 – 6108.
[4] S. A. Maier, M. L. Brongersma, P. G. Kik, H. A. Atwater, *Phys. Rev. B* **2002**, *65*, 193408.
[5] R. H. Baughman, A. A. Zakhidov, W. A. de Heer, *Science* **2002**, *297*, 787 – 792.
[6] M. Bottini, F. Cerignoli, L. Tautz, N. Rosato, A. Bergamaschi, T. Mustelin, *J. Nanosci. Nanotechnol.* **2006**, *6*, 3693 – 3698.
[7] L. Marty, A. M. Bonnot, A. Bonhomme, A. Iaia, C. Naud, E. Andre, V. Bouchiat, *Small* **2006**, *2*, 110 – 115.
[8] B. Kim, W. M. Sigmund, *Langmuir* **2004**, *20*, 8239 – 8242.
[9] A. Carrillo, J. A. Swartz, J. M. Gamba, R. S. Kane, N. Chakrapani, B. Q. Wei, P. M. Ajayan, *Nano Lett.* **2003**, *3*, 1437 – 1440.
[10] L. Q. Jiang, L. Gao, *Carbon* **2003**, *41*, 2923 – 2929.
[11] X. Hu, T. Wang, X. Qu, S. Dong, *J. Phys. Chem. B* **2006**, *110*, 853 – 857.
[12] D. Y. Wang, H. Mohwald, *J. Mater. Chem.* **2004**, *14*, 459 – 468.
[13] E. Gazit, *FEBS J.* **2007**, *274*, 317 – 322.
[14] E. Katz, E. Willner, *ChemPhysChem* **2004**, *5*, 1084 – 1104.
[15] K. T. Nam, D.-W. Kim, P. J. Yoo, C.-Y. Chiang, N. Meethong, P. T. Hammond, Y.-M. Chiang, A. M. Belcher, *Science* **2006**, *312*, 885 – 888.
[16] P. Asuri, S. S. Bale, S. S. Karajanagi, R. S. Kane, *Curr. Opin. Biotechnol.* **2006**, *17*, 562 – 568.
[17] M. B. Linder, G. R. Szilvay, T. Nakari-Setala, M. E. Penttila, *FEMS Microbiol. Rev.* **2005**, *29*, 877 – 896.
[18] A. Moisala, A. G. Nasibulin, D. P. Brown, H. Jiang, L. Khriachtchev, E. I. Kauppinen, *Chem. Eng. Sci.* **2006**, *61*, 4393 – 4402.
[19] A. G. Nasibulin, D. P. Brown, P. Queipo, D. Gonzalez, H. Jiang, E. I. Kauppinen, *Chem. Phys. Lett.* **2006**, *417*, 179 – 184.
[20] J. G. H. Wessels, *Annu. Rev. Phytopathol.* **1994**, *32*, 413 – 437.
[21] J. Hakanpaa, G. R. Szilvay , H. Kaljunen, M. Maksimainen, M. Linder, J. Rouvinen, *Protein Sci.* **2006**, *15*, 2129 – 2140.
[22] G. R. Szilvay, A. Paananen, K. Laurikainen, E. Vuorimaa, H. Lemmetyinen, J. Peltonen, M. B. Linder, *Biochemistry* **2007**, *46*, 2345 – 2354.
[23] A. Paananen, E. Vuorimaa, M. Torkkeli, M. Penttila, M. Kauranen, O. Ikkala, H. Lemmetyinen, R. Serimaa, M. B. Linder, *Biochemistry* **2003**, *42*, 5253 – 5258.
[24] S. S. Karajanagi, H. Yang, P. Asuri, E. Sellitto, J. S. Dordick, R. S. Kane, *Langmuir* **2006**, *22*, 1392 – 1395.
[25] M. J. O'Connell, S. M. Bachilo, C. B. Huffman, V. C. Moore, M. S. Strano, E. H. Haroz, K. L. Rialon, P. J. Boul, W. H. Noon, C. Kittrell, J. P. Ma, R. H. Hauge, R. B. Weisman, R. E. Smalley, *Science* **2002**, *297*, 593 – 596.
[26] S. M. Bachilo, M. S. Strano, C. Kittrell, R. H. Hauge, R. E. Smalley, R. B. Weisman, *Science* **2002**, *298*, 2361 – 2366.

  

Angewandte Chemie
Eine Zeitschrift der Gesellschaft Deutscher Chemiker

# Supporting Information



69451 Weinheim, Germany

# Controlled hybrid nanostructures via protein mediated non-covalent functionalization of carbon nanotubes

*Katri Kurppa*, Hua Jiang, Géza R. Szilvay, Albert G. Nasibulin, Esko I. Kauppinen, Markus B. Linder*

**Materials.** Arc-discharge Single-walled carbon nanotubes used in solubilization experiments were purchased from Nanoledge, France and used as such. Functionalization studies were performed using as-produced (without chemical purification) SWNTs synthesized in a laminar flow aerosol reactor and collected directly from the gas phase downstream of the reactor by filtering.[1] For the synthesis of SWNTs carbon monoxide and ferrocene were used as a carbon source and a catalyst precursor, respectively.[2] HFBI and NCysHFBI were produced and purified according to previously reported protocols.[3, 4] Bovine serum albumin (BSA) was purchased from Sigma-Aldrich.

**Solubilization and UV-Vis.** The NCysHFBI-SWNT and HFBI-SWNT samples were prepared by adding 1 ml of the aqueous protein solution to a known amount of the SWNTs. For comparison of the solubilization capabilities of different protein scaffolds BSA was used. A solution of each protein was prepared in deionized water (0.03 mM, 1 ml) and mixed with 0.2 mg of SWNTs. The mixture was vortexed slightly, then subjected to ultrasonication in a tip sonicator (Soniprep 150) for 2x1 min at 26 µm. Sonication yielded a dense black mixture, which was centrifuged at 20 800 rcf. The liquid was removed carefully from the pellet containing undissolved SWNTs and the centrifugation was repeated. The resulting supernatant was used in experiments as such. UV-spectra were collected from water dilutions on a Varian or a Perkin-Elmer Lambda 950 UV-Vis spectrometer.

**Circular dichroism.** Solutions of HFBI-SWNTs or NCysHFBI-SWNTs were prepared as described above. Instead of using the supernatant, the pellet from the second centrifugation step was resuspended in deionized water and sonicated briefly to remove unbound protein. The CD spectra were recorded on a JASCO model J-720 CD spectrometer with a 1-mm cell and a bandwidth of 1 nm at room temperature.

**AuNP labeling of NCysHFBI.** The disulphide bonded dimer $(NCysHFBI)_2$ was selectively reduced to monomeric NCysHFBI with dithiotreitol. The monomeric NCysHFBI was conjugated to Monomaleimido Nanogold particles (Nanoprobes Inc.) according to supplier's instructions. The reaction mixture was purified by RP-HPLC using a gradient 0.1% TFA / 0.1% TFA in acetonitrile as the eluent. Fractions of 0.5 ml were collected into eppendorf tubes containing 80 µl 1 M sodium acetate pH 5. The first peak was confirmed to be the protein conjugate by CNT solubilization capability, functionality in TEM analysis and MALDI-TOF, which displayed an array of peaks separated by the gold atomic mass of 197 g/mol between 5000 and 20000 Da. The purified solution of NCysHFBI-AuNP was used to solubilize SWNTs by sonication as described above. The centrifuged solution was removed from the pellet and the pellet was resuspended in a 0.2 mg/ml aqueous solution of $(NCysHFBI)_2$ and sonicated vbriefly in a tip sonicator. The resulting gray solution was centrifuged at 6800 rcf for 5 min and the supernatant was used in experiments as such.

**Transmission electron microscopy.** A Philips CM200 electron microscope equipped with a schottky-type field emission gun was used and operated at accelerating voltage of 200 kV or 80 kV. A Gatan 794 multiscan CCD camera (1k x 1k) was employed for digital recording. A few microliters of the sample solution were dried on copper grids coated with a holey carbon film. The sample was allowed to stabilize in vacuum for fifteen minutes to several hours prior to imaging.

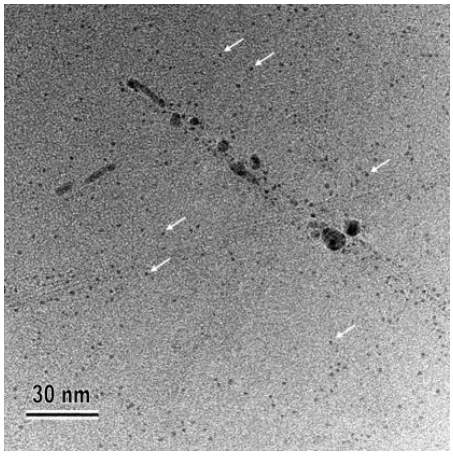


**Figure 1.** When unconjugated $(NCysHFBI)_2$-SWNT and gold NP's are mixed in solution, a random distribution of gold nanoparticles in the protein film is seen. The larger dark spheres in all images are catalyst particles. Some of the free nanoparticles are marked by the arrowheads for clarity

**References:**

[1] A. Moisala, A.G. Nasibulin, D.P. Brown, H. Jiang, L. Khrichtchev, E.I. Kauppinen *Chem. Eng. Sci.* **2006**, *61*, 4393-4402.
[2] A.G. Nasibulin, D.P. Brown, P. Queipo, P. Gonzalez, H. Jiang, E.I. Kauppinen *Chem. Phys. Lett.* **2006**, *417*, 179-184.
[3] G.R. Szilvay, T. Nakari-Setälä, M.B. Linder *Biochemistry* **2006**, *45*, 8590-8598.
[4] M.B. Linder, K. Selber, T. Nakari-Setälä, M.Q. Qiuo, M.R. Kula, M. Penttilä *Biomacromolecules* **2001**, *2*, 511-517.

# III

Kurppa, Katri; Hytönen, Vesa; Nakari-Setälä, Tiina; Kulomaa, Markku; Linder, Markus. 2014. Molecular engineering of avidin and hydrophobin for functional self-assembling interfaces. Elsevier Science. Colloids and Surfaces B: Biointerfaces, volume 120, pages 102-109. ISSN: 0927-7765. DOI: 10.1016/j.colsurfb.2014.05.010.

Colloids and Surfaces B: Biointerfaces 120 (2014) 102–109

Contents lists available at ScienceDirect

Colloids and Surfaces B: Biointerfaces

journal homepage: www.elsevier.com/locate/colsurfb

# Molecular engineering of avidin and hydrophobin for functional self-assembling interfaces☆

Katri Kurppa[a,*], Vesa P. Hytönen[b,c], Tiina Nakari-Setälä[a], Markku S. Kulomaa[b], Markus B. Linder[a,d]

[a] VTT Technical Research Institute of Finland, Tietotie 2, PO Box 1000, FI-02044 Espoo, Finland
[b] BioMediTech, University of Tampere and Tampere University Hospital, Biokatu 6, FI-33014 Tampere, Finland
[c] Fimlab Laboratories, Biokatu 4, FI-33520 Tampere, Finland
[d] Aalto University, Department of Biotechnology and Chemical Technology, Kemistintie 1, FI-00076 Espoo, Finland

ARTICLE INFO

*Article history:*
Received 18 November 2013
Received in revised form 3 February 2014
Accepted 11 May 2014
Available online 22 May 2014

*Keywords:*
Hydrophobin
Avidin
Protein engineering
Nanomaterial
Biofunctional surface

ABSTRACT

Control over the functionality of interfaces through biomolecular engineering is a central tool for nanoscale technology as well as many current applications of biology. In this work we designed fusion proteins that combined the surface adhesion and interfacial activity of a hydrophobin–protein together with the high affinity biotin-binding capability of an avidin–protein. We found that an overall architecture that was based on a circularly permuted version of avidin, dual-chain avidin, and hydrophobin gave a highly functional combination. The protein was produced in the filamentous fungus *Trichoderma reesei* and was efficiently purified using an aqueous two-phase partitioning procedure. The surface adhesive properties were widely different compared to wild-type avidin. Functional characterization showed that the protein assembled on hydrophobic surfaces as a thin layer even at very low concentrations and efficiently bound a biotinylated compound. The work shows how the challenge of creating a fusion protein with proteins that form multimers can be solved by structural design and how protein self-assembly can be used to efficiently functionalize interfaces.



## 1. Introduction

Molecular-level control of the structure and function of interfaces is of key importance in numerous biological systems, ranging from adhesion and signal transduction to the building of larger structural assemblies. Similarly, new technological development is focused toward the use of controlled interfaces for nanostructured systems. Ideally molecular self-assembly can be used for full control of interfaces, orienting molecules in a specific way and determining how they interact with other molecules in their surroundings. Such nanostructure-controlled systems are used for example to find new ways of detecting signals and for making materials with new functional properties. This leads to a new base for technologies for biosensors, the compatibility of implantable devices, and the construction of high-performance biomimetic nanomaterials [1,2].

Examples show that biological systems provide several potential solutions for achieving molecularly well-defined systems. DNA assemblies are very promising because they are extremely versatile for creating structural assemblies [3]. However, in nature proteins are the primary molecules that provide chemical and physical functions. Proteins have the advantage that they show an astounding variety of functions, but we are still in the very early stages in being able to use first principles in designing new functions in protein-based systems. Although there are substantial difficulties in designing new proteins, we can in many cases use natural structures as components and fuse them together into chimeric variants that combine desired functions. The challenge herein is to design the overall architecture of the system so that the desired functions can be utilized. In this work we link together the interfacial assembly functionality of a hydrophobin protein with the affinity binding functionality of an avidin protein.

Hydrophobins are extracellular proteins produced by filamentous fungi [4–6]. In fungal growth they have a multitude of roles that involve controlling interfaces in different ways, for example allowing aerial growth through reducing surface tension or

☆ This work was performed at the Technical Research Institute of Finland (VTT), Tietotie 2, P.O. Box 1000, FI-02044.

* Corresponding author. Tel.: +358 40 197 3041/+358 40 197 3041; fax: +358 20 722 7071.
*E-mail address:* katri.kurppa@vtt.fi (K. Kurppa).

http://dx.doi.org/10.1016/j.colsurfb.2014.05.010
0927-7765/

functioning as adhesives. Through structural analysis it is understood that the basis for the function of hydrophobins is their amphiphilic structure, which is due to a relatively large hydrophobic patch on the surface of the protein. This structure causes the hydrophobins to assemble at interfaces and form adhesive films on hydrophobic surfaces [7–9]. Hydrophobins have a tendency to aggregate and exhibit complicated self-assembly features. Based on the occurrence of hydrophobic and hydrophilic amino acids in the amino acid sequence, the hydrophobins have been divided in two classes, class I and class II [10]. Generally the class I hydrophobins form insoluble aggregates, whereas many of the class II hydrophobins have been found to be soluble by formation of dimers, tetramers or even higher types of oligomers [11]. These properties have led to the use of hydrophobins in advanced material applications such as the functionalization of nanomaterials such as carbon nanotubes and graphene [12,13].

Chicken avidin is a tetrameric egg-white protein that binds the small molecule D-biotin (vitamin H) with an exceptionally high ($K_d \sim 10^{-15}$ M) affinity [14]. Like avidin, streptavidin which is of bacterial origin is also a widely used tool in biotechnology applications, and the term (strept)avidin collectively refers to chicken avidin and streptavidin [15,16]. The wild-type avidin is a tetrameric protein in which four identical chains come together to form the functional assembly. Therefore the wild-type avidin binds four biotin molecules. The subunits are not functional unless assembled as a tetramer [17,18]. The very high affinity, specificity and multivalency, has made the (strept)avidin–biotin technology widely used in applications of life sciences and nanotechnology [19–21]. The popularity of the biotin–avidin system for functionalization is supported by the very easily performed coupling reactions in which biotin activated with different reactive groups can be chemically bound to a variety of compounds. Thousands of biotin-functionalized molecules are readily available commercially.

The insight that hydrophobins show very promising features for modification and control of interfaces lead us to explore how fusion proteins should be constructed in order to utilize this property in a wider and more functional way. The aim of this work was to construct a fusion protein that could combine the surface-assembling properties of hydrophobins with the biotin-binding functionality of avidin. We used the class II hydrophobin HFBI from *Trichoderma reesei* because it was expected to be efficiently purified by two-phase extraction and can be handled without irreversible aggregation [10]. The produced fusion protein was anticipated to readily assemble on interfaces and provide controlled and oriented biotin-mediated linking functionality. In addition to the functionality of the engineered fusion protein we were interested in the most efficient molecular design of the chimeric protein. This was addressed by fusing the hydrophobins to either the subunit of the avidin tetramer or a modified dual-chain avidin unit. The dual-chain avidin is a result of duplication and fusion of two circularly permuted avidin subunit chains, resulting in a structure in which two monomer chains have been fused into one polypeptide chain [22]. In the dual-chain avidin (dcAvd), the functional quaternary structure is formed by two peptide chains, but retaining the overall native four-binding site arrangement, i.e. forming a pseudotetramer. The designed constructs HFBI–Avd and HFBI–dcAvd result in different stoichiometry of hydrophobin units and the functional quaternary structure of avidin (Fig. 1).

## 2. Materials and methods

### 2.1. Cloning of HFBI–Avd and HFBI–dcAvd

The Avi and dcAvd cassettes were released from the plasmid pGemT-easy(attL1-ompA-AVD-attL2) and pGemT-easy(attL1-ompA-dcAvd-attL2) [23] (named p2768 (Avd) and p2769 (dcAvd)) with *Kpn*I and *Nde*I (New England Biolabs, Ipswich, USA). The cassette was subcloned into the corresponding restriction sites of a shrimp alkaline phosphatase treated fungal expression vector pTNS29 carrying a cbhI promoter and HFBI as an N-terminal fusion partner. The resulting plasmids pTNS47 (containing the Avd gene) and pTNS48 (containing the dcAvd gene) were transformed into DH5α *Escherichia coli* strain by electroporation.

The expression cassettes containing the HFBI–Avd or HFBI–dcAvd inserts were released with *Sph*I (New England Biolabs, Ipswich, USA) from the plasmids and co-transformed with pTNS48/7 and the selection plasmid pToC202 (acetamide resistance (Amd+)) in *T. reesei* strain Rut-C30 Δ*hfb2* VTT D-99676 as described previously [24]. The obtained Amd+ transformants were tested for high HFBI–Avd or HFBI–dcAvd expression in microtiter plate and shake flask cultivations and analyzed for hydrophobin by Western blot analysis.

### 2.2. Production and purification of HFBI–Avd and HFBI–dcAvd

The *T. reesei* strains VTT D-051057 (HFBI–Avd) VTT D-051059 (HFBI–dcAvd) were cultivated in a bioreactor for 72 h in media containing 40.0 g/l lactose, 4.0 g/l peptone, 1.0 g/l yeast extract, 4.0 g/l

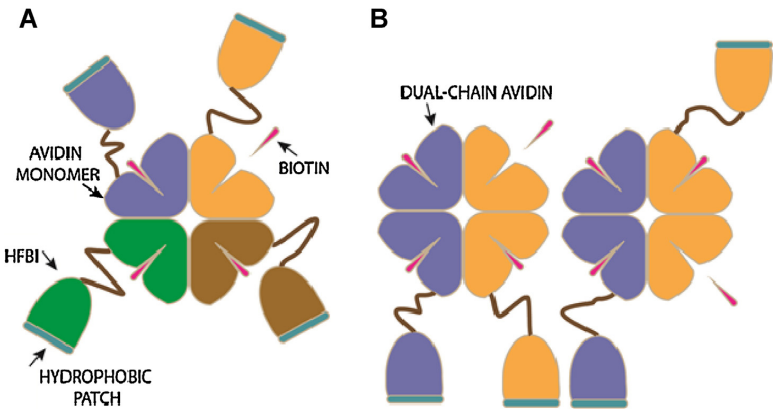


**Fig. 1.** (a) Schematic presentation of HFBI–Avd construct. (b) Schematic representation of the HFBI–dcAvd construct, which contains avidin assembly (pseudotetramer) resembling the native tetramer. Hydrophobins are also known to form multimers in solution through interaction of the hydrophobic patches.


**Fig. 2.** Amino acid sequences of HFBI–Avd and HFBI–dcAvd. The linker region fusing two circularly permuted avidins together is indicated by vertical arrow.

$KH_2PO_4$, 2.8 g/l $(NH_4)_2SO_4$, 0.6 g/l $MgSO_4 \cdot 7H_2O$, 0.8 g/l $CaCl_2 \cdot 2H_2O$ and 2.0 ml/l trace elements. Cultivations were performed at pH 3–5 with constant agitation at 28 °C.

HFBI–Avd was released from the mycelium by mixing the mycelium pellet with 0.2 M Tris buffer at pH 7.5 containing 2% sodium dodecyl sulfate (SDS). Further purification was performed by buffer exchange using a 10 DG desalting column (Bio-Rad) to 20 mM phosphate buffer pH 7.5. Residual SDS was removed using Q-Sepharose (GE-Healthcare, Buckinghamshire, UK) equilibrated in the same buffer but containing 20% ethanol. Under these conditions the protein was found in the flow through while the SDS remained in the column.

HFBI–dcAvd was purified from the culture supernatant by a two-phase extraction procedure [25]. The cell culture was centrifuged at 4000 rpm and 6 °C for 30 min. The supernatant was extracted with a non-ionic detergent Berol 532 (Akzo Nobel, Amsterdam, The Netherlands) and back-extracted into aqueous buffer using isobutanol. The extract was further purified by ion-exchange chromatography eluting from a MonoS column (GE Healthcare, Buckinghamshire, UK) using a PBS gradient (20 mM sodium phosphate, 0–1 M NaCl, pH 7.5). Two peaks were observed in the chromatography run (Fig. 3b), of which only the latter was detected with Western blot using antibodies against avidin. MALDI-TOF spectrometry was performed in the Institute of Biotechnology at the University of Helsinki. The amino acid sequences of HFBI–Avd and HFBI–dcAvd are presented in Fig. 2.

### 2.3. Biotin-binding capacity of HFBI–dcAvd

Characterization of biotin-binding capacity was performed only for HFBI–dcAvd, as the HFBI–Avd construct proved poorly soluble. Fluorescence quenching of the Trp-residues in the biotin binding site was followed by titration of HFBI–dcAvd with free biotin (Sigma Aldrich). Biotin (100 nM) was added in 1 μl aliquots to a solution of HFBI–dcAvd (1 ml, 500 nM) in PBS (0.1 M sodium phosphate, 0.15 M NaCl, pH 7.2) followed by mixing for 1 min. The sample was excited at 280 nm and the fluorescence at 350 nm was followed and compared to an identically performed control experiment with avidin (Sigma Aldrich, St. Louis, US). The obtained fluorescence intensity in relation to the maximum intensity ($F/F_0$) was plotted against the fraction of biotin added. A linear fitting was performed to the beginning of the curve and the part after reaching quenching maximum. The cross section of these fits was used to estimate the maximum fraction of biotin bound (Table 1).

The number of functional biotin-binding sites was determined also using [$^3$H]-biotin (GE Healthcare, Buckinghamshire, UK). A reaction mixture containing HFBI–dcAvd (20 μl, 0.0325 μM) or avidin, PBS (500 μl) and [$^3$H]-biotin (20 μl, 0.125 μM) was incubated at RT (20–22 °C) for 1–2 h. Three parallel 160 μl samples were filtered through Whatman GF/C glass fiber filters with 10 000 *MW* cut-off (GE Healthcare, Buckinghamshire, UK). The filter was rinsed thoroughly with 10 ml ice-cold deionized water to remove unbound [$^3$H]-biotin and immersed in Optiphase scintillation

**Table 1**
Characterization of HFBI–dcAvd biotin binding.

| Protein | Determination of biotin-binding sites[a] | | Dissociation of 8,9[$^3$H] biotin 50 °C |
|---|---|---|---|
| | No of sites[b] | No of sites[c] (quenching, %) | $k_{diss}$ ($10^{-6}$ $s^{-1}$) |
| Avidin | 3.3 ± 0.1 | 3.4 (53) | 4.3 ± 0.7 |
| HFBI–dcAvd | 2.9 ± 0.6 | 2.4 (33) | 7.6 ± 0.8 |
| Avidin[d] | – | 3.3 (48) | 4.2 |
| dcAvd[d] | – | 3.9 (51) | 3.0 |

[a] Values calculated per avidin tetramer and per HFBI–dcAvd dimer.
[b] [$^3$H]-biotin assay.
[c] Estimated by fluorescence quenching.
[d] From Nordlund et al.

cocktail (Perkin Elmer, Waltham, US). All HFBI–dcAvd or avidin was assumed to bind to the filter. The number of the biotin binding sites was calculated from the measured radioactivity, corrected by the counting rate, and the specific activity of the used [$^3$H]-biotin.

### 2.4. Biotin affinity of HFBI–dcAvd

Measuring of biotin affinity was feasible only in the case of HFBI–dcAvd, as the HFBI–Avd construct was insoluble after purification. Biotin dissociation of HFBI–dcAvd was measured according to the protocol of Klumb et al. [26]. Two reaction mixtures containing [$^3$H]-biotin (2.4 μl, 1.48 TBq/mmol, 37 MBq/ml) and BSA (4 μl, 10 mg/ml) in PBS (4 ml, 0.1 M sodium phosphate, 0.15 M NaCl pH 7.2) were prepared. Aliquots of 300 μl were filtered by centrifugal ultrafiltration through Millipore Ultrafree 10 000 *MW* cut-off filters (Merck Millipore, Billerica, US). Three samples of 30 μl were drawn from both reactions and the activities were assayed for radioactivity in a liquid scintillation counter. To the initial reaction mixtures was then added HFBI–dcAvd (105 μl, 0.15 mg/ml) or avidin (10 μl, 0.32 mg/ml). The reaction mixtures were incubated at the desired temperature for 15 min. Samples were taken and filtered as previously. Scintillation was counted from the filtrates of the HFBI–dcAvd or avidin solution with the added [$^3$H]-biotin to ensure that all labeled biotin was retained in the filter together with the protein. Excess of free biotin (42 μl, 1 mg/ml) was then added to both reactions. Incubation at the desired temperature was continued and scintillation was counted from the filtrates of samples taken at 60 min intervals. The dissociation rate constant $k_{diss}$ was determined from the slope of the plot of ln(fraction biotin bound at time $t$) vs. time [26]. The equilibrium constant $K_d$ can be calculated from $K_d \sim k_{on,\,WT}/k_{off,HFBI-dcAvd}$ using the biotin-binding association rate constant of wild-type avidin $k_{on,\,WT} = 7 \times 10^7$ M/s [14]. The half-times of biotin binding $t_{1/2}$ were calculated using the equations of the first order exponential decays fitted to the plots of (fraction biotin bound at time $t$) vs. $t$ by setting $y = 0.5$ and solving for $t$. Dual-chain avidin has been previously found to be indistinguishable from wild-type avidin in this assay [27].

### 2.5. Surface adhesion

The functionality of the HFBI moiety and surface binding capacity of HFBI–dcAvd were tested by following binding to a hydrophobic surface with an E4 quartz-crystal microbalance with dissipation monitoring (QCM-D; Biolin Scientific, Stockholm, Sweden) [28,29]. QCM crystals (5 MHz AT-cut quartz crystals, Biolin Scientific, Sweden) were spin-coated with polystyrene according to supplier's instructions. Polystyrene petri dishes were dissolved in toluene to a final concentration of 0.5% (w/v). Gold sensor crystals were cleaned by soaking in hot (75 °C) $NH_3/H_2O_2$ solution and subsequent treatment in an UV/ozone chamber (Bioforce Nanosciences, Inc., Ames, US) for 10 min per side. The clean gold crystals were immediately spin-coated with two to three drops of the 0.5% (w/v) polystyrene solution at 2000 rpm of for 20 s. The coated crystals were dried at 80 °C for 30 min and rinsed with EtOH and water prior to use in experiments.

In order to measure binding of HFBI–dcAvd, the polystyrene coated crystals were subjected to a solution of HFBI–dcAvd in PBS buffer (0.1 M sodium phosphate, 0.15 M NaCl, pH 7.2) in the QCM-D instrument. A fresh sample solution was reloaded one to two times, until changes in frequency were no longer observed and the surface was observed to be saturated. The bound layer was rinsed with PBS after every sample loading to remove nonspecifically bound material. Binding of biotinylated substrates was tested by adding a biotinylated fusion of green fluorescent protein and hevein protein (bGH) at 68 μg/ml to the HFBI–dcAvd layer followed by a buffer rinse. For reference non-biotinylated GFP-hevein (GH) was used at the same concentration.

The measured frequency responses $\Delta f$ were used to calculate the mass of protein bound, $\Delta m$, using the Sauerbrey relation (Eq. (1)),

$$\Delta m = -\frac{C \times \Delta f}{n_3} \quad (1)$$

where $C = 17.7$ ng/Hz/cm$^2$ for a 5 MHz quartz crystal and $n_3 = 3$, the overtone number.

Dissipation $D$ describes the dampening of the crystal's oscillation by the adhered molecules and can thus be used to understand the viscoelastic properties of the studied surface layers. $D$ is defined as:

$$D = \frac{E_{lost}}{2\pi E_{stored}} \quad (2)$$

where $E_{lost}$ is the energy lost during one oscillation cycle and $E_{stored}$ is the total energy stored in the oscillator.

## 3. Results

The fusion proteins HFBI–Avd and HFBI–dcAvd were produced successfully in *T. reesei*. After cultivation, HFBI–Avd was found to be adhered to the fungal mycelium while HFBI–dcAvd was found as a soluble protein in the culture medium. Since both proteins were produced with signal sequences for secretion, the different locations of the proteins indicated different solubility characteristics. HFBI–Avd could be released from the mycelium by adding 2% SDS. Attempts to remove the SDS from the extract solution by ion exchange showed that the protein could be retained in solution after SDS removal only by adding ethanol to a concentration of at least 20%. If no ethanol was added the HFBI–Avd precipitated rapidly.

In the case of HFBI–dcAvd different behavior was observed. Two-phase extraction from cell culture supernatant with Berol 532 and isobutanol yielded a 100-fold concentration of the protein confirmed by a well-resolved band in SDS-PAGE (Fig. 3a). Bands of higher molecular weight seen in SDS-PAGE (Fig. 3a, left panel) but not detected in the anti-HFBI Western blot (Fig. 3a, right panel) represent extracellular cellulases originating from *T. reesei*. The ion exchange chromatography run produced two well separated peaks (Fig. 3b) that were analyzed by Western blotting, SDS-PAGE and MALDI-TOF mass spectrometry. The latter peak showed a mass of 42 kDa as well as a positive result in Western blot analysis. The difference in mass of 4 kDa compared to the mass calculated from the amino acid sequence (38 kDa) was assumed to result from glycosylation. This was confirmed by deglycosylation of HFBI–dcAvd with endoglucanase Endo H followed by SDS-PAGE and Western analysis (data not shown). The avidin sequence has one site for N-linked glycosylation at reside Asn-17 in wild-type avidin and dcAvd has thus two glycosylation sites. There are no glycosylation sites on HFBI. From 1 l of supernatant we purified 0.5 mg of HFBI–dcAvd, corresponding to a 50% overall yield.

The effective number of biotin-binding sites per HFBI–dcAvd dimer was determined by using radioactive biotin (Table 1). The value was compared to an estimation obtained from measuring intrinsic tryptophan fluorescence quenching. The radioactivity assay gave a value of $2.9 \pm 0.6$ for the number of biotin binding sites of HFBI–dcAvd, which was well in accordance with the value approximated by fluorescence quenching (2.4). As a reference the same experiments were performed for wild-type avidin, which showed slightly higher number of binding sites. Dissociation rate constants for biotin binding were also determined for HFBI–dcAvd and wild-type avidin by competition of radiolabeled biotin and cold biotin (Table 1) [26]. The dissociation constant for HFBI–dcAvd

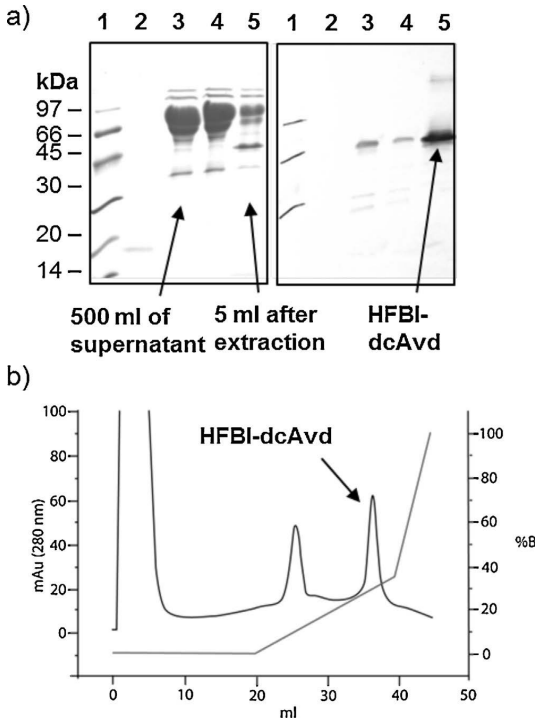


**Fig. 3.** (a) SDS-PAGE gel and Western blot with hydrophobin antibody detection of HFBI–dcAvd purification illustrate the efficiency of the two-phase extraction procedure. Lanes: (1) Molecular weight marker (2) Wild-type avidin (3) Sample of supernatant (15 μl). Total supernatant volume in the purification was 500 ml. (4) Residue (lower phase of two-phase extraction) (5) Back-extracted protein (upper phase of two-phase extraction). Total amount of recovered protein was 5 ml, i.e. concentrated 100-fold during the two-phase separation. (b) Ion-exchange chromatogram of HFBI–dcAvd purification.

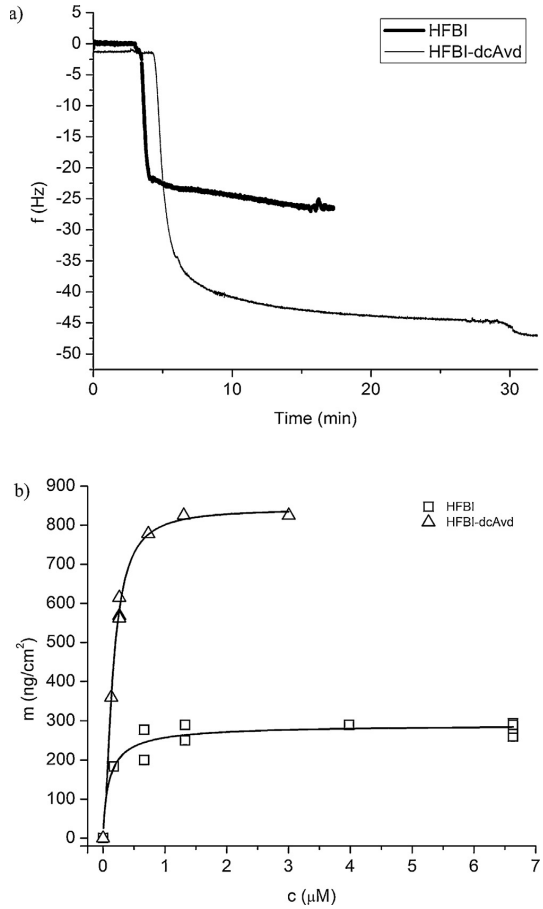


**Fig. 4.** (a) Typical QCM-D sensograms displaying the binding profile of HFBI–dcAvd and native HFBI to polystyrene surface. (b) Binding isotherms for HFBI–dcAvd and HFBI show the amount of HFBI–dcAvd bound m (ng/cm$^2$) to a polystyrene surface as a function of HFBI–dcAvd concentration, $c$ (μM). The lines represent a fit of the one-site Langmuir equation to the data set.

was measured to be $7.6 \pm 0.8 \times 10^{-6}\,s^{-1}$ and for wild-type avidin $4.3 \pm 0.7 \times 10^{-6}\,s^{-1}$.

Self-assembly into surface bound monolayers as well as the substrate binding capacity of HFBI–dcAvd were studied by quartz crystal microbalance measurements (QCM-D). Protein was injected on the polystyrene surface at different concentrations to determine equilibrium binding (Fig. 4a). A −45 Hz change in the oscillation frequency was measured, which translates to a Sauerbrey mass of 825 ng/cm$^2$ (Eq. (1)). No additional binding was observed during subsequent loadings of the HFBI–dcAvd solution. The dissipation energy values were typically low ($\leq 1 \times 10^{-6}$) for both the wild-type HFBI and HFBI–dcAvd. When protein concentrations were as low as 10 μg/ml (0.2 μM) or less, multiple loadings of the sample and longer binding times were required to reach the saturation level. A HFBI–dcAvd solution at a concentration of 50 μg/ml (1.3 μM) resulted in saturation of the surface immediately. Measurements at a range of concentrations gave binding isotherms represented in Fig. 4b. The wild-type HFBI displayed distinctive fast binding and saturation of the surface, while HFBI–dcAvd reached saturation more gradually. The amounts of mass bound presented in Fig. 4b have been calculated from the frequency response of the first sample loading.

The polystyrene sensor crystals were either commercially available polystyrene coated crystals or the polystyrene surface was self-fabricated by spin-coating on commercial gold crystals. Depending on the spin-coating process, the HFBI–dcAvd monolayer resulted in a different frequency response at saturation, suggesting a difference in the surface roughness of the two polystyrene surfaces (data not shown). The same behavior was not observed in the case of HFBI. To ensure reproducible layers, all of the experiments for the binding isotherm were measured on self-fabricated polystyrene surfaces. The amount of HFBI–dcAvd bound on different self-fabricated polystyrene crystals was found to vary by less than 5%, A biotinylated substrate was successfully immobilized on polystyrene via the HFBI–dcAvd monolayer (Fig. 5a). A biotinylated fusion protein of green fluorescent protein and hevein (bGH, 35 kDa) bound to the HFBI–dcAvd surface (42 kDa, 0.01 mg/ml) in a ratio 1:1 of HFBI–dcAvd and bGH, as estimated by comparing the molar amounts calculated from the measured Sauerbrey masses of the HFBI–dcAvd and bGH layers, 670 ng/cm$^2$ and 530 ng/cm$^2$, respectively (Fig. 5a and b). Immobilization of bGH via a HFBI–dcAvd layer resulted in only small increase in dissipation ($1.3 \times 10^{-6}$), indicating a rigid layer structure (Fig. 5c). The control experiment where bGH was subjected to a layer of wild-type HFBI showed a significantly lower amount of bound bGH (70 ng/cm$^2$).

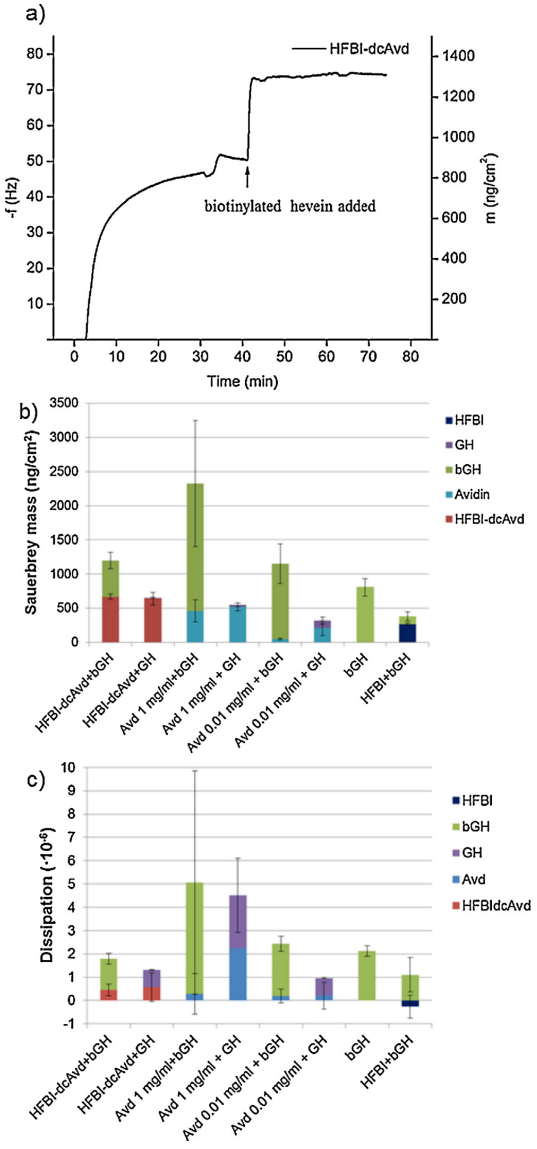


**Fig. 5.** QCM-D measurements displaying the differences of the HFBI–dcAvd and physisorbed avidin in binding a biotinylated GFP-hevein (bGH). (a) QCM-D measurement data demonstrating the functionality of the HFBI–dcAvd scaffold on a polystyrene surface. The arrow marks the addition of the biotinylated substrate (GFP-hevein). (b) Sauerbrey masses of examined protein layers. (c) Dissipation values are a measure of viscoelasticity of the adhered layer.

In contrast to HFBI–dcAvd wild-type avidin physisorbed on polystyrene with poor efficiency, as a 0.1 mg/ml concentration yielded a Sauerbrey mass of only ~100 ng/cm$^2$. This value is lower than expected for avidin monolayer on an ideally flat surface (580 ng/cm$^2$). Increasing the avidin concentration to 1 mg/ml produced a layer of 490 ng/cm$^2$, which is comparable to the mass of an avidin monolayer (Fig. 5b). However, binding of avidin was not reproducible as conveyed by the large standard deviation of parallel QCM-D measurements (Fig. 5b and c). The structure of the avidin layer was unordered, as was displayed by elevated dissipation values. The Sauerbrey mass of bGH on the physisorbed avidin layer was on average 1860 ng/cm$^2$. This translates to a molar ratio of 7:1 of bGH to avidin, which is clearly too high for a specifically bound, ordered molecular layer. Also the dissipation values for bGH bound to physisorbed avidin were high, in the range of 2.2–4.7 × 10$^{-6}$, confirming the formation of a soft, unordered layer.

A notable amount (1100 ng/cm$^2$) of bGH was bound on wild-type avidin also in the case where the mass of the avidin layer did not correspond to a monolayer coverage (Fig. 5b and c). This result was explained by the observed nonspecific binding of the biotinylated protein bGH on the polystyrene surface (800 ng/cm$^2$). Nonspecific binding was even more pronounced for the biotinylated protein bGH than for the nonbiotinylated GH, which is explained by the charge neutralizing effect of the biotinyl modification.

## 4. Discussion

Here we have shown how avidin and hydrophobin can be fused together to create chimeric proteins that have the dual functionality of assembling at interfaces and binding strongly to biotin. First, we investigated how the fusion protein should be constructed taking into account the functional tetrameric structure of avidin, and second, we showed how the engineered fusion protein functioned in making avidinylated surfaces by molecular self-assembly. Two different protein architectures were investigated, HFBI–Avd and HFBI–dcAvd. In the construct HFBI–Avd, each HFBI was tethered to one avidin subunit. This stoichiometry leads to an avidin-tetramer where each tetrameric complex comprised four HFBI units (Fig. 1a). Characterization showed that this construct was poorly soluble. The likely reason for this was that the four HFBI units could further interact with the hydrophobins of other HFBI–Avd complexes, leading to a poorly soluble network. For the wild-type hydrophobin such interactions increase solubility because the multimerization provides shielding of hydrophobic patches [11]. However, it is likely that in this case the shielding resulted in an overall lower solubility because of the structural constraints. Due to the poor solubility of the HFBI–Avd construct it was unfeasible to use in functional testing. Previously similar problems in relation to constructing fusion proteins of avidin have been reported due to its multivalency. In the case of S-layer avidin fusions a separate step was required to recombine fused and non-fused avidin in a functional ratio of three wild-type avidin monomers and one fusion protein [30]. We found such an approach impractical and not supportive of our goals of having a straightforward procedure enabled by protein design.

The strategy involving the fusion of HFBI with a dual-chain variant of avidin (dcAvd) to produce the chimeric protein (HFBI–dcAvd) resulted in a soluble and functional protein. As shown in Fig. 1b, the fusion of the polypeptide chains of two avidin monomers into a dual-chain avidin was designed to form an equivalent quaternary structure to that of avidin, however composed of only two polypeptide chains. Therefore, the dual-chain avidin dimer contains only two hydrophobins, as opposed to four hydrophobin domains in the HFBI–Avd tetramer. The dimerization of HFBI–dcAvd can lead to two different configurations, with HFBI molecules on the same side of the dcAvd moiety or on opposite sides (Fig. 1b) [31]. The HFBI–dcAvd construct resulted in a soluble protein that was readily produced and purified. The functionality of the HFBI–dcAvd was corroborated already during initial purification steps by noting that multimeric assembly did not interfere with the two-phase surfactant purification procedure [25]. Experiments to assess the biotin-binding behavior of HFBI–dcAvd confirmed that the fusion protein had a similar functionality as the wild-type avidin for

binding its ligand, biotin [32]. The slight difference in values of dissociation constant for biotin-binding does not indicate a significant difference in functionality for HFBI–dcAvd compared to wild-type avidin.

QCM-D was used as a method to characterize the functionality of HFBI–dcAvd for forming self-assembled interfaces. These measurements yielded binding isotherms and approximations of surface binding affinity of both proteins. From these experiments it could be seen that HFBI and its fusion protein HFBI–dcAvd behaved similarly and for both a maximum binding capacity was reached. These mass values obtained at saturation were compared to estimations calculated on the basis of known structures of HFBI and avidin. The experimental value for the maximal amount of HFBI bound to the surface (290 ng/cm$^2$) corresponded to a surface area per molecule of 4.3 nm$^2$ calculated using a molecular mass of 7.5 kDa. This value is well in agreement with the structure of HFBI which has a diameter of about 2 nm [5]. The corresponding calculation for HFBI–dcAvd (maximal amount bound 825 ng/cm$^2$, *MW* 42 kDa) gave an area per molecule of 8.5 nm$^2$. This value suggests a dense packing of the fusion protein. The dense packing is also confirmed by the low dissipation values. However, the 15 amino acid linker is roughly 6 nm long, estimated on the basis of C—N and C—C bond lengths (1.3–1.5 Å) and thus allows relative movement of the fusion protein partners. While the presented molecular areas indicate molecular packing comparable to a molecular monolayer, the values still remain estimates due to the long, flexible linker and the roughness of the applied polystyrene surfaces. The 95% confidence interval for the dissociation constants for HFBI binding on polystyrene was between 0.02 and 0.2 μM, and for HFBI–dcAvd 0.1 to 0.5 μM. Despite the overlap between the confidence intervals, the binding profile displayed by the QCM sensograms suggests that the HFBI–dcAvd fusion protein has a slightly lower polystyrene binding affinity. This could be due to interference of the molecular binding mechanisms of HFBI due to the relatively large fusion partner.

Next we analyzed the functional properties of the HFBI–dcAvd in comparison to wild-type avidin by using self-assembled surfaces of these proteins and by investigating how a biotinylated protein bound to the surface. In general, the attachment of such compounds to functionalized surfaces is affected by a number of different factors. The orientation of the surface-functionalization proteins determines the loading capacity on the surface as well as the subsequent position of the immobilized compounds. Another direct result of controlled orientation is enhanced reproducibility. Bound proteins are also likely to be more protected from denaturing surface interactions when correctly positioned. The surface coverage that can be obtained using molecular scaffolds is determined by the size of the surface scaffold molecule as well as the size of the bound compound. Steric clashing of the functional domain may disrupt the self-assembly of the surface-binding compound leading to a suboptimal surface layer. Minimization of unspecific binding to the surface is also a desired effect in many applications. Taking in account all these issues, the outcome is clearly much reliant on the individual properties of the compounds to be immobilized and many problems are highly case-dependent.

HFBI–dcAvd formed an effectively functionalized, rigid molecular surface for immobilization of biotinylated molecules. At the same concentration (0.01 mg/ml), wild-type avidin bound weakly to polystyrene. Using the natural rubber allergen hevein (GH) we investigated in more detail how the hydrophobin-fused avidin differs from wild-type avidin in surface functionalization (Fig. 5). We noticed that at a higher concentration (1 mg/ml) more avidin was adsorbed, but the structure and reproducibility of the avidin surface were poor compared to HFBI–dcAvd. The formed avidin layers bound the biotinylated hevein (bGH) in a seemingly high amount. Considering the poor reproducibility and softness of the surface layer and observed nonspecific binding of bGH to both the bare polystyrene as well as the avidin surfaces, the difference to the HFBI–dcAvd mediated immobilization was clear. HFBI–dcAvd performed very predictably, binding the biotinylated antigen (bGH) in a 1:1 molar ratio (HFBI–dcAvd monomer to bGH) while exhibiting very low binding of the non-biotinylated antigen (GH). Control experiments revealed notable nonspecific absorption of bGH to the bare polystyrene surface. Nonspecific absorption played a role also when immobilizing bGH on the avidin treated surface, taken the observed unexpectedly high molar ratio of bGH to avidin. Binding of the non-biotinylated GH on the avidin layers was low, indicating that the non-specific binding was enhanced by biotinylation, possibly due to an increase in protein hydrophobicity. However, this nonspecific binding was significantly diminished by the HFBI surface.

While the QCM-D measurements confirmed that HFBI–dcAvd forms stable monolayers on hydrophobic surfaces, a clear improvement over avidin functionalization was seen in the layer structures as revealed by the dissipation values. The high functionality and dense packing of HFBI–dcAvd indicates that its structural conformation is well suited for surface binding. This means that the hydrophobin domains are likely to be directed to the same side of the protein or at least that if the hydrophobins are positioned diagonally, this does not sterically prevent the binding. Therefore HFBI–dcAvd functionalization introduced two important characteristics to polystyrene: (1) lowered nonspecific binding and (2) capability to immobilize biotinylated molecules in highly ordered fashion.

Dissipation values obtained in QCM-D measurements describe the energy loss of a freely oscillating crystal (Eq. (2)). Hence, any viscoelastic layer adhered to the crystal will cause an elevated dissipation value, as the layer is not coupled to the crystal movement and dampens the oscillation. The dissipation values for a wild-type HFBI surface are well below $1 \times 10^{-6}$ units, as were the measured dissipation values for the HFBI–dcAvd layer [33,34]. When bGH was immobilized on HFBI–dcAvd, the increase in dissipation was significantly lower than when bGH was immobilized on avidin (Fig. 5c). The large dissipation values imply that the layer structure was loose and thus weakened, possibly as a result of larger complex formation at the surface. We also noticed large variations in the amount of avidin immobilized on the polystyrene surface, whereas the HFBI–dcAvd layers were reproducible (Fig. 5b). When bGH was introduced on a wild-type HFBI surface only very little protein was bound, showing that the wild-type HFBI surface acts as a blocking layer.

## 5. Conclusions

We have shown how protein engineering can be used to combine the surface adhesive self-assembly properties of hydrophobin proteins and the use of the high affinity of avidin to bind its ligand, biotin, for functionalizing surfaces. The combination of these functionalities was challenging because of the properties of both proteins to form quaternary structures and assemblies in solution. The fusion approach allowed also the use of an aqueous-two phase method to purify the protein in a very efficient way.

Overall, this work elucidates the clear advantages that can be gained by methods of genetic engineering and self-assembly. Control over fusion protein stoichiometry can lead to improved results when managed at the molecular engineering stage. Organized and controlled surface functionalization is important in bio-interface engineering in relation to many fields of technology. The nanometer size-scale of the components, controlled interactions and individual multimerization habits of both protein partners make feasible also expansion of the application scope for nanotechnological purposes.

## Acknowledgments

We are grateful to Dr. Henri Nordlund, deceased in July 2008, for his participation and ideas in the early stages of this work. We thank Mrs. Riitta Suihkonen and Mrs. Arja Kiema for assistance in protein production and purification. Mr. Michael Bailey is acknowledged for work on the fermentations and Dr. Marja-Leena Laukkanen for kindly delivering the biotinylated GFP-hevein protein for immobilization studies. This research was supported by grants MNT-ERA.net/TEKES 40407/09 and GraNBis from the Finnish Funding Agency for Technology and Innovation (Tekes) and grants SA 136288, 140978 and 123099 from the Academy Finland. All authors except TN-S are members of the The National Doctoral Programme in Informational and Structural Biology (ISB).

## References

[1] E. Busseron, Y. Ruff, E. Moulin, N. Giuseppone, Nanoscale 5 (2013) 7098.
[2] H.D. Espinosa, J.E. Rim, F. Barthelat, M.J. Buehler, Prog. Mater. Sci. 54 (2009) 1059.
[3] V. Linko, H. Dietz, Curr. Opin. Biotechnol. 24 (2013) 555.
[4] M.B. Linder, G.R. Szilvay, T. Nakari-Setala, M.E. Penttila, FEMS Microbiol. Rev. 29 (2005) 877.
[5] J. Hakanpaa, G.R. Szilvay, H. Kaljunen, M. Maksimainen, M. Linder, J. Rouvinen, Protein Sci. 15 (2006) 2129.
[6] H.A.B. Wosten, M.L. de Vocht, Biochim. Biophys. Acta (BBA)—Rev. Biomembr. 1469 (2000) 79.
[7] A. Paananen, E. Vuorimaa, M. Torkkeli, M. Penttila, M. Kauranen, O. Ikkala, H. Lemmetyinen, R. Serimaa, M.B. Linder, Biochemistry 42 (2003) 5253.
[8] R. Serimaa, M. Torkkeli, A. Paananen, M. Linder, K. Kisko, M. Knaapila, O. Ikkala, E. Vuorimaa, H. Lemmetyinen, O. Seeck, J. Appl. Crystallogr. 36 (2003) 499.
[9] G.R. Szilvay, A. Paananen, K. Laurikainen, E. Vuorimaa, H. Lemmetyinen, J. Peltonen, M.B. Linder, Biochemistry 46 (2007) 2345.
[10] J.G.H. Wessels, Ann. Rev. Phytopathol. 32 (1994) 413.
[11] G.R. Szilvay, T. Nakari-Setala, M.B. Linder, Biochemistry 45 (2006) 8590.
[12] K. Kurppa, H. Jiang, G.R. Szilvay, A.G. Nasibulin, E.I. Kauppinen, M.B. Linder, Angew. Chem. Int. Ed. 46 (2007) 6446.
[13] P. Laaksonen, M. Kainlauri, T. Laaksonen, A. Shchepetov, H. Jiang, J. Ahopelto, M.B. Linder, Angew. Chem. Int. Ed. 49 (2010) 4946.
[14] N.M. Green, Biochem. J. 89 (1963) 585.
[15] N.M. Green, Methods Enzymol. 184 (1990) 51.
[16] O.H. Laitinen, H.R. Nordlund, V.P. Hytonen, M.S. Kulomaa, Trends Biotechnol. 25 (2007) 269.
[17] O. Livnah, E.A. Bayer, M. Wilchek, J.L. Sussman, Proc. Nat. Acad. Sci. U.S.A. 90 (1993) 5076.
[18] L. Pugliese, A. Coda, M. Malcovati, M. Bolognesi, J. Mol. Biol. 231 (1993) 698.
[19] P. Ringler, G.E. Schulz, Science 302 (2003) 106.
[20] J. Turkova, J. Chromatogr. B 722 (1999) 11.
[21] M. Liss, B. Petersen, H. Wolf, E. Prohaska, Anal. Chem. 74 (2002) 4488.
[22] H.R. Nordlund, O.H. Laitinen, V.P. Hytonen, S.T.H. Uotila, E. Porkka, M.S. Kulomaa, J. Biol. Chem. 279 (2004) 36715.
[23] V.R. Hytonen, O.I.H. Laitinen, T.T. Airenne, H. Kidron, N.J. Meltola, E.J. Porkka, J. Horha, T. Paldanius, J.A.E. Maatta, H.R. Nordlund, M.S. Johnson, T.A. Salminen, K.J. Airenne, S. Yla-Herttuala, M.S. Kulomaa, Biochem. J. 384 (2004) 385.
[24] M. Penttila, H. Nevalainen, M. Ratto, E. Salminen, J. Knowles, Gene 61 (1987) 155.
[25] M. Linder, K. Selber, T. Nakari-Setala, M.Q. Qiao, M.R. Kula, M. Penttila, Biomacromolecules 2 (2001) 511.
[26] L.A. Klumb, V. Chu, P.S. Stayton, Biochemistry 37 (1998) 7657.
[27] V.P. Hytonen, H.R. Nordlund, J. Horha, T.K.M. Nyholm, D.E. Hyre, H. Kulomaa, N.J. Porkka, A.T. Marttila, P.S. Stayton, O.H. Laitinen, M.S. Kulomaa, Proteins-Struct. Funct. Bioinf. 61 (2005) 597.
[28] M. Rodahl, F. Hook, C. Fredriksson, C.A. Keller, A. Krozer, P. Brzezinski, M. Voinova, B. Kasemo, Faraday Discuss. 107 (1997) 229.
[29] F. Hook, M. Rodahl, P. Brzezinski, B. Kasemo, Langmuir 14 (1998) 729.
[30] D. Moll, C. Huber, B. Schlegel, D. Pum, U.B. Sleytr, M. Sara, Proc. Nat. Acad. Sci. U.S.A. 99 (2002) 14646.
[31] V.P. Hytonen, J. Horha, T.T. Airenne, E.A. Niskanen, K.J. Helttunen, M.S. Johnson, T.A. Salminen, M.S. Kulomaa, H.R. Nordlund, J. Mol. Biol. 359 (2006) 1352.
[32] H.R. Nordlund, V.P. Hytonen, J. Horha, J.A.E. Maatta, D.J. White, K. Halling, E.J. Porkka, J.P. Slotte, O.H. Laitinen, M.S. Kulomaa, Biochem. J. 392 (2005) 485.
[33] M. Linder, G.R. Szilvay, T. Nakari-Setala, H. Soderlund, M. Penttila, Protein Sci. 11 (2002) 2257.
[34] M.S. Gruner, G.R. Szilvay, M. Berglin, M. Lienemann, P. Laaksonen, M.B. Linder, Langmuir 28 (2012) 4293.

# IV

Soikkeli Miikka; Kurppa, Katri; Kainlauri, Markku; Arpiainen, Sanna; Paananen, Arja; Gunnarsson, David; Joensuu, Jussi; Laaksonen, Päivi; Prunnila, Mika; Linder, Markus; Ahopelto, Jouni. 2016. Graphene Biosensor Programming with Genetically Engineered Fusion Protein Monolayers. American Chemical Society. ACS Applied Materials and Interfaces, volume 8, issue 12, pages 8257–8264. ISSN: 1944-8244. DOI:10.1021/acsami.6b00123.

ACS APPLIED MATERIALS & INTERFACES

Research Article

www.acsami.org

# Graphene Biosensor Programming with Genetically Engineered Fusion Protein Monolayers

Miika Soikkeli,[†,§] Katri Kurppa,[†,§] Markku Kainlauri,[†,§] Sanna Arpiainen,[†,§] Arja Paananen,[†] David Gunnarsson,[†] Jussi J. Joensuu,[†] Päivi Laaksonen,[†,⊥] Mika Prunnila,[†] Markus B. Linder,[†,‡] and Jouni Ahopelto*[,†]

[†]VTT Technical Research Centre of Finland Ltd., P.O. Box 1000, FI-02044 VTT, Espoo, Finland

[‡]School of Chemical Technology, Aalto University, P.O. Box 6100, FI-00076 AALTO, Espoo, Finland

Supporting Information

**ABSTRACT:** We demonstrate a label-free biosensor concept based on specific receptor modules, which provide immobilization and selectivity to the desired analyte molecules, and on charge sensing with a graphene field effect transistor. The receptor modules are fusion proteins in which small hydrophobin proteins act as the anchor to immobilize the receptor moiety. The functionalization of the graphene sensor is a single-step process based on directed self-assembly of the receptor modules on a hydrophobic surface. The modules are produced separately in fungi or plants and purified before use. The modules form a dense and well-oriented monolayer on the graphene transistor channel and the receptor module monolayer can be removed, and a new module monolayer with a different selectivity can be assembled in situ. The receptor module monolayers survive drying, showing that the functionalized devices can be stored and have a reasonable shelf life. The sensor is tested with small charged peptides and large immunoglobulin molecules. The measured sensitivities are in the femtomolar range, and the response is relatively fast, of the order of one second.

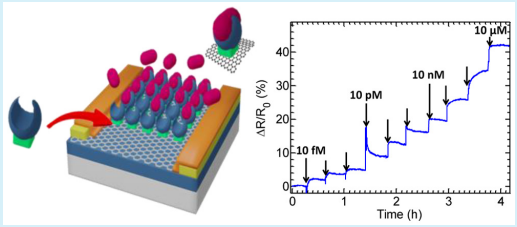


**KEYWORDS:** *graphene, biosensor, fusion protein, hydrophobin, self-assembly, Debye length*

## 1. INTRODUCTION

Health and well-being are recognized as one of the growing challenges in today's aging society requiring easy-to-use monitoring tools for daily life. One of the emerging trends is preventive health care, which is turning research toward point-of-care diagnostics and qualitative and quantitative detection of biological and chemical species such as disease markers.[1] In many cases, culturing and labeling are required, which make diagnostics slow and sometimes even cumbersome, directing the efforts to development of label-free techniques. Quantitative label-free charge based detection of analytes has been recently demonstrated with carbon nanotube (CNT), graphene, and semiconductor nanowire based sensors.[2−5] Regarding graphene, different forms varying from functionalized reduced graphene oxide (rGO) mixtures to pristine graphene have been utilized in sensors.[6−10] Graphene field effect transistors (GFETs) are extremely sensitive to charges residing in the vicinity of the graphene channel.[11] Charges have a strong effect on the position of the Dirac peak, which provides a measure of the amount of charge carried by the analytes. Because most biomolecules, such as antibodies, DNA, peptides, proteins, and lipids, are inherently charged, their detection with field effect sensors is essentially label-free. Compared to other FET-type sensors, for example, silicon nanowires, GFETs have similar charge sensitivity but larger surface area for functionalization, higher chemical stability, and much larger fabrication tolerances. The main challenges are related to biorecognition, particularly to the reliable and reproducible immobilization of the receptor layer for selective binding of the desired analyte.

Hydrophobin proteins have been optimized by evolution to assemble at interfaces.[12] The proteins have a hydrophobic patch, which binds relatively strongly to hydrophobic surfaces, such as graphene, through van der Waals interactions and forms a dense monomolecular layer with a specific molecular orientation.[13−16] Hydrophobin binding on graphene has been previously utilized to exfoliate graphene[15] and to employ hydrophobin fusion proteins as binders in graphene−nanofibrillous cellulose composites.[17] Hydrophobins have also been used with immobilized glucose oxidase in amperometric sensing of glucose on platinum,[18] in multiwall carbon nanotube electrodes,[19] and with immobilized choline oxidase for choline detection on gold electrodes.[20]

In this work, we report on a generic biosensor concept, which combines the high charge sensitivity of the GFET with receptor modules that are produced separately providing both

Received: January 5, 2016
Accepted: March 10, 2016
Published: March 10, 2016

  

DOI: 10.1021/acsami.6b00123
ACS Appl. Mater. Interfaces 2016, 8, 8257−8264

the immobilization and sensing functions. Receptor modules are fusion proteins with the receptor molecule genetically attached to an HFBI hydrophobin anchor, which provides the immobilization. The modules are produced in fungi or plants using fusion techniques and are purified before use. The attachment relies on directed self-assembly, resulting in a dense and well-oriented monolayer of the modules on the GFET channel. The approach enables a single step in situ functionalization of the sensor with purified receptor modules and also in situ removal of the modules and refunctionalization, that is, programming. In addition, it is shown that the module monolayers on GFET survive drying and rewetting without losing sensitivity to analyte, thus making it possible to realize disposable chips that are sensitized to a preselected analyte. We first demonstrate the sensor concept using receptor modules with HFBI anchor and $Z_E$ peptide as the receptor to detect the $Z_R$ peptide. The advantage of these helical peptides is their small size, which should not hinder the self-assembly of the hydrophobins on graphene, and their relatively well-defined charge. As a more realistic test case, we use HFBI-Protein A receptor modules and immunoglobulin analyte. Protein A is known to bind different immunoglobulin subclasses, with highest affinity to the members of the IgG class, and was applied here to detect IgG1 antibody. The sensor device and measurement configuration are schematically depicted in Figure 1.

## 2. EXPERIMENTAL SECTION

**2.1. Fabrication of the Graphene Field Effect Transistors.** GFETs were fabricated from graphene grown by photothermal chemical vapor deposition (PT-CVD) on copper foil (Alfa Aesar, 99.999%).[21] Monolayer graphene was transferred using a sacrificial poly(methyl methacrylate) (PMMA) support onto a silicon substrate covered with a 300 nm thick thermal silicon dioxide layer. The $SiO_2$ surface was treated with hexamethyldisilazane (HMDS) to promote adhesion and to enhance the electrical characteristics of graphene.[22] The copper foil was etched in alkaline solution. PMMA support was removed in subsequent ultrasonic baths of acetone, isopropanol, and deionized water, followed by a 3 h anneal at 350 °C in vacuum. The clean graphene surface was protected with a 20 nm thick $TiO_2$ layer grown by atomic layer deposition (ALD). To initiate the ALD growth, a 1 nm thick layer of Ti was first evaporated on graphene and was allowed to oxidize. Graphene was patterned using optical lithography and oxygen plasma. The electrical contacts were formed by thin evaporated Ti/Au (5/50 nm) metallization and lift-off. The electrodes around the channels were protected from the liquid environment with a 85 nm thick $TiO_2$ layer grown by ALD. Channels (30 $\mu$m × 190 $\mu$m graphene) were opened in polysilicon etch, and the chips were wire bonded to chip carriers.

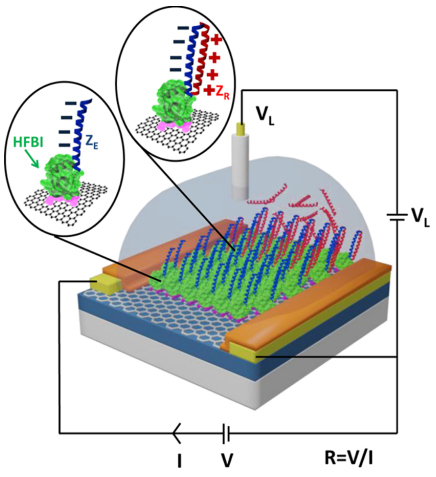


**Figure 1.** Functionalized GFET biosensor and measurement configuration shown schematically. $V_L$ is the liquid gate voltage and R is the graphene channel resistance. In this case, the GFET channel is functionalized with a monolayer of HFBI-$Z_E$ receptor modules and the charge of the modules define the resistance of the channel, that is, fix the position of the Dirac peak. The analyte molecules bound by the receptors shift the position of the peak and the amount of the shift provides information on the concentration of the analyte in the sample.

**2.2. Receptor Modules and Analytes.** HFBI-Protein A modules were produced in transient expression mode in *Nicotiana tabacum* plants via agroinfiltration as described previously.[23] Proteins were extracted for purification by homogenizing frozen leaves in PBS buffer supplemented with 2% (W/V) sodium ascorbate and 1 mM EDTA (4× buffer volume/leaf weight). The homogenate was clarified twice by centrifugation (10 min at 3220*g* at 4 °C). The supernatant was warmed to RT and mixed with Triton X-114 (3% w/v, Sigma-Aldrich, USA). The phases were allowed to separate at room temperature. The top (detergent-poor) phase was removed, and the detergent phase was washed with isobutanol (10× volume/detergent mass). After buffer exchange, the extract was polished by affinity chromatography using a Streptactin macroprep column according the manufacturers protocol (IBA, Germany).

The fusion protein HFBI-$Z_E$ was produced in the filamentous fungus *Trichoderma reesei*.[15] The fusion proteins were purified by standard two-phase extraction procedure as described previously.[23,24] Proteins were diluted to the concentration of 0.1 mg/mL in the buffer solution (100 mM sodium phosphate pH 7). This concentration has been found to suit best to QCM investigations with hydrophobin fusions.

Sequences of $Z_E$ and $Z_R$ regions:[25]

$Z_E$, L E I E A A F L E Q E N T A L E T E V A E L E Q E V Q R L E N I V S Q Y R T R Y P G L;

$Z_R$, L E I R A A F L R R R N T A L R T R V A E L R Q R V Q R L R N E V S Q Y E T R Y G P L.

The analyte for HFBI-$Z_E$ was a synthetic peptide $Z_R$ (5 kDa, Biomatik Co., Ontario, Canada) and for HFBI-Protein A antibody IgG1 lambda (150 kDa, Sigma-Aldrich, St.Louis, USA).

The estimation of net charges of the peptides and hydrophobin was carried out by summing the charges of each of the amino acids using the p$K_a$ values. For $Z_E$ and $Z_R$, the assumption was that all the side chains can have effect on the net charge. For HFBI, the cysteine amino acids were excluded from the net charge calculation since it is known that they form sulfur bridges with each other thus stabilizing the hydrophobin structure, and not affecting the net charge.[26]

**2.3. Atomic Force Microscopy (AFM).** Topography images of HFBI-Protein A and HFBI-$Z_E$ layers on graphene were captured with NanoScopeV Multimode8 AFM (E scanner, Bruker). As deposited CVD graphene on catalytic metal surface (Pt) and CVD graphene transferred on $SiO_2$ were used as substrates. Self-assembly of the receptor module layers was performed in identical conditions that were used for GFET sensor programming. Freshly prepared module layers were imaged first in the buffer solution (100 mM NaP, pH 7) in ScanAsyst mode using ScanAsyst-Fluid+ cantilevers for $SiO_2$ samples (the images are shown in the Supporting Information) and Fluid cantilevers for Pt samples (Bruker, $f_0$ = 150 kHz, k = 0.7 N/m) with a scan rate of 1.6 Hz. After imaging in buffer, the module layers were rinsed gently with buffer and milli-Q water and dried under $N_2$. Samples were stored in a container under $N_2$ for 1−3 h before imaging in dry state. Images of dry module layers were recorded in the ScanAsyst mode in air using ScanAsyst-Air cantilevers (Bruker, $f_0$ = 70 kHz, k = 0.4 N/m) with a scan rate of 1.6 Hz. These conditions were used also for the clean graphene surfaces. Rewetting of module layers


DOI: 10.1021/acsami.6b00123
ACS Appl. Mater. Interfaces 2016, 8, 8257−8264

was carried out by placing buffer solution on the sample surface and starting imaging in buffer within 5−15 min. Imaging was performed as described above for the freshly prepared samples. Images were flattened to remove possible tilt in the image data, and no further image processing was performed. The NanoScope Analysis software (Bruker) was used for image processing and analysis.

**2.4. Quartz Crystal Microbalance (QCM-D) Measurements.** A QCM-D (E4, Biolin Scientific, Sweden) was used to measure the binding of HFBI-Protein A and HFBI-$Z_E$ modules on hydrophobic substrates and the binding of the corresponding analytes to the receptor modules. Polystyrene coated 5 MHz quartz crystals were purchased ready-made at Biolin Scientific or spin-coated on gold coated crystals according to supplier's protocol. Binding on graphene was tested with CVD graphene transferred on the crystals. The crystals were rinsed with ethanol and MQ water and dried with $N_2$ prior to measurement. Buffer solution was 100 mM sodium phosphate at pH 7. In analysis, solution of HFBI-$Z_E$ or HFBI-Protein A diluted in the buffer (100 $\mu$g/mL, 500 $\mu$L) was pumped into the measurement chamber at 0.1 mL/min rate. The adsorbed layer was next rinsed with the buffer. Treatment was repeated, but additional binding was not detected. The analyte solution was then injected into the chamber and rinsed with the buffer to monitor selective binding.

**2.5. Electrical Measurements and Fluidic Setup.** All the measurements were performed using a single GFET. The sensor was analyzed using a fluidic chamber formed by mechanically clamping a cover to the sensor chip with an O-ring sealing. The polyether ether ketone (PEEK) cover had tubing for liquid inlet and outlet and for a Ag/AgCl reference electrode (1 mm diameter leak free reference electrode by Harvard Apparatus). The functionalization of the graphene channel was carried out using a similar cover without the electrode. A computer controlled syringe pump system was used to feed controlled amounts of protein and buffer solutions into the chamber. The liquid gate potential was controlled by applying a voltage to the Ag/AgCl reference electrode by a semiconductor parameter analyzer (HP4142B). The resistance of the graphene channel was measured in 4-point configuration using a lock-in amplifier with 100 nA AC-bias at a frequency of 11.433 Hz. The silicon substrate of the graphene sensor chip was grounded. The data have not been normalized.

**2.6. Sensor Analysis.** Before each series of measurements, the graphene surface was cleaned with 3 mL of acetone and ethanol and 10 mL of DI water. Then 3 mL of the buffer was introduced, and the resistance of the graphene channel was recorded as a function of liquid potential after 25 min stabilization. The sensor was functionalized by flushing with HFBI-$Z_E$ or HFBI-Protein A solution (100 $\mu$g/mL) for 3 min at 0.3 mL/min of flux. The surface was let to stabilize for 60 min, rinsed with the buffer solution for 5 min, and dried with $N_2$. The fluidic chamber was replaced by a clean one, and the sensor was rinsed again with the buffer and channel resistance measured. Sensitivity measurements were performed with the analytes described in the Receptor Modules and Analytes section above, with 1 min of pumping and 25 min of stabilization for each concentration. To test the effect of the buffer concentration on the sensitivity, the clean sensor was first measured in 10 mM and 100 mM NaP buffers. Then the sensor was functionalized with HFBI-$Z_E$ receptor modules as described above and measured in the 10 mM buffer and subsequently in the 100 mM buffer solution.

## 3. RESULTS AND DISCUSSION

**3.1. Directed Self-Assembly and Surface Coverage.** High surface coverage and packing density of the receptor modules are essential to obtain high sensitivity via optimal net affinity of the specific analyte and to prevent unspecific binding from the analyte medium. It has been shown earlier that HFBI proteins form a full dense monolayer on highly ordered pyrolytic graphite.[16] In this work, we have investigated the surface coverage of the HFBI-$Z_E$ and HFBI-Protein A receptor modules formed by a single step directed self-assembly. The surface coverage was studied using AFM both in liquid and dry conditions. AFM images of a clean CVD graphene surface on platinum as well as both HFBI-$Z_E$ and HFBI-Protein A functionalized surfaces are shown in Figure 2. The surfaces

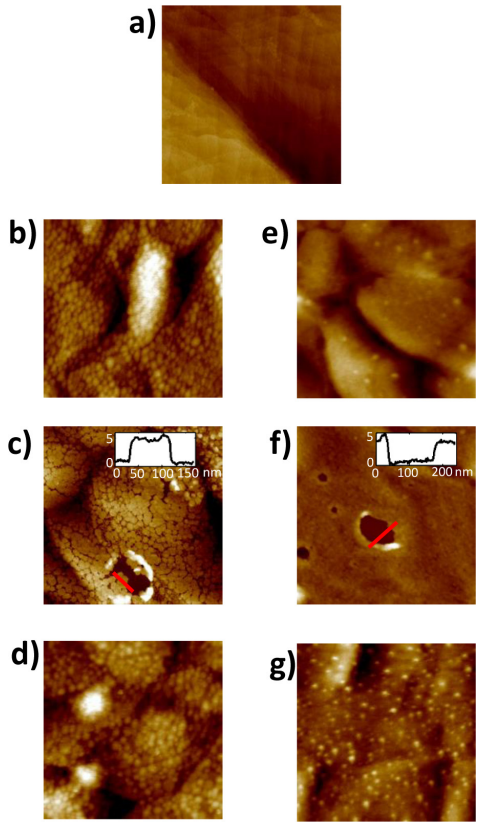


**Figure 2.** AFM topography images of clean, HFBI-$Z_E$, and HFBI-Protein A receptor module layers on CVD graphene on platinum. (a) Clean graphene surface on platinum before any functionalization. (b) Surface after HFBI-$Z_E$ functionalization in 100 mM pH 7 NaP buffer, (c) after drying in $N_2$, and (d) after rewetting in the buffer. (e) Surface after HFBI-Protein A functionalization in 100 mM pH 7 NaP buffer, (f) after drying, and (g) after rewetting in the buffer. For both of the receptor modules, protein film shrinkage and possible mechanical forces during the drying tend to create cracks in the film, but damage is healed in both cases after 5 min of rewetting in the buffer. The height profiles of the dried samples in the insets of panels c and f correspond to the red lines in the same panels. The thickness of both the dried HFBI-$Z_E$ and HFBI-Protein A layers is 4−5 nm, corresponding to a typical thickness of a monomolecular fusion protein layer after drying. The image size is 1 × 1 $\mu m^2$ and height scale 15 nm in all the images.

were imaged in wet state in sodium phosphate buffer immediately after the functionalization, after drying for a few hours in $N_2$, and finally after rewetting in the buffer. Both receptor modules form a dense surface monolayer layer immediately after the functionalization. Drying can induce some cracks in the layer but after rewetting in the buffer solution the module monolayer is healed and no cracks can be


DOI: 10.1021/acsami.6b00123
ACS Appl. Mater. Interfaces 2016, 8, 8257−8264

observed. The thicknesses of both dried HFBI- $Z_E$ and HFBI-Protein A layers are within 4−5 nm, which fits well to the thickness of a monomolecular layer of hydrophobins in the dry state.[27] The results are similar on graphene transferred onto $SiO_2$, and the corresponding AFM images can be found in the Supporting Information.

**3.2. Quartz Crystal Microbalance Measurements.** The AFM results are further confirmed by the QCM analysis showing that the self-assembly of the HFBI-$Z_E$ modules on a hydrophobic polystyrene surface creates a rigid monolayer with surface coverage close to unity (see Supporting Information). The QCM data of self-assembly of HFBI-Protein A receptor modules on hydrophobic polystyrene surface and the subsequent response to introduction of IgG1 analyte are shown in Figure 3.

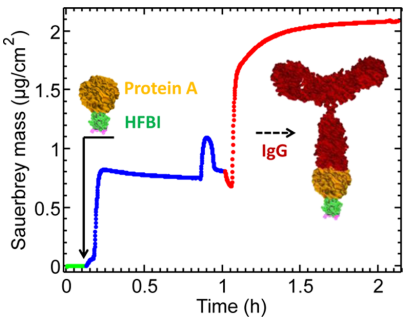


**Figure 3.** QCM sensogram showing the formation of the HFBI-Protein A receptor module layer on hydrophobic polystyrene surface together with the subsequent binding of the IgG1 analyte. The blue curve shows the mass increase due to the self-assembly of the monolayer of the receptor modules, and the red shows the subsequent binding of the analyte. The hump at the end of the blue curve is due to a rinse pulse with the buffer.

The Sauerbrey mass of the HFBI-Protein A monolayer corresponds to an average 3.2 ± 0.2 nm spacing between the molecules (see Supporting Information). This agrees with the estimated diameter of the Protein A part of the HFBI-Protein A fusion,[28] suggesting formation of a uniform and dense surface coverage, agreeing with the AFM results. From the QCM data, the IgG1 binding ratio to the receptor modules was found to be roughly 50−60% at 8 nM analyte concentration (see Supporting Information for details). The HFBI-Protein A module binding on different hydrophobic surfaces such as polystyrene (Figure 3) and CVD graphene transferred to the quartz crystal gave similar results, verifying the hydrophobicity-mediated adhesion (see Supporting Information).

**3.3. Sensor Response.** Charged zipper peptide pair $Z_E$-$Z_R$ was used to demonstrate the operation principle of the sensor. These peptides are well suited to test the operation and sensitivity due to their same but opposite charges and small size not hindering the formation of a uniform module monolayer on graphene, as shown in Figure 2. The estimation of the charge states of HFBI protein and $Z_E$ and $Z_R$ peptides as a function of pH is shown in Figure 4, panel a. HFBI has a nearly neutral net charge around pH 7, and the total charges of $Z_E$ and $Z_R$ are −7e and +7e, respectively. Consequently, the net charge of HFBI-$Z_E$ receptor module is expected to be −7, which will be compensated by the charge of the $Z_R$ analyte during binding

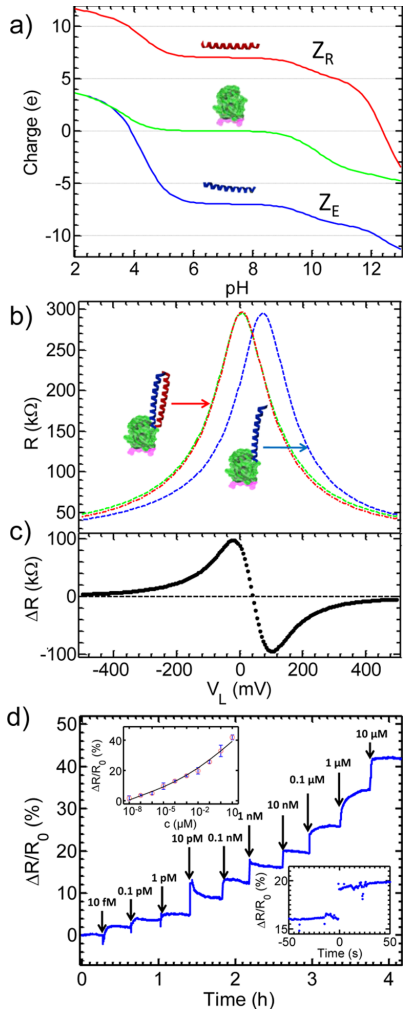


**Figure 4.** (a) Calculated charge of the peptides $Z_E$ (blue) and $Z_R$ (red) and the hydrophobin protein HFBI (green) as a function of pH. (b) Resistance of the graphene channel as a function of the liquid potential for clean graphene surface (green), with HFBI-$Z_E$ receptor module surface functionalization (blue) and after selective binding of $Z_R$ from 10 $\mu$M analyte solution (red). (c) Resistance difference ΔR arising from the $Z_R$ binding, that is, subtraction of the blue curve from the red curve. (d) Sensor response at increasing $Z_R$ analyte concentration. The arrows indicate the introduction of the analyte and the concentrations. The calibration curve defined as the average response measured at each concentration level (error bars 2$\sigma$) is shown in the top inset. Initial and end states in panel d correspond to the blue and red curves in panel b. (bottom inset) Close-up of the response curve showing the abrupt rise of the signal as for 10 nM step.

by ionic bridging between the matching amino acids.[25] The $Z_R$ concentration of 10 $\mu$M is expected to provide an ideal 1:1 binding ratio with $Z_E$ (see Supporting Information).

The response of the sensor was measured with only buffer solution introduced, after in situ self-assembly of a HFBI-$Z_E$


DOI: 10.1021/acsami.6b00123
ACS Appl. Mater. Interfaces 2016, 8, 8257−8264

module layer, and after binding of the $Z_R$ analyte. After functionalization with HFBI-$Z_E$ receptor modules, the sensor was dried, and the fluidic chamber was replaced with a clean one to avoid possible memory effects in the liquid feeding tubing. The shift of the Dirac peak and the corresponding relative change in the channel resistance arising from the functionalization and introduction of the analyte are plotted in Figure 4, panels b and c, respectively. All the measurements were carried out in 100 mM sodium phosphate buffer at pH 7. The shift of the Dirac peak toward more positive voltage indicates that the HFBI-$Z_E$ complex carries negative charge, (blue curve in Figure 4b) consistent with the calculations shown in Figure 4, panel a. Introduction of the peptide $Z_R$ in 10 $\mu$M analyte solution (red curve in Figure 4b) returned the Dirac peak position close to the value of the clean sensor state (green curve in Figure 4b), indicating effectively zero net charge of the peptide pair. The sensitivity was investigated at constant liquid gate voltage $V_L$ by introducing the $Z_R$ analyte in increasing concentrations as shown in Figure 4, panel d and measuring the channel resistance at constant $V_L$. The liquid gate bias $V_L$ = 0 V was selected to optimize the response by producing maximum $\Delta R$.

The dynamic range of detection was found to extend from 10 fM at least up to 10 $\mu$M analyte concentration. Already 10 fM analyte concentration induced a saturated response of 2% in the relative change of the channel resistance at constant $V_L$, an order of magnitude higher than the noise level in the measurement. The detector response was fast, typically less than 1 s, reflecting the immediate receptor−analyte binding process (see the bottom inset in Figure 4d). After the initial response, the stabilization to the biological equilibrium can be affected by curls in the fluidic chamber and mobile charges in the sensor substrate. At very low analyte concentration, the association rate is strongly limited by the finite mass transport in the buffer.[29]

The response of HFBI-Protein A receptor module functionalization to IgG1 analyte was investigated in the same way as with the HFBI-$Z_E$ module and $Z_R$ analyte. The response was measured using the same GFET device after in situ solvent cleaning followed by functionalization with the new receptor modules. Again, the modules form a full monolayer on graphene by self-assembling, as shown in Figure 2, panels e−g. Binding of the HFBI-Protein A receptor module was found to induce a negative shift of the Dirac peak, and the subsequent IgG1 binding further increased the shift, indicating detection of positive charge in both cases. The exact charge of IgG1 is not known. The shift of the Dirac peak and the corresponding change in resistance are shown in Figure 5, panels a and b. The sensor sensitivity and the related calibration curve at liquid potential $V_L$ = 75 mV are shown in Figure 5, panel c. A response of about 3% in the relative change of the channel resistance was obtained at the lowest concentration of 80 fM, and the dynamic range was found to extend at least up to 80 nM concentration, which was the highest concentration tested. The temporal response of HFBI-Protein A to IgG1was similar to the HFBI-$Z_E$ $Z_R$ system, that is, fast initial response and slower saturation.

The selectivity of the sensor was studied by functionalizing the graphene surface with HFBI-$Z_E$ receptor modules and using 80 nM IgG1 analyte. IgG1 analyte showed less than 1% response compared to the 42% response in $\Delta R/R$ with 10 $\mu$M $Z_R$ analyte. In addition, the selectivity was tested using clean graphene channel with no functionalization and also with HFBI

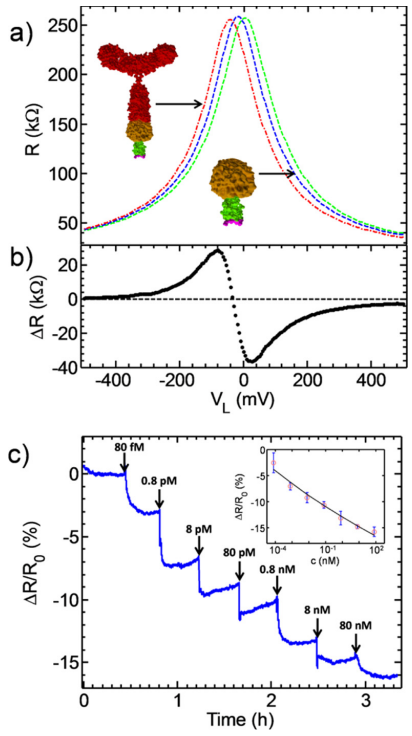


**Figure 5.** Sensor response to IgG1 with HFBI-Protein A as the receptor module. (a) Resistance of the graphene channel as a function of the liquid gate potential for a clean sensor (green), surface functionalized with HFBI-Protein A receptor modules (blue), and after binding of IgG1 from 80 nM analyte solution (red). (b) Resistance difference $\Delta R$ arising from the IgG1 binding. (c) Sensor response at increasing IgG1 concentrations and the calibration curve (inset). The arrows indicate the introduction of the analyte and the concentrations. Initial and end states correspond to the blue and red curves in panel a.

anchor protein monolayer functionalization. The response was measured with 10 $\mu$M $Z_R$ analyte. Both of the non-functionalized and GFET functionalized only with HFBI proteins gave an order of magnitude smaller shift of the Dirac peak than the sensor with HFBI-$Z_E$ module functionalized surface. Data for selectivity measurements are shown in the Supporting Information.

The measured sensitivity is rather surprising taking into account that the measurements were performed in high ionic strength buffer. The polarizability of the buffer liquid leads to screening of the charge of the analytes, which will limit the sensitivity of the GFET, and consequently, the structure of the immobilized layer has an important role in optimizing the performance of the sensor.[30] Hydrophobins are 3 nm tall,[13] and they self-assemble into a dense molecular monolayer on hydrophobic surfaces (see Figure 2). The liquid content remaining inside these layers has been estimated to be only in the range of 10−30%.[31] It is not precisely known how the ionic screening occurs in such a system. The confinement and the small amount of liquid in the protein layer most likely reduce the overall polarizability.[32] Therefore, it can be expected that the double layer formation by mobile ions in the liquid takes


DOI: 10.1021/acsami.6b00123
ACS Appl. Mater. Interfaces 2016, 8, 8257−8264

place mainly above and in between the proteins of the receptor modules, with some contribution arising from the volume of mobile liquid inside the proteins. The effective detection range and the charge sensitivity were investigated with the HFBI-$Z_E$ receptor module monolayer at low analyte concentrations and in two different buffer strengths. The $Z_E$ peptide is linked to the N-terminus of HFBI, which is located in the upper half of the HFBI as illustrated in Figure 6. Each of the $Z_E$ charges,

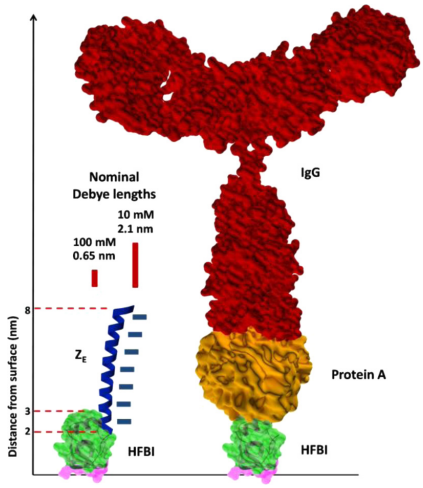


**Figure 6.** Illustration of the sizes and the relevant length scales related to the response of the sensor. The nominal Debye lengths in 10 mM and 100 mM buffer solutions are shown by red bars. The effective detection distance from the graphene surface found in the measurements is much larger than the bulk solution Debye lengths.

distributed evenly along the 5−6 nm $\alpha$ helix,[33] has a different effect on the resistance of the graphene channel due to the different distance and different screening. The sensitivity to the $Z_E$ charges at 100 mM buffer indicates the effective detection range to be at least 2.5 nm. When the Debye length in the buffer was tripled to 2.1 nm by decreasing the ionic strength of the buffer to 10 mM, the sensor response increased 6% due to a 25% (6 mV) larger shift of the Dirac peak (see Supporting Information for the data), showing that screening plays a role but the effect is not directly proportional to the Debye length in the bulk of the buffer. Because of the sensitivity to the Debye length, it is expected that the there are certain limitations in the applicability of the sensor at very high ionic strengths. However, a measurable signal for selective detection at conditions close to physiological conditions was obtained.

The case of HFBI-Protein A receptor module and IgG1 analyte is more problematic. Protein A is larger molecule than HFBI, and steric hindrance during self-assembly can affect the formation of the receptor layer on the graphene channel. However, as shown by the AFM images in the Figure 2 and by the QCM results, the HFBI-Protein A receptor modules form a dense monolayer and the reasoning of reduced screening should apply also here, extending the detection range of the charge carried by the large biomolecules. The size of the fusion receptors suggests the distance of the binding site of IgG1 to be at least 5 nm from the graphene surface, which is in accordance with layer thicknesses estimated from QCM and the AFM data. This is again significantly larger than the subnanometer Debye length in the buffer solution. The IgG1 molecules are large (~15 nm), and the sensor is expected to detect only part of the charges of the molecule. The net charge of the IgG1 molecules at pH 7 is positive (pI 8−9.5), which is consistent with the measured response. The amount and location of the charge within the IgG1 molecule is not known, and the orientation of the molecule can depend on the binding ratio to Protein A. At low analyte concentrations, the IgG1 molecules have enough space to lie down on top of the Protein A layer, but at high binding ratios, these molecules are probably standing perpendicular to the surface due to the Coulomb repulsion forces. The limited volume of liquid inside the dense IgG1 molecule layer might enhance the effective detection range at high analyte concentrations. However, the experimental data show that the GFET functionalized with the receptor module monolayer has high sensitivity even for large molecules in strong ionic buffer and is label-free and selective. The conditions chosen for the study simulate the blood plasma, showing the applicability of the technology for blood analytics. At neutral pH, the hydrophobin layer has neutral or slightly negative charge, which repels negatively charged albumins and fibrinogen and therefore suits perfectly for a passive layer for supporting the actual sensing motifs. The sensing group itself is specific for binding of the analyte, which limits the risks of false positive responses.

## 4. CONCLUSIONS

In this work, we have demonstrated the concept of a modular and programmable label-free biosensor. The receptor modules, consisting of an anchor for immobilization and receptor for recognition, are separately produced by biological fusion and prepurified before use. The receptor moiety can be selected to match the analyte to be detected, and the anchoring moiety is always the HFBI hydrophobin protein. It is shown that the receptor modules form a dense oriented monomolecular layer by a single step directed self-assembly on the graphene channel of the GFET used for charge detection. Because most of the biological molecules carry charge, specific labeling is not required. The GFET provides very high charge sensitivity and is fabricated by rather standard microelectronics processing techniques, facilitating mass production of the sensors. The sensitivity of the biorecognition in both model systems is high, with 3% response recorded for below 100 fM analyte concentrations in high ionic strength buffer. The potential to build in selectivity is demonstrated by cross-checking with immunoglobulin analyte and a sensor functionalized with receptor modules for peptide analyte, resulting an order of magnitude smaller shift in the position of the Dirac peak and, consequently, much smaller $\Delta R/R$ response with the IgG1 analyte compared to the peptide analyte. However, several challenges remain to be solved when working with real samples due to their complexity. It is shown that the same device can be programmed to detect different analytes by changing the receptor module layer in situ. The possibility to dry the receptor module layer on the sensor without compromising the performance will be essential for preprogrammed sensor assays in point-of-care applications exploiting disposable sensor chips.

## ■ ASSOCIATED CONTENT

### Supporting Information

The Supporting Information is available free of charge on the ACS Publications website at DOI: 10.1021/acsami.6b00123.



DOI: 10.1021/acsami.6b00123
ACS Appl. Mater. Interfaces 2016, 8, 8257−8264

Additional information about SPR and QCM-D analysis, AFM images, calculation of theoretical Debye length and measurements with different buffer concentrations (PDF)

## AUTHOR INFORMATION


### Corresponding Author

*E-mail: jouni.ahopelto@vtt.fi.

### Present Address

[⊥]School of Chemical Technology, Aalto University, P.O. Box 16200, FI-00076 AALTO, Finland.

### Author Contributions

[§]These authors contributed equally to this work.


### Notes

The authors declare no competing financial interest.

## ACKNOWLEDGMENTS

This research was supported by TEKES project GraNBis, Academy of Finland Centre of Excellence in Atomic Layer Deposition, Academy of Finland Centre of Excellence in Molecular Engineering of Biosynthetic Hybrid Materials Research and grant no. 250898, and the European Union Seventh Framework Programme under grant agreement no. 604391 Graphene Flagship. Ingmar Stuns and Sampo Sorvisto are acknowledged for the fluidic cell. We thank Riitta Suihkonen, Anne Ala-Pöntiö, and Teresa Blomqvist for help with production and purification of HFBI−$Z_E$.

## REFERENCES


(1) Ngoepe, M.; Choonara, Y.; Tyagi, C.; Tomar, L.; du Toit, L.; Kumar, P.; Ndesendo, M.; Pillay, V. Integration of Biosensors and Drug Delivery Technologies for Early Detection and Chronic Management of Illness. *Sensors* **2013**, *13*, 7680−7713.

(2) Stine, R.; Mulvaney, S. P.; Robinson, J. T.; Tamanaha, C. R.; Sheehan, P. E. Fabrication, Optimization and Use of Graphene Field Effect Sensors. *Anal. Chem.* **2013**, *85*, 509−521.

(3) Pumera, M. Graphene in Biosensing. *Mater. Today* **2011**, *14*, 308−315.

(4) Jacobs, C. B.; Peairs, M. J.; Venton, B. J. Review: Carbon Nanotube Based Electrochemical Sensors for Biomolecules. *Anal. Chim. Acta* **2010**, *662*, 105−127.

(5) Chen, K.; Li, B.; Chen, Y. Silicon Nanowire Field-effect Transistor-based Biosensors for Biomedical Diagnosis and Cellular Recording Investigation. *Nano Today* **2011**, *6*, 131−154.

(6) Kuila, T.; Bose, S.; Khanra, P.; Mishra, A. K.; Kim, N. H.; Lee, J. H. Recent Advances in Graphene-based Biosensors. *Biosens. Bioelectron.* **2011**, *26*, 4637−4648.

(7) Ohno, Y.; Maehashi, K.; Matsumoto, K. Label-free Biosensors Based on Aptamer-modified Graphene Field-effect Transistors. *J. Am. Chem. Soc.* **2010**, *132*, 18012−18013.

(8) Mannoor, M. S.; Tao, H.; Clayton, J. D.; Sengupta, A.; Kaplan, D. L.; Naik, R. N.; Verma, N.; Omenetto, F. G.; McAlpine, M. C. Graphene-based Wireless Bacteria Detection on Tooth Enamel. *Nat. Commun.* **2012**, *3*, 763.

(9) Cui, Y.; Kim, S. N.; Jones, S. E.; Wissler, L. L.; Naik, R. R.; McAlpine, M. C. Chemical Functionalization of Graphene Ena-bled by Phage Displayed Peptides. *Nano Lett.* **2010**, *10*, 4559−4565.

(10) Borini, S.; White, R.; Wei, D.; Astley, M.; Haque, S.; Spigone, E.; Harris, N.; Kivioja, J.; Ryhänen, T. Ultrafast Graphene Oxide Humidity Sensors. *ACS Nano* **2013**, *7*, 11166−11173.

(11) Novoselov, K. S.; Geim, A. K.; Morozov, S. V.; Jiang, D.; Zhang, Y.; Dubonos, S. V.; Grigorieva, I. V.; Firsov, A. A. Electric Field Effect in Atomically Thin Carbon Films. *Science* **2004**, *306*, 666−669.

(12) Wessels, J. G. H. Hydrophobins, Unique Fungal Proteins. *Mycologist* **2000**, *14*, 153−159.

(13) Linder, M. B.; Szilvay, G. R.; Nakari-Setälä, T.; Penttilä, M. E. Hydrophobins: The Protein-amphiphiles of Filamentous Fungi. *FEMS Microbiol. Rev.* **2005**, *29*, 877−896.

(14) Kurppa, K.; Jiang, H.; Szilvay, G. R.; Nasibulin, A. G.; Kauppinen, E. I.; Linder, M. B. Controlled Hydrid Nanostructures through Protein-Mediated Noncovalent Functionalization of Carbon Nanotubes. *Angew. Chem.* **2007**, *119*, 6566−6569.

(15) Laaksonen, P.; Kainlauri, M.; Laaksonen, T.; Shchepetov, A.; Jiang, H.; Ahopelto, J.; Linder, M. B. Interfacial Engineering by Proteins: Exfoliation and Functionalization of Graphene by Hydrophobins. *Angew. Chem., Int. Ed.* **2010**, *49*, 4946−4949.

(16) Kivioja, J.; Kurppa, K.; Kainlauri, M.; Linder, M. B.; Ahopelto, J. Electrical Transport through Ordered Self-assembled Protein Monolayer Measured by Constant Force Conductive Atomic Force Microscopy. *Appl. Phys. Lett.* **2009**, *94*, 183901.

(17) Laaksonen, P.; Walther, A.; Malho, J. M.; Kainlauri, M.; Ikkala, O.; Linder, M. B. Genetic Engineering of Biomimetic Nanocomposites: Diblock Proteins, Graphene and Nanofibrillated Cellulose. *Angew. Chem., Int. Ed.* **2011**, *50*, 8688−8691.

(18) Zhao, Z.; Qiao, M.; Yin, F.; Shao, B.; Wu, B.; Wang, B.; Wang, X.; Qin, X.; Li, S.; Yu, L.; Chen, Q. Amperometric Glucose Biosensor Based on Self-assembly Hydrophobin with High Efficiency of Enzyme Utilization. *Biosens. Bioelectron.* **2007**, *22*, 3021−3027.

(19) Wang, X.; Wang, H.; Huang, Y.; Zhao, Z.; Qin, X.; Wang, Y.; Miao, Z.; Chen, Q.; Qiao, M. Noncovalently Functionalized Multi-wall Carbon Nanotubes in Aqueous Solution Using the Hydrophobin HFBI and Their Electroanalytical Application. *Biosens. Bioelectron.* **2010**, *26*, 1104−1108.

(20) Zhao, Z.; Wang, H.; Qin, X.; Wang, X.; Qiao, M.; Anzai, J.; Chen, Q. Self-assembled Film of Hydrophobins on Gold Surfaces and Its Application to Electrochemical Biosensing. *Colloids Surf., B* **2009**, *71*, 102−106.

(21) Riikonen, J.; Kim, W.; Li, C.; Svensk, O.; Arpiainen, S.; Kainlauri, M.; Lipsanen, H. Photo-thermal Chemical Vapour Deposition of Graphene on Copper. *Carbon* **2013**, *62*, 43−50.

(22) Lafkioti, M.; Krauss, B.; Lohmann, T.; Zschieschang, U.; Klauk, H.; Klitzing, K.; Smet, J. H. Graphene on a Hydrophobic Substrate: Doping Reduction and Hysteresis Suppression under Ambient Conditions. *Nano Lett.* **2010**, *10*, 1149−1153.

(23) Joensuu, J. J.; Conley, A. J.; Lienemann, M.; Brandle, J. E.; Linder, M. B.; Menassa, R. Hydrophobin fusions for high-level transient protein expression and purification in Nicotiana benthamiana. *Plant Physiol.* **2010**, *152*, 622−633.

(24) Linder, M. B.; Qiao, M.; Laumen, F.; Selber, K.; Hyytiä, T.; Nakari-Setälä, T.; Penttilä, M. E. Efficient Purification of Recombinant Proteins Using Hydrophobins as Tags in Surfactant-based Two-phase Systems. *Biochemistry* **2004**, *43*, 11873−11882.

(25) Zhang, K.; Diehl, M. R.; Tirrell, D. A. Artificial Polypeptide Scaffold for Protein Immobilization. *J. Am. Chem. Soc.* **2005**, *127*, 10136−10137.

(26) Hakanpää, J.; Szilvay, G. R.; Kaljunen, H.; Maksimainen, M.; Linder, M. B.; Rouvinen, J. Two crystal structures of Trichoderma reesei hydrophobin HFBI—the structure of a protein amphiphile with and without detergent interaction. *Protein Sci.* **2006**, *15*, 2129−2140.

(27) Szilvay, G. R.; Paananen, A.; Laurikainen, K.; Vuorimaa, E.; Lemmetyinen, H.; Peltonen, J.; Linder, M. B. Self-assembled hydrophobin protein films at the air-water interface: structural analysis and molecular engineering. *Biochemistry* **2007**, *46*, 2345−2354.

(28) Gouda, H.; Torigoe, H.; Saito, A.; Sato, M.; Arata, Y.; Shimada, Y. Three-dimensional Solution Structure of the B Domain of Staphylococcal Protein A: Comparisons of the Solution and Crystal Structures. *Biochemistry* **1992**, *31*, 9665−9672.

(29) Duan, X.; Li, Y.; Rajan, N. K.; Routenberg, D. A.; Modis, Y.; Reed, M. A. Quantification of the Affinities and Kinetics of Pro-tein Interactions Using Silicon Nanowire Biosensors. *Nat. Nanotechnol.* **2012**, *7*, 401−407.

(30) Stern, E.; Wagner, R.; Sigworth, F. J.; Breaker, R.; Fahmy, T. M.; Reed, M. A. Importance of the Debye Screening Length on Nanowire Field Effect Transistor Sensors. *Nano Lett.* **2007**, *7*, 3405−3409.




DOI: 10.1021/acsami.6b00123
*ACS Appl. Mater. Interfaces* 2016, 8, 8257−8264

(31) Krivosheeva, O.; Dėdinaitė, A.; Linder, M. B.; Tilton, R. D.; Claesson, P. M. Kinetic and Equilibrium Aspects of Adsorption and Desorption of Class II Hydrophobins HFBI and HFBII at Silicon Oxynitride/water and Air/water Interfaces. *Langmuir* **2013**, *29*, 2683−2691.
(32) Fernandez Stigliano, A. Breakdown of the Debye Polarization Ansatz at Protein-Water Interfaces. *J. Chem. Phys.* **2013**, *138*, 225103.
(33) Berg, J. M.; Tymoczko, J. L.; Stryer, L. *Biochemistry*, 5th ed.; W.H. Freeman and Company: New York, 2002.



DOI: 10.1021/acsami.6b00123
*ACS Appl. Mater. Interfaces* 2016, 8, 8257−8264

# SUPPORTING INFORMATION

# Graphene biosensor programming with genetically engineered fusion protein monolayers

*Miika Soikkeli‡[1], Katri Kurppa‡[1], Markku Kainlauri‡[1], Sanna Arpiainen‡[1],Arja Paananen[1], David Gunnarsson[1], Jussi J. Joensuu[1], Päivi Laaksonen[1†], Mika Prunnila[1], Markus B. Linder[1,2], Jouni Ahopelto[1]**

[1]VTT Technical Research Centre of Finland, PO. Box 1000, FI-02044 VTT, Espoo, Finland
[2] Aalto University, School of Chemical Technology, PO. Box 6100, FI-00076 AALTO, Espoo, Finland

†Present Address: Aalto University, School of Chemical Technology, P.O. Box 16200, FI-00076 AALTO, Finland

‡These authors contributed equally to this work

***jouni.ahopelto@vtt.fi**

**Protein interactions**

Surface-plasmon resonance measurements (SPR) (Autolab ESPRIT) were carried out to study the binding ratio of HFBI-$Z_E$ and $Z_R$. HFBI-$Z_E$ was bound on a hexanethiol-treated gold surface and the binding of $Z_R$ was measured at different concentrations. The bound amount was monitored before and after buffer rinse. A nonlinear regression curve was fitted to the data. The data shows, that the $B_{max}$, binding capacity, before buffer rinse is 2.7 μM and the corresponding dissociation constant $K_D$ is 5.7 μM. The values after buffer rinse were 1.7 μM and 4.7 μM for binding capacity and dissociation constant, respectively.

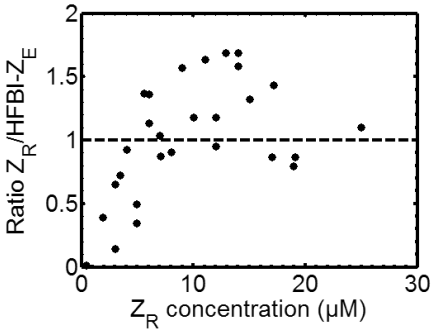


**Figure S1.** Concentration dependence of analyte binding ratio to receptor molecules. SPR data showing the binding of $Z_R$ to a HFBI-$Z_E$ layer on a hydrophobic hexanethiol SAM surface.

**QCM-D analysis**

In the QCM-D measurements the measured frequency responses Δf were used to calculate the mass of protein bound, Δm, using the Sauerbrey relation

$$\Delta m = -\frac{C \cdot \Delta f}{n_5}$$

where C = 17.7 $ngHz^{-1}cm^{-2}$ for a 5 MHz quartz crystal and n = 5, the overtone number.

High affinity binding of the HFBI-$Z_E$ protein to a hydrophobic polystyrene surface was confirmed in the measurements. The Sauerbrey mass calculated on the basis of the frequency change is about 270 $ng/cm^2$, which is in the range of the monolayer mass (MW 12 kDa). The dissipation of the unmodified HFBI layer on polystyrene is <1, indicating a very rigid, compact layer. For the HFBI-$Z_E$ at pH 7, the dissipation is in the range of 2 – 2.5. This is a result of the $Z_E$ peptide chains extending outward from the surface. At pH 5 the dissipation is zero, indicating a more compact layer structure (unpublished data). Addition of the $Z_R$ peptide to the HFBI-$Z_E$ layer at pH 7 resulted in a decrease of the dissipation. However, there was no corresponding change in frequency. This finding can most likely be attributed to either a molecular rearrangement upon binding of the zipper peptides or water being expelled from the underlying

HFBI-$Z_E$ layer. The SPR data together with the reported GFET measurements confirm however the binding of the zipper peptides $Z_E$ and $Z_R$ in a 1:1 ratio (Fig. S1). The possibility of such molecular rearrangements or changes in packing density should be taken into consideration when evaluating and designing biosensors.

QCM-D measurements of HFBI-Protein A revealed that the fusion protein formed a stable layer with a mass of 752 ng/cm$^2$. This value corresponds to a molecular area of 9 nm$^2$ (for MW 44 kDa). The reported diameter of the HFBI molecule is 2 nm [1], and the attached Protein A partner is likely to affect the area taken up by the protein. The dimensions of the Protein A part of the fusion molecule cannot be exactly determined due to the absence of a crystal structure. Herein, an approximate length of 4.5 nm and a diameter of 2.5 nm of the *Staphylococcus aureus* Protein A subunit B (Protein Data Bank ID 1BDC) were used to evaluate the scale of the molecular area of HFBI-Protein A. Molecular packing and surface roughness account for deviations from theoretical estimation. The antibody bound to the HFBI linked Protein A surface with high-affinity resulting in a mass increase of 1330 ng/cm$^2$. The measures masses translate to a rough 1.9 : 1 molar ratio of HFBI-Protein A : IgG. The binding ratio can be possibly tuned by adding free HFBI to the HFBI-Protein A to act as a spacer (unpublished results).

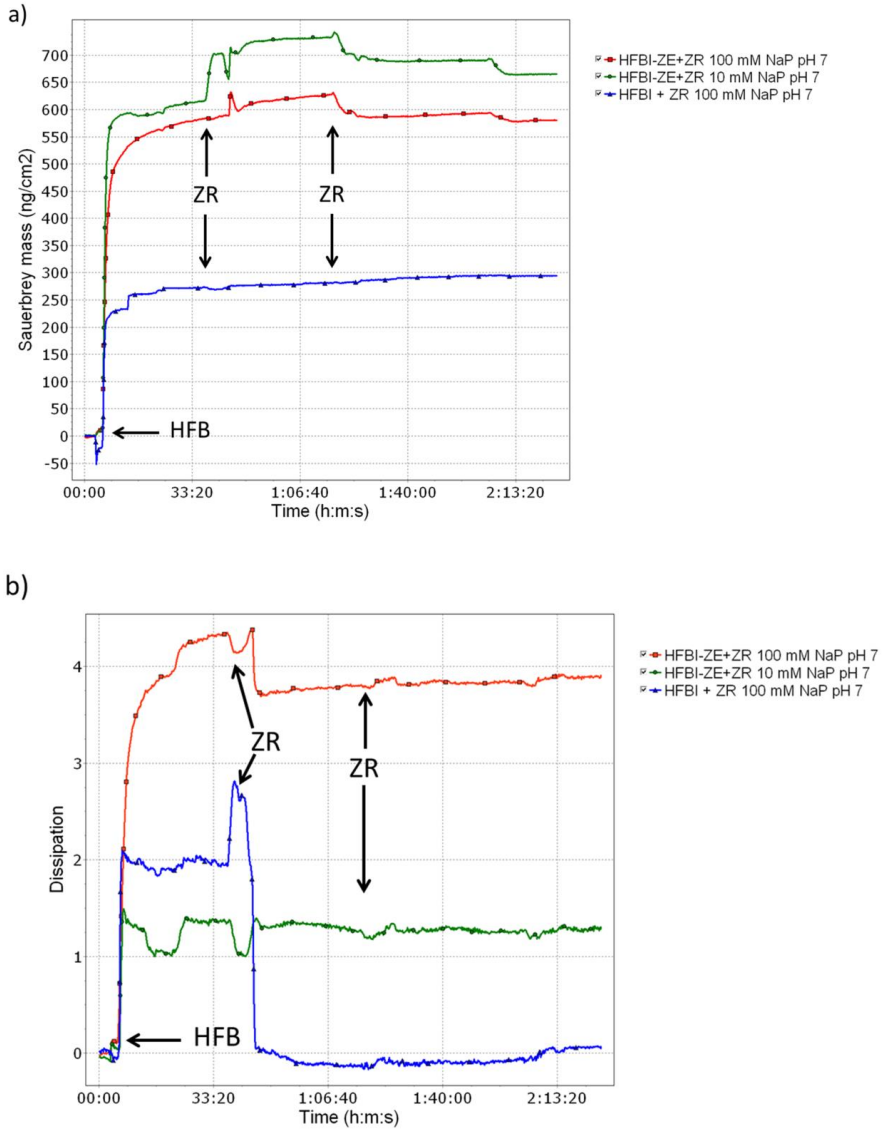


**Figure S2.** QCM analysis of receptor and analyte attachment on hydrophobic surfaces a) QCM-D sensograms showing the Sauerbrey masses (a) and dissipation values (b) of the positive peptide $Z_R$ to the hydrophobin fusion HFBI-$Z_E$ at phosphate concentration of 100 mM (red curve) and 10 mM (green curve). The unmodified HFBI was measured as a negative control (blue curve).

QCM-D measurements of HFBI-Protein A were also performed on graphene attached to silicon dioxide surface. The surface coverage of graphene on silicon dioxide was only 25 %, and reference QCM analysis was made on pure silicon dioxide to estimate the effect of the surrounding areas. The QCM results with crystals having distinct areas with different mass per unit area are only indicative, because the method is based on an analysis of uniformly covered QCM plate. It may be that the whole plate resonates in some undefined mode or the resonance overtone peak consists of two distinct resonance peaks originating from the different areas, from which only the stronger is recorded. This favors both larger surface area and higher uniformity and stiffness in the attached mass in the selection of the recorded signal.

The measurement results are shown in Figure S3. The addition of HFBI-Protein A results in a Sauerbrey mass increase of 750 ng/cm$^2$ for graphene on $SiO_2$ surface and 800 ng/cm$^2$ for $SiO_2$ surface. After washing with buffer the corresponding masses are 440 ng/cm$^2$ and 540 ng/cm$^2$, respectively. The addition of IgG analyte increases the Sauerbrey masses to 940 ng/cm$^2$ and 640 ng/cm$^2$, respectively. The behavior of the HFBI-Protein A related signal before and after rinsing is rather similar in both cases, so it is not possible to conclude that the masses recorded from graphene on $SiO_2$ surface are related to the graphene covered part of the surface. However, the

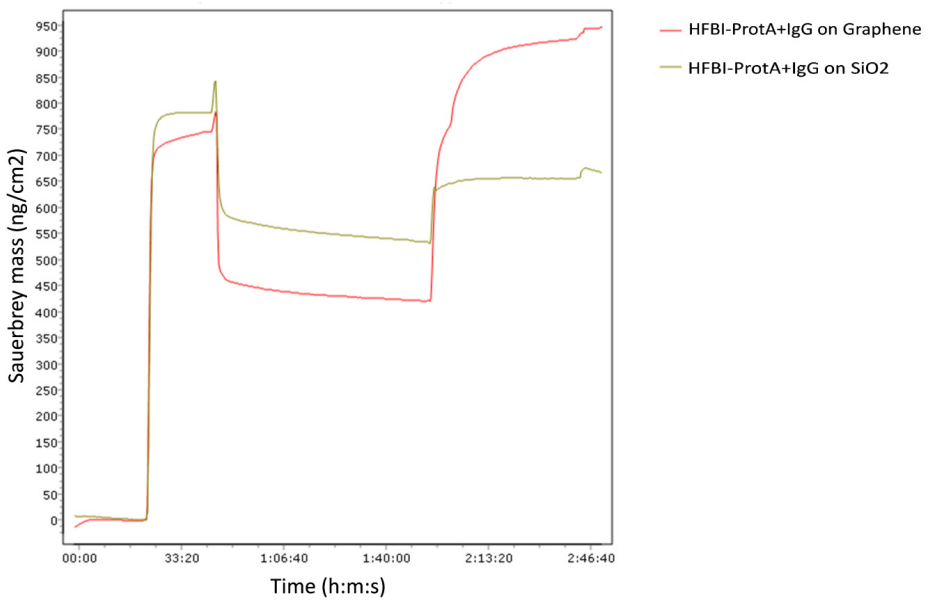


**Figure S3.** QCM analysis of receptor and analyte attachment on graphene with 25 % coverage on silicon dioxide (red) and silicon dioxide reference surface (brown). QCM-D sensograms showing the Sauerbrey masses of the IgG adsorbed to the hydrophobin fusion HFBI – Protein A at phosphate concentration of 100 mM.

amount of IgG analyte attaching on the graphene on $SiO_2$ surface is 5 times higher than on the reference $SiO_2$ surface, indicating that the graphene covered part greatly affects the overall signal. Even though the Sauerbrey mass of adsorbed HFBI-Protein A layer and the sequential IgG layer cannot be reliably determined from the QCM data due to the thickness and structure of the adsorbed protein layer, the results are indicative and show the functionality of the surface. It is noteworthy that the mass increase with IgG introduction is similar in shape to that of the IgG analyte attaching on the fusion protein coated polystyrene surface (Figure 5). This indicates that similar processes are taking place on surfaces. The higher amounts of IgG attached to the surface containing graphene most likely originates from the optimal orientation of the Protein A molecules via fusion protein, thus enabling much higher binding of IgG analytes. On the $SiO_2$ surface orientation of HFBI-Protein A fusion proteins is less controlled, and results in a protein layer where Protein A molecules are only randomly available for binding of IgG analytes.

The HFBI fusion based receptors can also be used in other detection schemes, for example with silicon nanowire FETs that however need to be covered with a hydrophobic layer in order to achieve the oriented self-assembly. The conditions for the functionalization of the hydrophobic HMDS layer on $SiO_2$ were tested by QCM analysis with set consisting of hydrophiliced quartz, HMDS covered quartz and polystyrene crystals. The amounts of HFBI attaching to polystyrene and HMDS covered quartz from a 50 µg/ml HFBI at pH 7 varied between 250 – 300 ng/cm$^2$, whereas there was no attachment on the hydrophilized quartz. HMDS was also found stable against 3 hour exposures to pH 7 and pH 8. It could also be cleaned from the HFBI with 60% ethanol, after which a new layer of HFBI was attached with as high surface coverage as before the cleaning.

**Atomic force microscopy imaging of the functionalization layers**

Both HFBI-$Z_E$ and HFBI-Protein A functionalized surfaces shown in Fig. S4 were studied immediately after functionalization, after drying and finally after re-wetting. Both cases show dense coverage of the surface immediately after the functionalization. Drying causes some tearing of the surface but after re-wetting the coverage is again dense and no tearing can be observed. Also in this case white spots caused likely by the buffer solution were observed in the images. The amount of white spots on the graphene surface on $SiO_2$ was higher than on platinum samples, which did not have a clear reason. The origin of similar white spots has earlier been presented to be nanobubbles on the surface.[2] Despite the spots the protein layer underneath them is uniform and dense also on the graphene surface on $SiO_2$.

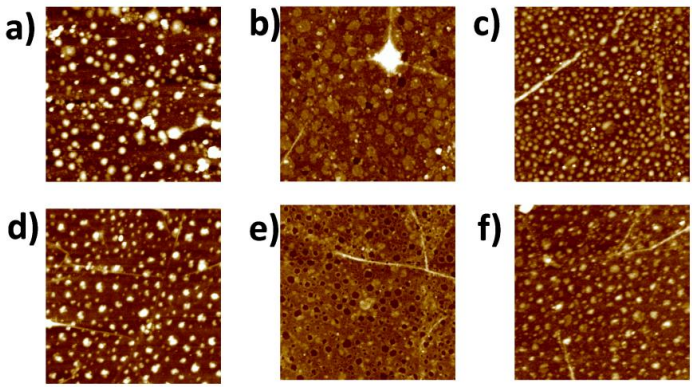


**Figure S4**. Atomic force microscopy topography images of HFBI-ZE and HFBI-Protein A receptor module layers on CVD graphene on $SiO_2$. a) Surface after HFBI-ZE functionalization in 100 mM pH 7 NaP buffer, b) after drying in $N_2$ and c) after re-wetting in the buffer. d) Surface after HFBI-Protein A functionalization in 100 mM pH 7 NaP buffer, e) after drying and f) after re-wetting in the buffer. For both of the receptor modules protein film shrinkage and possible mechanical forces during the drying tend to create cracks in the film but damage is healed in both cases after 5 min re-wetting in the buffer. The image size is 1 x 1 $\mu m^2$ and height scale 15 nm in all the images.

**Calculation of theoretical Debye length**

Ionic strength *I* of the sodium phosphate buffers (10 mM and 100 mM) were calculated from the equation

$$I = \frac{1}{2}\sum_{i=1}^{n} c_i z_i^2,$$

where the concentrations *c* of the ionic species of charge *z* where considered according to the equilibrium

$$H_3PO_4 \overset{pK_{a1}}{\rightleftharpoons} H_2PO_4^- + H^+ \overset{pK_{a2}}{\rightleftharpoons} HPO_4^{2-} + 2H^+ \overset{pK_{a3}}{\rightleftharpoons} PO_4^{3-} + 3H^+$$

$pK_{a1} = 2.148$; $pK_{a2} = 6.865$; $pK_{a3} = 12.319$

The Debye length $\kappa^{-1}$ in 10 mM and 100 mM sodium phosphate buffers for a theoretical planar surface was given by the equation

$$\kappa^{-1} = \sqrt{\frac{\varepsilon_r \varepsilon_0 k_B T}{2 N_A e^2 I}},$$

where $\varepsilon_r$ = relative permittivity of water, $\varepsilon_0$ = relative permittivity of vacuum, $k_B$ = Boltzmann's constant, $T$ = temperature, $N_A$ = Avogadro's constant, $e$ = elemental charge and $I$ = ionic strength. The theoretical Debye lengths in 10 mM and 100 mM sodium phosphate buffers were calculated to be about 2.1 nm and 0.65 nm, respectively. The Debye length in 100 mM sodium phosphate buffer solution as a function of pH is shown in Fig. S5.

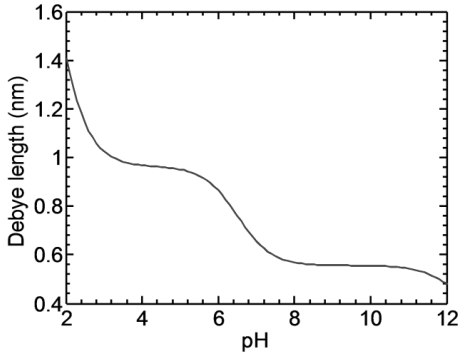


**Figure S5.** Dependence of Debye screening length on pH. Debye length as a function of pH in 100 mM sodium phosphate buffer. Debye length in 100 mM sodium phosphate buffer at pH 7 is about 0.65 nm.

**Sensor measurement as a function of ionic concentration of the buffer**

The effect of buffer concentration on the detected response as the measured resistance as a function of liquid potential for the 10 mM and 100 mM solutions with clean surface and HFBI-$Z_E$ functionalized surface are shown in Fig. S6. The Dirac peaks of clean curves (dashed red and black) have been shifted to 0 mV to compare the change caused by the buffer solutions. The Dirac peaks with HFBI-$Z_E$ in 10 (red) mM and 100 mM (black) buffers are at 29 mV and 23 mV,

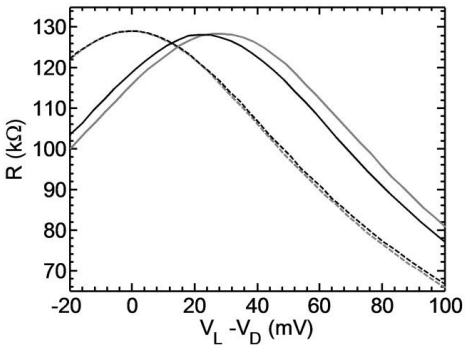


**Figure S6**. The effect of buffer concentration on sensor response. Resistance of graphene channel as a function of liquid potential for 10 mM (red) and 100 mM (black) pH 7 sodium phosphate buffer solutions. The data has been shifted to set the Dirac peaks of both clean curves (dashed red and black) at 0 mV. The shift caused by the attachment of HFBI-$Z_E$ in 10 mM (red) is 26 % larger than in 100 mM (black).

respectively. Thus the increase of the Debye length from 0.65 nm to 2.1 nm increased the detected shift of the Dirac peak by about 26 %, which corresponds to 6 % increase in detector response.

**Selectivity of the sensor functionalization**

The selectivity of sensor was studied by using 10 µM ZR analyte on pure graphene surface (Fig. SI7 a) and HFBI functionalized surface (Fig. SI7 b) in the 100 mM NaP pH 7 buffer solution. The attachment of 10 µM $Z_R$ analyte on pure graphene caused - 7 mV shift of the Dirac peak (4 % in $\Delta R\backslash R_0$ at -50 mV). HFBI functionalization of graphene caused - 4 mV shift of Dirac peak and adding the 10 µM $Z_R$ analyte caused additional - 9 mV shift of the Dirac peak (6 % in $\Delta R\backslash R_0$ at -50 mV). Both of these responses are nearly a decade smaller than the - 67 mV Dirac peak shift caused by the 10 µM $Z_R$ analyte on HFBI-$Z_E$ functionalized surface.

Further studies on selectivity were also made by using 80 nM IgG analyte with HFBI-$Z_E$ functionalized sensor in the 100 mM NaP pH 7 buffer solution (in Fig. S8). The detected response was - 2 mV shift of the Dirac peak (0.9 % in $\Delta R\backslash R_0$ at -50 mV), which is clearly smaller than the response caused with the same analyte on HFBI-Protein A functionalized surface or with 10 µM $Z_R$ analyte on HFBI-$Z_E$ functionalized surface.

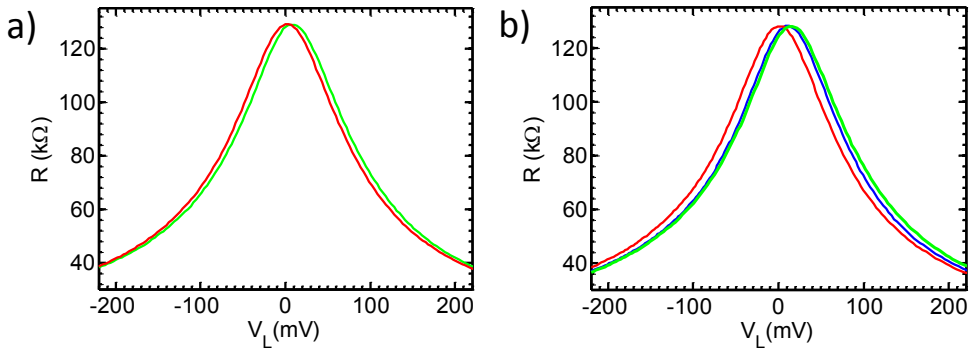


**Figure S7**. a) Response of clean graphene FET channel to small charged analytes. Resistance of the graphene channel as a function of the liquid potential for clean graphene (green) and after non-selective binding of $Z_R$ from 10 µM analyte (red). b) GFET response with bare HFBI functionalization: resistance of the graphene channel as a function of the liquid potential for clean graphene (green), with HFBI surface functionalization (blue) and after non-selective binding of $Z_R$ from 10 µM analyte (red).

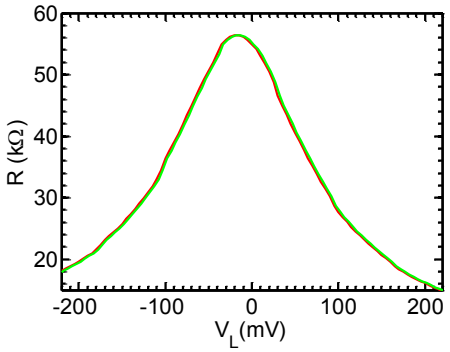


**Figure S8**. Sensor response to large analytes with unspecific binding. Resistance of the graphene channel as a function of the liquid potential for HFBI-$Z_E$ functionalized graphene (green) and after non-selective binding of IgG from 80 nM analyte (red).

## REFERENCES

(1) Hakanpää, J.; Szilvay, G. R.; Kaljunen, H.; Maksimainen, M.; Linder, M. B.; Rouvinen, J. Two Crystal Structures of Trichoderma Reesei Hydrophobin HFBI – The Structure of a Protein Amphiphile with and without Detergent Interaction. *Protein Sci.* **2006,** 15, 2129-2140.

(2) Bhushan, B,; Pan, Y.; Daniels, S. AFM Characterization of Nanobubble Formation and Slip Condition in Oxygenated and Electrokinetically Altered Fluids. *J. Colloid Interface Sci.* **2013**, 392, 105-116.

Aalto-DD 90/2017
VTT SCIENCE 153

Proteins have become a central focus of research in the fields of biotechnology and material development. Nature has created detailed and precise function to these molecules, which can be harnessed to build new materials and applications. The art of protein engineering may be used to join and modify elements in new combinations.

This research focuses on the design and use of fusion proteins of hydrophobin protein HFBI. Hydrophobins are small fungal proteins with interfacial function. A central theme throughout this research was to evaluate aspects such as protein component stoichiometry, material geometry and charge effects, as well as holistic factors influencing application design. The results presented in this thesis demonstrate the design and use of protein functionalities for creation of biomolecular assemblies based on the self-assembly of hydrophobin HFBI.

ISBN 978-952-60-7428-3 (printed)
ISBN 978-952-60-7427-6 (pdf)
ISSN-L 1799-4934
ISSN 1799-4934 (printed)
ISSN 1799-4942 (pdf)

978-951-38-8539-7 (printed)
978-951-38-8538-0 (pdf)
2242-119X
2242-119X (printed)
2242-1203 (pdf)

**Aalto University**
**School of Chemical Engineering**
**Department of Bioproducts and Biosystems**
**www.aalto.fi**

**BUSINESS + ECONOMY**

**ART + DESIGN + ARCHITECTURE**

**SCIENCE + TECHNOLOGY**

**CROSSOVER**

**DOCTORAL DISSERTATIONS**